Phase Transition and Structure Formation in Systems with Finite Number of Particles with Finite Volume

Akinori Awazu

February 2001

Doctoral Thesis at Osaka Prefecture University

Contents

Chapter 1

General Introduction

Surprisingly rich behaviors are often displayed in systems which consist of hard spheres or granular particles. The motivation of our present investigation is to understand characters and mechanism of complex behaviors of various many body systems through the investigation of systems only with the above simple elements; hard spheres and granular particles.

Hard sphere is regarded as one of the simplest object to model each molecule which has its own volume. Here, interactions between them involve only particle-particle elastic collisions through which the total energy is conserved. This has been used in order to investigate the microscopic dynamics of fluids or solids. On the other hand, granular particle, the system with large number of which we call granular materials, is macro-scale particle, also, with finite volume. Like hard spheres, these particles interact only by their direct collisions. However, since each particle is macroscopic, particle-particle collisions are inelastic and frictions work between particles (Table. 1.1). Usually, the number of particles in granular materials is finite, which means thermo-dynamic limit is not applicable. This is another remarkable aspect of them.

In several situations in both hard spheres system and granular materials, the finite volume effect of each particle can be the origin of their complex behaviors. For example,

Particle's type	Scale	Interaction	Energy
Hard sphere	Micro-scale (Molecular)	Elastic collision	Conservation
Granular particle	Macro-scale (Sand, Glass beads)	Inelastic collision & Friction	Dissipation

Table 1.1: Comparison of hard spheres and granular particles.

systems consisting of large number of hard spheres are well known to exhibit various complex behaviors such as the liquid-solid phase transition, the glass transition, etc. (see chapter 2). The degree of complexities can be expected to increase if interactions between particles become dissipative like granular materials. In reality, local and global states in granular materials exhibit spatial and temporal variations such as convection, size segregation, slugging, and stick-slip motion depending on environmental conditions (see chapter 2). In granular materials and hard spheres systems realizing glassy states, moreover, the frictional force, the pressure, and other characteristic quantities of a state often depend on the history before the state is realized (see chapter 2).

To study these issues is, equivalently, to treat strongly non-stationary states with large fluctuations, for which no effective methods for analysis have been developed. So, by introducing some model systems which are simplified but include intrinsic aspects of each phenomenon, we can uncover the essential and universal features of systems beyond each. In the former part of this thesis, we focus on the fundamental properties of hard spheres systems and granular materials such as the phase transition, and the characters of the transport of several quantities in these systems. On the other hand, in the latter part, we discuss the mechanism of pattern formations and the time evolution of these patterns.

The detailed organization of this thesis is as follows. In chapter 2, we review recent investigations of phase transition in many hard spheres systems, and those of some typical phenomena observed in granular materials. In chapter 3, we discuss the solid-liquid and the glass-like phase transition of the system which consists of two hard spheres in a rectangular box. In chapter 4, also using the two hard spheres system, we discuss the appearance of the static and the dynamic frictions, and the variance between them. In these two chapters, we show that the appearance of the solid-liquid and the glass-like phase transitions and the transition of the static-dynamic frictions, are generally observed if the system is influenced by the effect of excluded volume. In chapter 5, we discuss the transition of the effective dimension of strongly excited granular materials in a pipe associated with the variance of the pipe width. Up to this chapter, we discuss the basic properties of the systems which consist of particles with finite volume. In the subsequent three chapters, on the contrary, we discuss mainly the mechanism of spatial structure formation. In chapter 6, we discuss the size segregation of granular materials in a rotating drum. In chapter 7, we discuss the jam formation of the traffic flow on a high way with two lanes. Similar jam formation is seen in the flow of granular materials in a slim pipe which is one of the most important and elementary character of the flow of granular materials. Discussions in chapter 7 are strongly related to those in chapter 5, where the stability of jams is discussed through multi-dimensional effects of the system. In chapter 8, we discuss general characters of jam formation using simple models in which interactions between elements have a little complexities. In chapter 9, we summarize present investigations.

Chapter 2

Background

In this chapter, we overview recent investigations of several phenomena realized in hard spheres systems and granular materials. So far, numerous number of reports have been published on the studies of these systems, and are still drastically increasing. Thus, we pick up and introduce only a limited number of topics related to our discussions in the following chapters.

Section 2.1 is the review of recent investigations of phase transitions which are observed in systems consisting of particles with hard core potentials. The purpose of this section is to introduce the background of our discussions in chapter 3 and chapter 4. For this purpose, we introduce, mainly, the outline of numerical studies for Alder transition and the disappearance of this transition. Adding to the introduction of the liquid-solid phase transition, we overview the phenomena observed in the glass transition. Section 2.2 is the review of recent investigations of granular materials. First, we introduce the recent studies of the fluidized deep granular bed, in particular, the roll formation, the bubbling and the slugging. Appearance of these phenomena is directly related to the motivation of studies in chapter 5. Second, we overview recent studies of phenomena seen in one dimensional granular flows and traffic flows. Discussions in chapter 7 and chapter 8 are based on these studies. Third, we see the effect of inhomogeneity of particles' size of granular materials, in particular, the size segregation connecting to discussions in chapter 6. Finally, we introduce the experimental and numerical investigations of frictions which working on the granular layers reflecting history dependencies. In chapter 4, we discuss these history dependencies using a simple model. Related to topics with history dependencies, we introduce the investigations of the pressure distribution at the bottom of a sand pile.

2.1 Phase Transition of Many Hard Spheres System

In this section, phase transition and related phenomena observed in hard spheres systems are briefly reviewed. Also behaviors of particles systems with some other types of potential like r^{-12}, $d^{5/2}$, d^2, etc., are introduced because of the strong (and intrinsic as we believe) similarity of their behaviors to those in hard spheres systems.

In 1957, Alder and Wainwright, and Wood and Jacobson reported simulations of two dimensional systems with hard disks by, respectively, a Molecular Dynamics (MD) simulation, and the Monte Carlo simulation (MC)[1]. As well as the work on the energy relaxation of a non-linear lattice system by Fermi, Pasta and Ulam[2], these works were starting points of computational studies of physics. In 1962, Alder and Wainwright reported the liquid-solid phase transition which was observed in the MD simulation of a two dimensional system with 870 hard disks along an isotherm[3]. Today, this transition is called Alder transition. In this simulation, the density versus pressure curve includes a 'loop' like the curve described by Van der Waals equation (so-called Van der Waals loop. Fig.2-1), rather than a jump in density which one would expect for an infinite system. They concluded from their observation of such a loop that this liquid-solid phase transition is the first order phase transition. They also observed the particle trajectories in the transition region, and displayed liquid-like and solid-like regions which became an evidence of solid-liquid coexistence (Fig.2-2 (a)). This belief was strengthened by Hoover and Ree who calculated the entropy of the solid-like state by the constrained cell method[4]. Other various particles with repulsive potentials displayed almost the same transitions e.g., r^{-12}[11], and Heltziam contact law[13]. Moreover, liquid-solid, gas-liquid, and gas-solid phase transition and the tri-critical point were observed in the system with Lennard-Jones particles which included also attractive potential [12].

In three dimensional systems, the phase transition from the solid state to the liquid state (melting) has been believed to be the first order phase transition[5, 6]. For two dimensional system, however, Kosterlitz and Thouless, Halperin and Nelson, and Young questioned this belief and proposed a theory, called KTHNY theory, derived from the discussions about behaviors of dislocations and disclinations[6]. This theory provided a melting scenario involving two second order phase transitions and the intermediate hexatic phase between the solid state and the liquid state[6, 7]. In this phase, the system is divided into some hexagonal domains by the grain boundaries which are made up of arrays of dislocations (Fig.2-2 (b)). Such an intermediate phase is actually observed in the two dimensional XY spin model at low temperature[8]. Strandburg reported a detailed

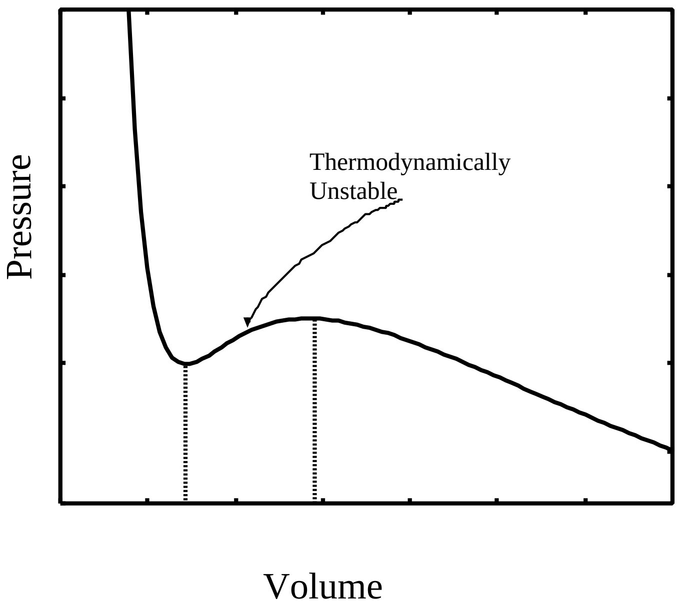

Figure 2.1: Loop of Van del Waals equation with low temperature.

review of this theory and related experiments and simulation results[9]. Configurations of the solid have the long-range bond-orientational order, and those of the liquid have the very short (exponentially decaying) bond-orientational order. KTHNY theory predicted that algebraic decay is realized in the intermediate hexatic phase. However, few clear evidences that such an intermediate hexatic phase appears instead of the coexistence of the solid and the liquid, have been demonstrated in simulations[10, 13]. Now, most of simulation results support that the melting of two dimensional systems with many spheres is the first order phase transition. Some of them also reported that the density gap between the solid state and the liquid state is much smaller than has long been believed[10]. However, some problems for these simulations, e.g., effects of finite system size, simulation time, boundary condition, etc., are still in discussion. In order to clarify the order of this transition, many simulations have been performed until now.

In order to discuss the liquid-solid phase transition of hard disks, a roughly approximated model called Correlated cell model was proposed[17]. In this model, single particle interacts, through elastic hard collisions, with scatters which are fixed on the sites of a two dimensional periodic lattice. The basic idea of this model is that the liquid-solid phase transition can be understood as a consequence of the cooperative motion of neighboring particles. In this model, it is assumed that periodically situated particles are moving with spatially uniform velocity through the periodically fixed scatters (Fig.2-3). Then, this

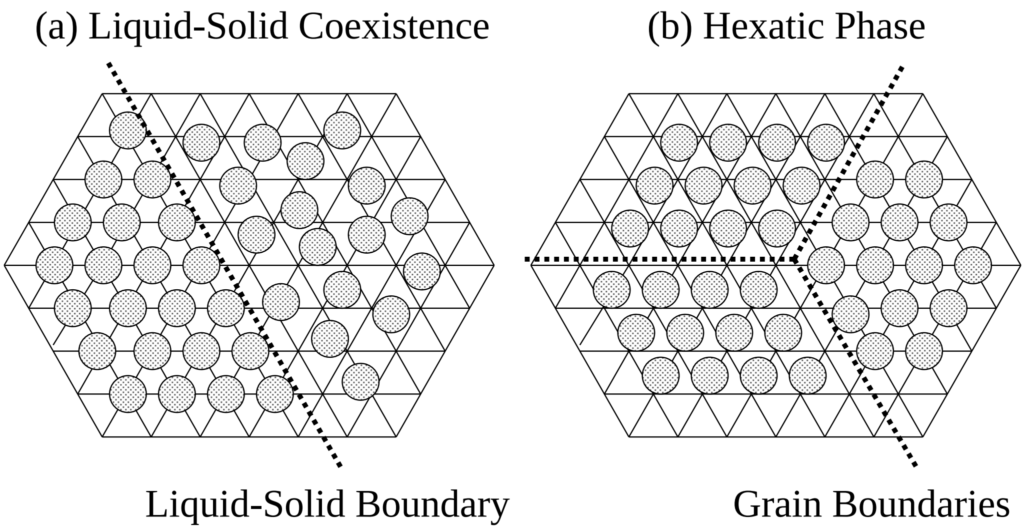

Figure 2.2: Particles configuration in (a) liquid-solid coexistence state and (b) hexatic phase.

system can be considered as the one body system, which is almost equivalent to Sinai Billiard[24]. In this system, the partition function can be calculated easily and the Van del Waals loop and a second order cusp are obtained[17]. Speedy focused on the other simplified situations in which a system consists of two hard disks in a two dimensional square region[20]. Under periodic boundary condition, this system is actually a one body system which is almost equivalent to the Correlated cell model. So, the Van der Waals loop and the second order cusps were observed. On the contrary, this loop and cusps disappear when two particles are confined in a square box with four rigid walls. Speedy concludes that the transition is the third order phase transition, and he regarded the transition as the 'glass transition'.

The applicability discussed in this section is not limited to the atomic scale nor to monodisperse particles. The influences of size polydispersity on the Alder transition has been investigated. First, this problem was discussed in colloidal dispersions[18]. In this discussion, the existence of the critical polydispersity beyond which the liquid state and the solid state merge was reported. By a MD simulation of particles which obey the Heltzian contact law, the same results were obtained[13]. In this simulation, the liquid branch of the density versus pressure curve was shown universal. The solid branch and coexist region change and the latter vanishes above a critical polydispersity. These phenomena are independent of characters of size dispersion like uniform, triangular, Gaussian, and binary dispersion. From the theoretical aspect, the critical polydispersity was calculated

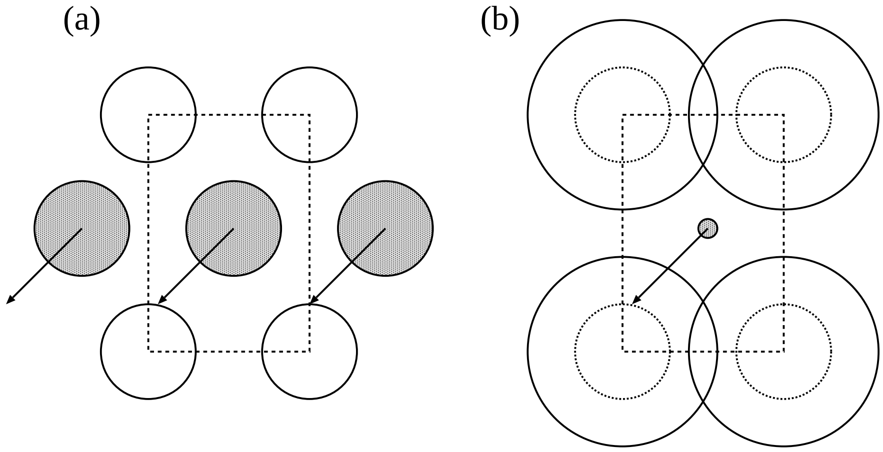

Figure 2.3: Geometry of the correlated cell model.

from the Density Functional Theory[19]. As will be mentioned in the next paragraph, the disappearance of the Van der Waals loop is one of the typical characteristic of the occurrence of the 'glass transition'.

In the previous two paragraphs, a term 'glass' appeared. Recently, so many reports for the glass have been published. Here, we look the brief outline of phenomena related to the glass transition. If liquid is cooled or compressed enough quickly, not quasi-statically, and paths through the solidification point, it enters the super-cooled liquid state, bypassing the crystallization[21, 22, 23, 24](Fig.2-4). If the quick cooling or compression is continued further, the system enters a state so-called the glass state. This phenomenon is called the 'glass transition'. This glass transition is a morphological transition of the system from the liquid to the non-crystalline solid, where the glass transition point, i.e. transition temperature, transition volume, etc., depends on the history, the speed of cooling or compressing, etc., unlike the liquid-solid phase transition point (see Fig. 2.4). The correlation of fluctuations of typical values of super-cooled liquid has a long relaxation time compared to those of a solid or a liquid. In super-cooled liquid, the following two types of relaxation processes are observed; i) β relaxation which appears in the earlier stage of this relaxation process, ii) α relaxation which is the longest relaxation in these processes[21, 22, 23]. After the system enters the glass state, the relaxation cannot be observed in finite obsevation time, which means, in a sense, the relaxation time becomes infinite. Still, the glass state looks stationary but is a non-equilibrium state which continues the relaxation in a strict meaning. Upon the entrance into the surpercooled liquid from the normal liquid state, thermodynamical values change smoothly which situation is

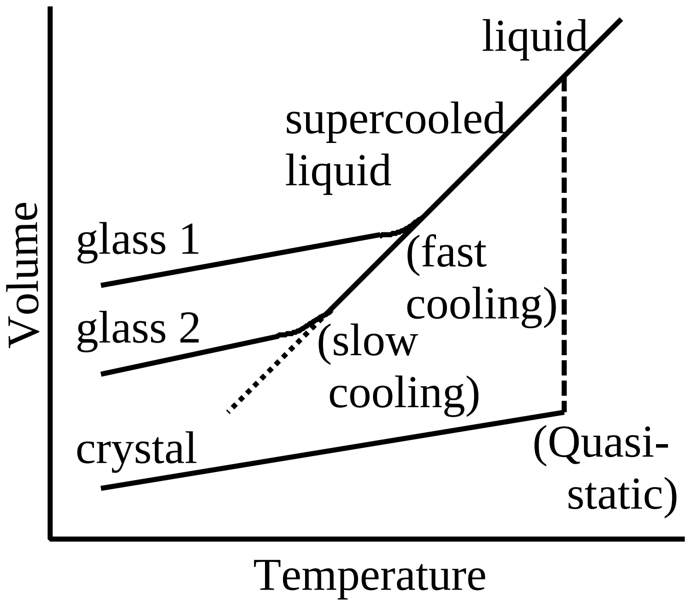

Figure 2.4: Relation between liquid, crystal, super-cooled liquid and glass.

different from the liquid-solid dicontinuous (first order) phase transition[22]. Actually in supercooled liquid states, and even in glass states, the observed spatial configurations are much more similar to those of liquid states than those of solid states. As getting closer to the glass transition point, however, the viscosity increases drastically[21]. Moreover, at the glass transition point, several quantities such as specific heat, compresivility, etc., also have singularities. Then, glass transition is considered as not a thermodynamical phase transition but the dynamical phase transition. The mechanism of such complex behaviors of the glass state and glass transition has been intensively investigated for these thirty years. Some theoretical models[15, 23, 25], some theories like Mode Coupling Theory[28], and so on, have been proposed and many MD simulations and Monte Carlo simulations have been performed[23, 24, 25, 26].

2.2 Structure Formations and Hysteresis of Granular Materials

The dynamics of granular materials has attracted much attention as not only that of typical and the simplest many body dissipative system in non-equilibrium state but also from industrial motivations[32, 33, 34]. Here, the term 'granular materials' indicates, for example, the sugar baking powder, sand or rock, sometimes a group of lesser planets, etc.. The discreteness of particles allows the granular materials to be fluidized, to exhibit fluid-like behaviors similar to hard spheres system. However, macroscopic characters of particles make the behaviors of fluidized granular materials to be extremely complex compared to those of usual fluids[32, 33, 34, 35]. Unlike usual molecular systems which are modeled as hard spheres systems, granular materials are dissipative. This indicates that the kinetic energy of the system decreases with time when no external force is added. Then, the system shows peculiar spatial patterns of density fluctuation[36, 34] even if we set an initial condition such that particles are distributed homogeneously with random velocities. In most of situations we consider, granular materials are held together mainly by gravity. So, if we leave granular materials in a vessel, particles settle on the bottom of vessel and nothing happens. In order to fluidize the system to observe the dynamics of granular materials, the energy injection is required.

One of the most popular experimental situation is that granular materials are shaken on a plate vibrating in vertical direction (Fig.2-5 (a))[38] $\sim$ [53, 104, 105, 106, 107]. The system in such situations are called Granular Vibrating Bed. If shallow granular layers are put on a vibrating plate, we can observe standing waves on the surface. It is remarkable that these standing waves create various cellular patterns or spiral patterns according to the change of the amplitude and the frequency of the vibration[38]. These phenomena of the granular vibrating bed have been reproduced by, for example, the DEM (distinct elements method[42]) simulations[39, 40] and phenomenological models[41]. When a granular bed with enough depth is strongly excited, we can observe the formation of a granular pile and a pair convection rolls inside the pile (Fig.2-5 (b))[37, 43, 44, 105]. In this case, it is observed that most of particles form a solid-like structure in bulk and only particles along side walls flow down to the bottom[43, 44]. Hence, characters of this convection are qualitatively different from those of Rayleigh Bernard convection in the real fluid. Moreover, we can observe another mode of convection, wherein particles move upward along side walls and downward in the middle if we add the stronger excitation(Fig.2-5 (c)). On the other hand, the multi-roll structure like Bernard convection is also observed when granular materials are excited more strongly in a wider vessel(Fig.2-5 (d))[45, 46, 47]. In the last situation, because most of particles are strongly fluidized, many characters of the system are similar to that of the real fluid. However, the number of rolls depends not only on the aspect ratio of the vessel but also on the strength of the excitation unlike the Bernard convection. The pair rolls structure of granular vibrating bed has been reproduced with the DEM simulations[43, 44, 47], stochastic model[52], phenomenological fluid models[53], etc.. On the contrary, the study of the production of multi-roll structure has not been advanced except a few performances of DEM simulations[46, 47].

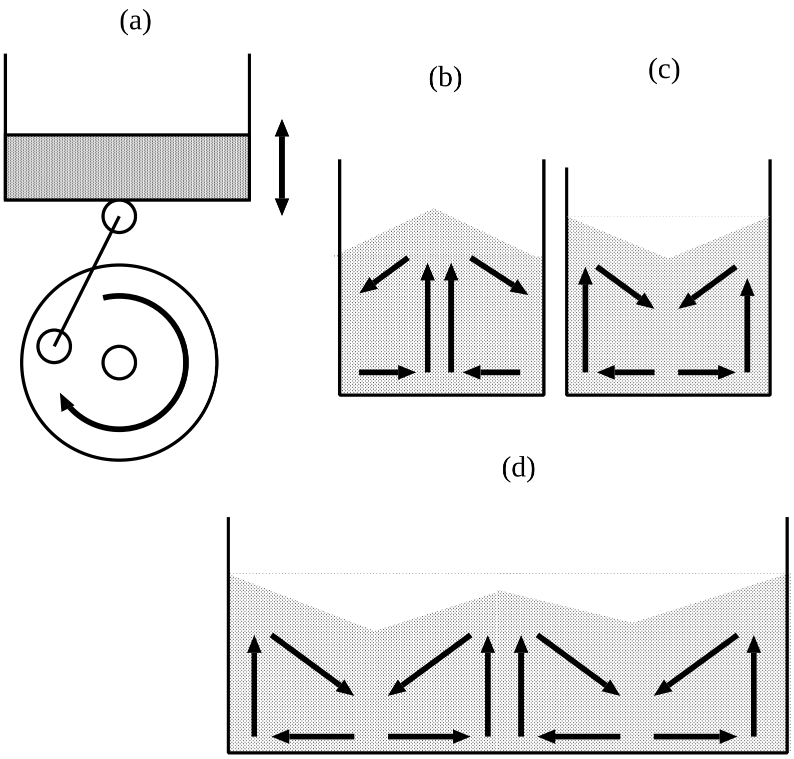

Figure 2.5: Illustration of vibrating bed((a)) and observed convections ((b)(c)(d)).

In the granular vibrating bed, two parameters, frequency and amplitude, are chosen to control the strength of the excitation. For the simplicity of the control, the system with a heat bath, instead of a vibrating plate, has been proposed for numerical simulation[54, 55, 56]. One of the essential advantages of this system is that we should consider only one parameter, temperature, which has no external time scales like the frequency. Here, the term 'temperature' is a tentative expression which indicates the strength of the excitation of particles by the energy source. With a simulation, the possibility of the hydrodynamic description of the behavior of one-dimensional situation was discussed, with a conclusion which indicated it is impossible[54]. Isobe et.al. simulated a two-dimensional case of this system with weak gravities[56]. They discussed transitions from the condensed granular state to the granular turbulence, and the statistical and hydrodynamic characters for each states. Some of results of this two-dimensional simulation reproduced the experimental observations in granular vibrating bed under weak gravity[57].

Mainly from the technological point of view, the system called Granular Fluidized Beds has been studied. Fluidized beds consist of granular materials confined in a high vessel, where fluid flow is injected from the source at the bottom. In experiments, the following states were realized by changing the flow rate of fluid from the source[35]. At low flow rate, particles rest at the bottom. When the flow rate exceed a critical value, particles start moving. This fluidized state consists of some phases, for instance, the homogeneous phase, the bubbling phase(Fig.2-6 (a)), the channeling phase, etc.. In the bubbling phase, pair convection rolls which consist of particles and fluid are observed in void regions. If the vessel is slim or the flow rate is larger, the slugging phase is realized(Fig.2-6 (b)). In order to discuss these phenomena, several two fluid models have been proposed in which the dynamics of particles was regarded as that of fluid[32, 60, 61]. The bubbling and the slugging were reproduced in these models. These two fluid models also have advantages in analytical treatments. However, the way to describe the mass of distinct particles as a continuum has not been established. Besides some ad hoc assumptions have been needed in order to describe the dynamics using these models. On the other hand, the direct simulation by modifying the Stokesian Dynamics was performed[63, 64]. In this simulation, hydrodynamic interactions between particles were seriously considered, and the slugging phase, the bubbling phase and the channeling phase were reproduced. Moreover, they predicted the existence of a kind of the fluctuation-dissipation relation among the diffusion of particles, the effective temperature, and the effective viscosity[64]. However, this method is associated by a serious problem that the amount of calculation to simulate a system with large number of particles is extremely large. Instead, in order

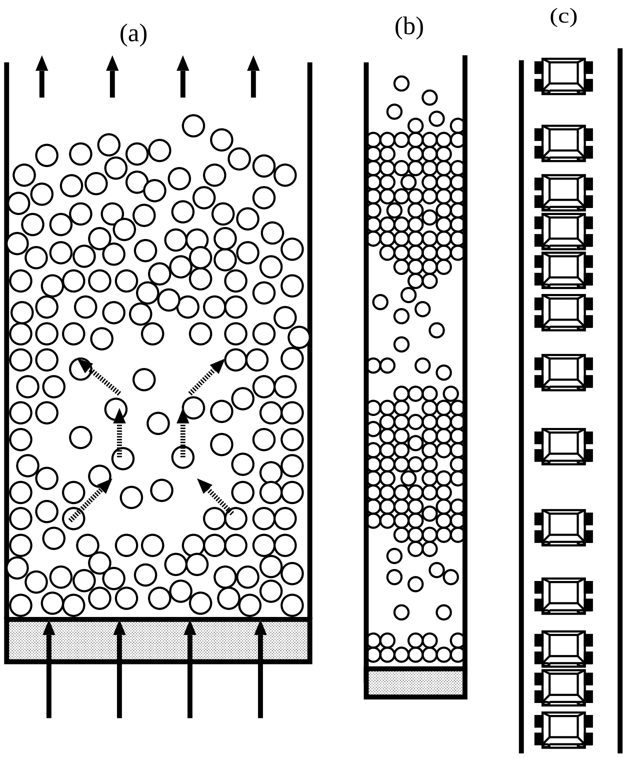

Figure 2.6: (a)Bubbling in fluidized bed, (b)slugging in a slim pipe, and (c)traffic jam.

to simulate the fluidized bed, a model which is modified from DEM with simplified hydrodynamic interactions has been often used[70]. This model was so much simplified as to lack some important terms of hydrodynamic interactions. Nonetheless, the bubbling could be observed in such a simplified model.

The interaction between fluids and granular materials plays a important roll also in much larger scale structure like desert dunes[133, 135]. Dunes seem to be the largest structures which consist of granular materials. According to the amount of available sand height and the temporal variation of wind directions, several forms of dune such as barchan dune, seif dune, star dune, etc. are reproduced[135].

The slugging is observed also in the situation that granular materials are poured from the top of a long slim pipe filled with fluid (air or water) with no injection from the bottom unlike fluidized bed (Fig.2-6 (b))[66, 88]. The appearance of the slugging phase in this situation is considered the same as that of the jamming phase of traffic flow on a high way(Fig.2-6 (c))[65, 67, 68, 69, 70]. In these systems, the phase transition from the free flow state to the slug (jam) flow state is observed with increasing the density of particles (cars). Moreover, a power low in the power spectra in the flow of particles (cars) is observed near the transition point[65, 66, 88]. In most cases, these systems have been regarded as one dimensional systems. So, many kinds of one dimensional models of the granular pipe flow and the traffic flow have been proposed[71]-[97]. As with the fluidized bed, hydrodynamic models[84] and the distinct particles (cars) models have been proposed[82, 97, 88, 89]. Most of traffic flow models define the optimal velocity determined by the local density of cars or the distance between a car and the preceding one, and assume that the force proportional to the difference between cars' velocity and the optimal velocity works on each car. In the case of granular flow, optimal velocity is determined from the considerations of hydro-dynamical interactions between particles[88]. The jam formation in these model systems under the periodic boundary condition have been studied analytically by the perturbative treatment of solitons and by more generalized ways. [85, 88, 89, 90, 94]. In one of these discussions, the exponent of power low in power spectra in the flow of particles was also determined by adding noise which is considered as the effect of the overtaking[89]. Moreover, in some cases, rigorous soliton type solutions were found for the jamming flow[92, 93]. From another point of view, a particles model with open boundary was studied[95] which study pointed out the necessity of the analysis for convective instabilities of each state in order to discuss a real particles flow system including, at least, an entrance and an exit. Differently from methods with differential equations, other models using the cellular automaton or the coupled map, have also been proposed in order to discuss these systems of particles flow[71][80]∼[97]. Other than the above studies, the transition from the free flow state to the jam flow state and the power low in the power spectra in the flow of particles had been reproduced earlier[75, 73, 86]. Recently, mathematical structures of cellular automaton models have been discussed and been related to equations with soliton solutions by the ultradiscrete method[97]. One of the advantages of these cellular automaton models is that we can easily extend a simple model to a more complex traffic flow model (multi lanes, traffic flow in cities, etc.), or to some systems other than the real traffic flow (Internet traffic, etc.)[91, 98]-[101, 102].

In section 2.1, we introduced the effects of size polydispersity on the Alder transition in hard spheres systems. Such size polydispersity causes several interesting phenomena also in the granular system as follows. When we shake or flow the mixtures of granular particles of different sizes, large particles and small particles usually separate spontaneously with each other[103]-[122]. This size segregation is one of the characteristic phenomena in granular materials. When we shake the granular mixture in a vessel, small particles tend to come down to the bottom and the large particles distribute above the bed of small particles[103]. (Dependences on the form of vessel, characters of friction and form of each particle, however, different types of the distribution of shaken granular mixtures have also been observed[104, 105, 106, 107].) On the other hand, we can see interesting patterns with size segregation when we pour polydisperse particles from upward to make a pile[108, 109], or put these mixtures in a horizontally rotating drum[112]∼[122]. When a pile is formed by toppling bi-disperse particles from a point, two types of separation patterns are realized as follows[108]. When the angle of repose[1] of large particles is smaller than that of small ones, large particles accumulate at the bottom and small particles accumulate at the upper part of the pile(Fig.2-7 (a)). This angle depends on the form and the frictional coefficient of each particles. On the other hand, when the angle of repose of large particles is larger than that of small ones, large and small particles segregate to form stripes which are parallel to the slope of pile(Fig.2-7 (b)). It is remarkable that these phenomena can be reproduced by a very simple cellular automaton model in which only the friction between large-large, small-large and small-small pairs of particles are accounted. On the other hand, mixtures of granular materials which are partially-filled in horizontally rotating drum realize the following two types of segregation patterns depending on the duration of rotation[112, 113]. At first, the radially segregated pattern appears where large particles accumulate near the walls of drum and small particles accumulate to the central region around the rotating axis(Fig.2-7 (c)). When the drum is rotated further, axially segregated pattern appears where the system evolves to form alternating bands one of which is rich in small particles and the other is rich in large particles(Fig.2-7 (d)). For these phenomena, by a DEM model and a very simple cellular automaton model, spatio-temporal evolutions were simulated in good agreement with the experimental results[115, 114]. These pattern formations were found to be described by an almost same mathematical model with Cahn-Hilliard equation which is known to model the phase separation process of binary alloys [113, 116]. Moreover, in the granular system with mono-disperse particles on a vibrating plate, a loop like the Van der Waals loop was observed in the relation between packing fraction and pressure[123]. As with the hard spheres system, in which interactions between particles cause no dissipation, this loop disappears above a critical polydispersity[123].

The statics of solid-like state of granular materials is also complex. In some cases, history dependency plays important roles. Frictions in granular layers, too, is an important subject not only of fundamental physics but also of the physics of earthquakes[126]. Recently, Nasuno and his coworkers considered an experiment on the friction of granular materials and its historical dependencies under the following simple situation[127]. Place

[1] The angle of repose of each particle is defined as the maximum angle of slope that the same size of particles can sustain.

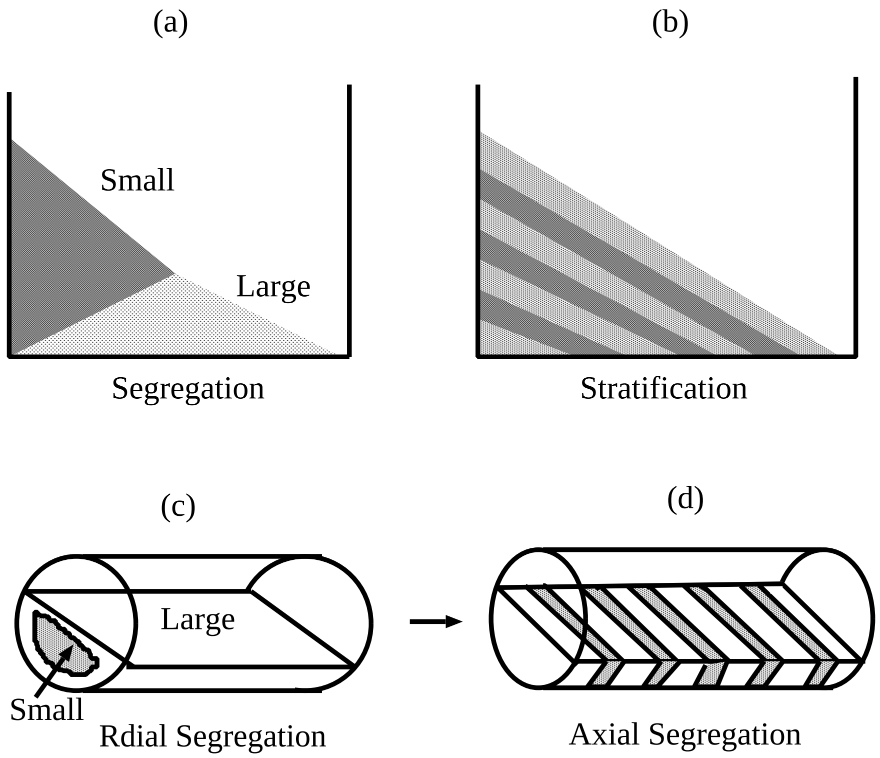

Figure 2.7: Segregation patterns (a)(b)in the pile, and (c)(d)in a horizontally rotating drum

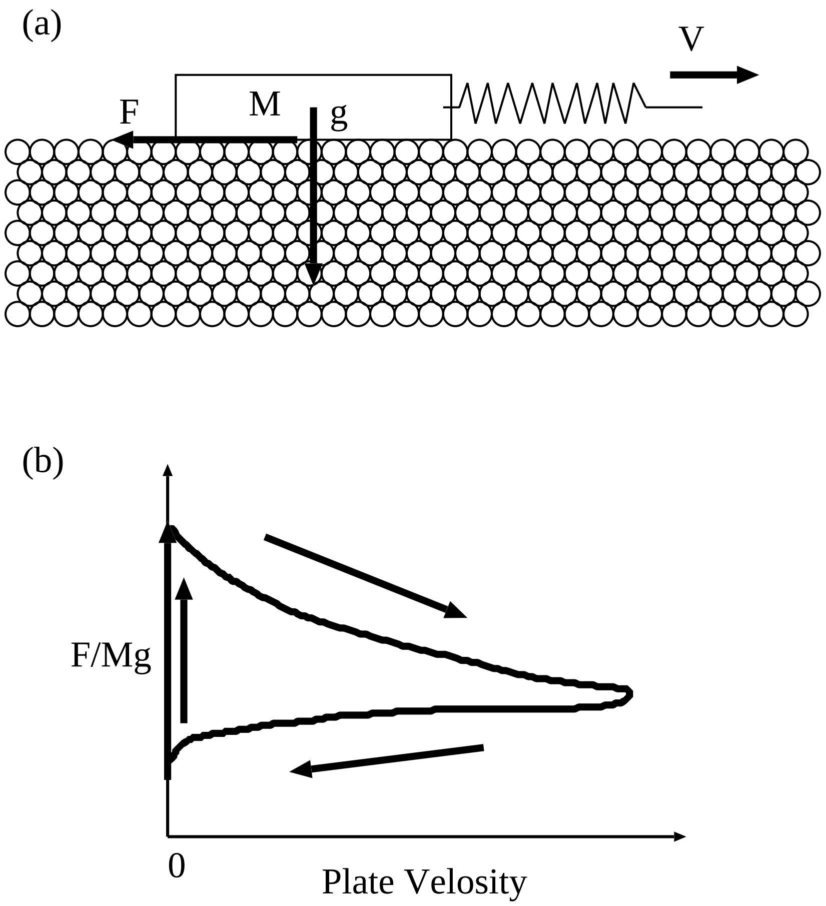

Figure 2.8: (a)Illustration of the experimental setup of granular frictions, and (b)Illustration of the observed hysteresis loop.

a plate with a spring on granular materials, and push (or pull) the spring at a constant speed in the horizontal direction (Fig. 2.8(a)). When the pushing speed is sufficiently low, we can see the stick-slip motion of the plate, while at high speeds, we can see a steady sliding of the plate. Similar phenomena have been observed even in the frictional dynamics of the paper-on-paper system and melt fractures in polymers[125, 128, 129]. Frictions of solid-on-solid system has been believed to satisfy the Coulomb-Amontons's laws as follows[125]; I)The magnitude of the friction is independent of the contact area between two objects. II)The magnitude of the friction is proportional to the normal reaction. III)The maximum static friction coefficient is larger than the dynamic friction, and the dynamic friction is constant independent of the sliding velocity. However, from sensitive measurements of frictional forces, Nasuno et.al found that the dynamic friction on granular layers is multi-valued and exhibit a hysteresis; The frictional force is less for decreasing than for increasing velocities[127] (Fig. 2.8(b)). A rough description of this hysteresis loop between the plate velocity and the frictional force is following. When the plate is pushed continuously but is sticked to the granular layer, the static friction working on this plate increases. When the plate starts to slip, the magnitude of the frictional force decreases as the plate velocity increases. However, the magnitude of the frictional force is almost constant while the plate velocity is decreasing until it stops again. Hayakawa proposed a simple phenomenological model which is modified from the phenomenological model proposed by Calson and Batista[131, 132]. His model reproduced some characteristic results in stick slip motion such as the hysteresis loop. However, a few unclear points, the definition of an order parameter etc., remain in this model. DEM simulations were also performed[130] to discuss these points[131]. It was remarkable that such a hysteresis was also observed at the relation between the velocity profile of the wind flow on sand[136].

Like the granular frictions, the pressure distribution of the granular materials also has the history dependencies. Now, we focus on the vertical pressure distribution along the bottom of granular pile. One usually expects the pressure has the global maximum near the center of the bottom. In some experiments, however, a local minimum point often appears near the center of the bottom. Such a minimum is called a dip. One of recent experimental investigations reported that the appearance of this dip depends on the history of the pile formation as follows[137]. The piles are formed either by toppling granular particles from a point source, or from a horizontally extended homogeneous source like rain. The pressure profiles resulting from localized source inputs have a clear dip while the results from homogeneous rain show no dip. The dip was reproduced in some simulations: the simulation of frictionless particles model, the Monte-Carlo simulation of force network, and the simulation of polygonal particles, etc.[138, 139, 140]. However, the relation between the history and the internal stress is still unclear because we have no effective method for universal treatments of system's history. In order to discuss this problem, also the character around the surface of the pile, velocity distribution of flowing or slowly moving particles, etc., are expected to be important[141, 142].

Chapter 3

Liquid-Solid Phase Transition of the System with Two Particles in a Rectangular Box

Abstract: In this chapter, we study the statistical properties of two hard spheres in a two dimensional rectangular box. In this system, the relation like Van der Waals equation is obtained between the width of the box and the pressure working on side walls. The auto-correlation function of each particle's position is calculated numerically. By this calculation near the critical width, the relaxation time until the correlation become zero gets longer according to the increase of the height of the box. Moreover, fast and slow relaxation processes like α and β relaxations observed in super cooled liquid are realized when the height of the box is sufficiently large. These relaxation processes are discussed with the probability distribution of relative position of two particles.

3.1 Introduction

Liquid-solid phase transition is one of the most familiar phenomena for us. This transition of a system with so many degrees of freedom has been studied through many kinds of analytical models and numerical models[14]. Among numerical studies, the liquid-solid phase transition is observed in systems containing $10^{1\sim4}$ hard or soft core particles by Monte-Calro simulation and Molecular Dynamics simulation[1, 3, 10, 12, 13]. The motions of individual particles (moleculars) are different between in the liquid phase and in the solid phase. In the former phase, particles can exchange their own positions one another, and each particle can wander all around the system. On the other hand, in the latter phase, particles cannot exchange their own positions, and they move only restricted small areas.

Now we consider a rectangular box containing two hard spheres with same diameter d. The height of the box is larger than $2d$. When the width of the box is larger than $2d$, these spheres can exchange their own positions (Fig.3.1 (a)). However, these particles cannot exchange their positions when the width of box is smaller than $2d$ (Fig.3.1 (b)). From these facts, we regard the former state and the latter state as the simplest forms of, respectively, the liquid state and the solid state. Then, a problem arises; In such a simple system near the critical width ($= 2d$) of the box, can we find characteristic phenomena like Alder transition[3, 10, 13] of the system with many hard spheres ? In this chapter, to understand this problem, we focus on statistical and dynamical properties of the spheres near the critical width of the box.

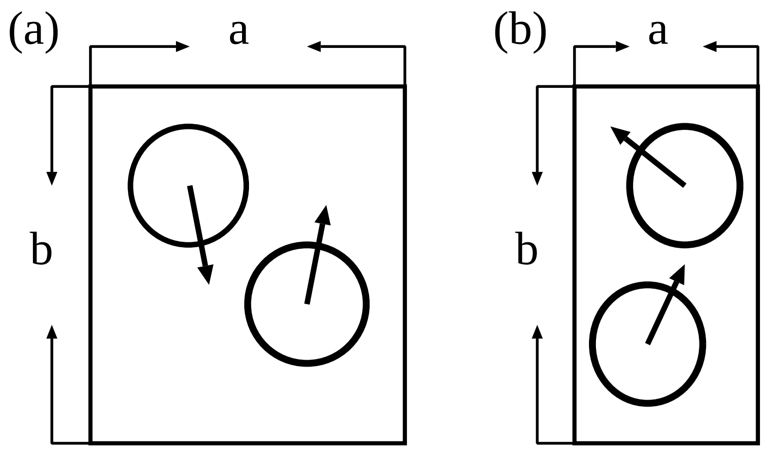

Figure 3.1: Illustration of two particles system in rectangular box. (a)Width of box is larger than sum of two diameters (Liquid state), and (b)width of box is smaller than sum of two diameters (solid state).

3.2 Simulation of two particles in a rectangular box

The system of our consideration consists of two dimensional hard sphere particles with unit mass and unit radius which are confined in a two-dimensional rectangular box. Here, the width and the height of the box are respectively a and b, and all the walls are rigid (Fig.3.1). The interactions between two particles and between a particle and a wall are realized only through hard core collisions. These tasks are implemented in the following manner; the tangential velocities to the collision plane are preserved, while the normal component of relative velocity Δv_n changes into $-\Delta v_n$. The total energy of this system is given as 1. Since this system consists of rigid spheres and rigid walls, the qualitative behaviors are independent of the total energy. We set $b > 4$ for most of our discussions which means these two particles can exchange their positions in horizontal direction with each other. Note, in our discussions, the state with $a > 4$ is regarded as the liquid state and the state with $a < 4$ is regarded as the solid state.

Figure 3.2 (a) and (b) are typical relations between the width a and the pressure P_a which works on side walls for each height $b = 4.3 \sim 6.7$. Here, P_a is defined as the time average of the impulses caused by the bouncing of particles on side walls per unit length per unit time. In these figures, the region of a, in which the volume compressibility is negative, appears for small b around the critical width $a^* = 4.0$. These curvatures are similar to the Van der Waals loop[14] or the loop of Alder transition[3, 10, 13] which includes the liquid-solid coexisting region. This negative volume compressibility seems to indicate the appearance of phase transition around the critical width $a^* = 4.0$ which distinguishes the solid state from the liquid state. If b becomes larger than a critical value $b^* \sim 6.0$, however, the form of this curvature is loosened, and the compressibility becomes positive for all a. In this case, we cannot observe the distinction between the liquid state and the solid state. Figure 3.2 (c) and (d) are typical relations between the width a and the pressure which works on upper and lower walls P_b for each height $b = 4.3 \sim 6.7$. Here, P_b is defined as the time average of the impulses caused by the bouncing of particles on upper and lower walls per unit length per unit time. Differently from the relation between a and P_a, P_b decrease monotonically with the increase of a. Such anisotropy seems one of the characteristic features of this system, which does not appear in the system with many hard spheres. If we focus only on the a-P_a relation, however, this system can be regarded as one of the simplest model to imitate the liquid-solid phase transition. Here, a and P_a correspond to, respectively, the volume and pressure of the system with many particles.

Now, we consider the counterpart of the above b in the system with many hard spheres

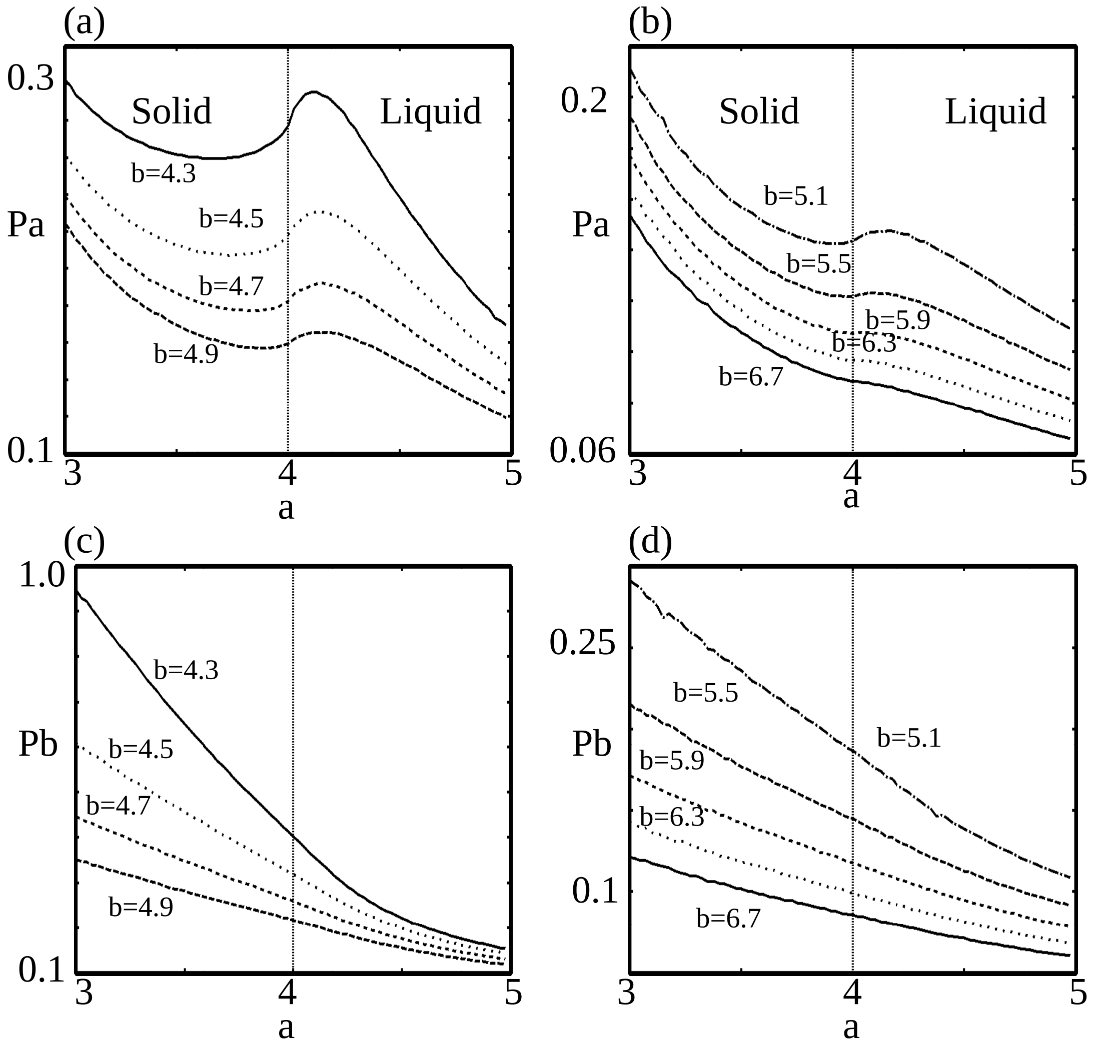

Figure 3.2: Relations between the width a and the pressure P_a with (a)$b = 4.3, 4.5, 4.7, 4.9$ (b) $b = 5.1, 5.5, 5.9, 6.3, 6.7$ in descending order, and that between the width a and the pressure P_b with (c)$b = 4.3, 4.5, 4.7, 4.9$ (d) $b = 5.1, 5.5, 5.9, 6.3, 6.7$.

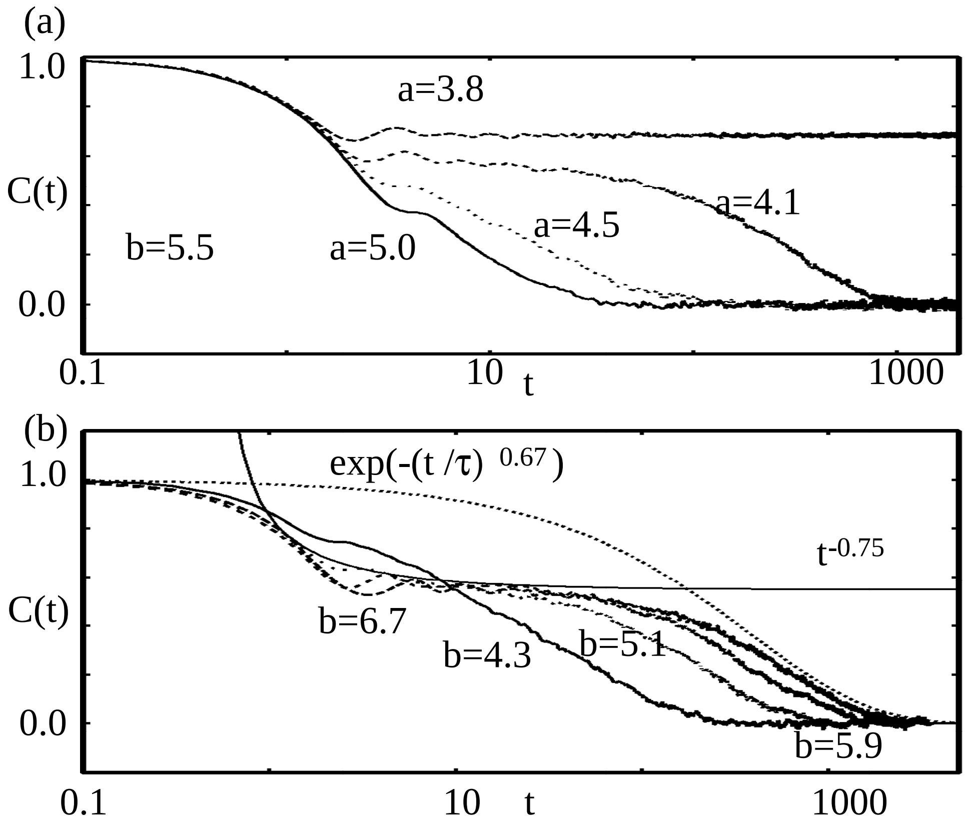

Figure 3.3: Auto-correlation function of each particle's position $C(t)$, respectively, (a)$a = 3.8, 4.1, 4.5, 5.0$ with $b = 5.5$, and (b)$b = 4.3, 5.1, 5.9, 6.7$ with $a = 4.1$. Fitting lines are $\sim t^{-0.75}$ and $\sim exp(-(t/\tau)^{0.67})$.

or in more general systems with many degrees of freedom. Figure 3.3 (a) is a typical auto-correlation functions of the position of each particle $C(t) =< \mathbf{x}(0)\mathbf{x}(t) > / < \mathbf{x}(0)\mathbf{x}(0) >$ in the solid state ($a = 3.8$) and liquid states ($a = 4.1$, $a = 4.5$, and $a = 5.0$ with $b = 5.5$). Here, $\mathbf{x}(t)$ is the position of a particle. In the liquid state, the relaxation process becomes slower as the width comes closer to the critical value. In the solid state ($a = 3.8$), the correlation function has a finite value for $t \to \infty$ because two particles cannot exchange their positions. Figure 3.3 (b) is the auto-correlation functions for $b = 4.3, 5.1, 5.9, 6.7$ near the critical width a^* ($a = 4.1$). These curvatures indicate that each relaxation process contains the fast and the slow relaxation processes for a little over the critical width. These fast and slow relaxations can be fitted with functions, respectively, $t^{-\beta}$ ($\beta \sim 0.75$) and $exp(-(\frac{t}{\tau})^{\alpha})$ ($\alpha \sim 0.67$, $\tau = constant$). By increasing b, the form of $C(t)$ changes as follows. i)The time at which the correlation becomes zero gets longer. ii)When b is larger than a critical value $b^{**} \sim 5.0$, the fast relaxation and the slow relaxation are separated clearly by the appearance of plateau. These relaxations are respectively similar to β and α relaxations of the density fluctuations in the super-cooled liquid[21, 22, 23]. The system which includes non-uniform molecules tends to become the super-cooled liquid state when it is cooled or compressed[21, 22, 23, 24, 25, 26]. Moreover, the liquid-solid coexisting region disappears in the system with many hard spheres when the size polydispersity of spheres is larger than a critical value[13]. From these facts, we expect that present two particles system imitates the phase transition of a system which consists of many non-uniform elements. Here, the quantity b corresponds to the dispersion of particles' characters like the size polydispersity in the system with many particles. In order to discuss the mechanism of above simulation results, we focus on the statistical properties of each particle's trajectory for each b near the width a^*.

3.3 Discussions from particles trajectories

Figure 3.4 (a), (b) and (c) are typical trajectories of centers of particles for, respectively, $b = 4.7$, $b = 5.7$ and $b = 6.7$ with $a = 4.1$. If the volume of the box is large enough and we can ignore the particles' volume, these trajectories fill the rectangular region which is enclosed by points $(\frac{a-d}{2}, \frac{b-d}{2})$, $(\frac{a-d}{2}, -\frac{b-d}{2})$, $(-\frac{a-d}{2}, \frac{b-d}{2})$ and $(-\frac{a-d}{2}, -\frac{b-d}{2})$ (Fig.3.4(c)). Here, d is the diameter of each particle which is set as 2 in our discussion. This means particles wander all around the box like ideal gas systems. When the size of box becomes small, however, the finite volume effect of particles become evident. Particularly, if the

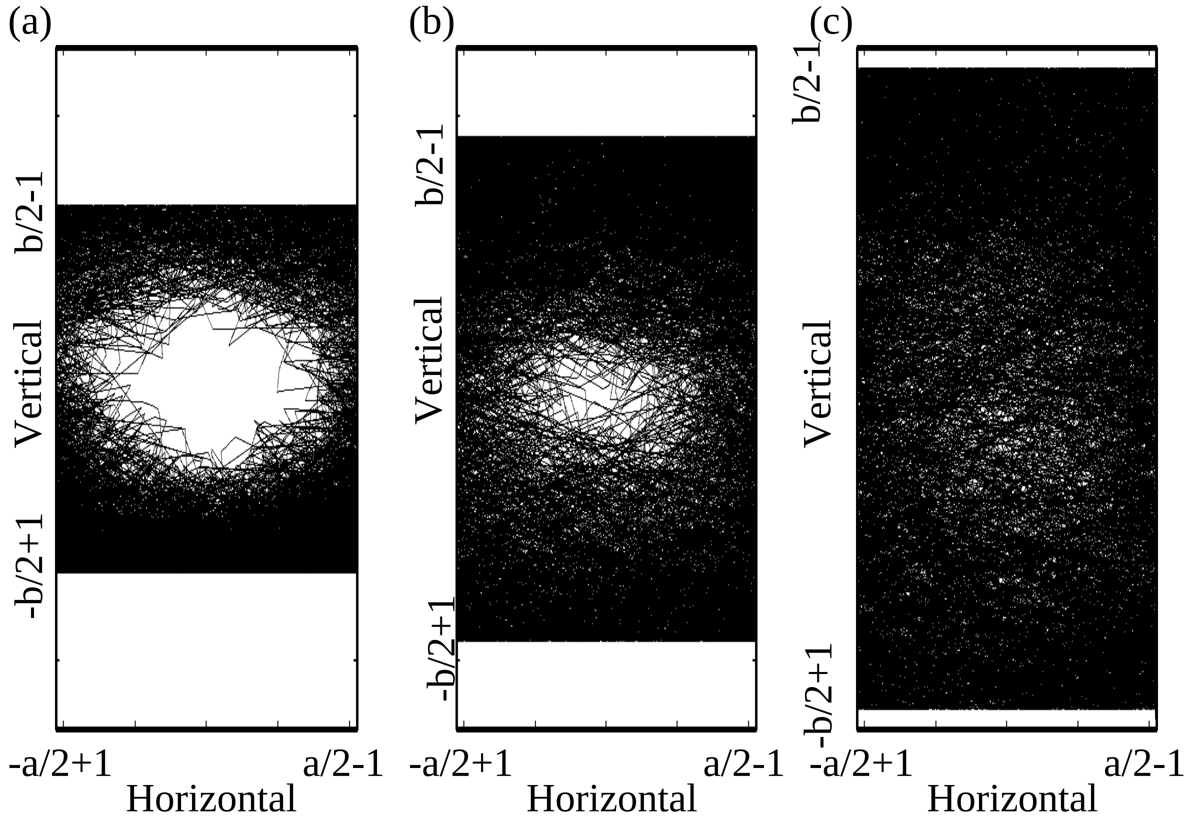

Figure 3.4: Typical trajectories of particles for, respectively, (a)$b = 4.7$, (b)$b = 5.7$ and (c)$b = 6.7$ with $a = 4.1$.

relation

$$(a-d)^2 + (b-d)^2 < (2d)^2 \tag{3.1}$$

is satisfied, a region appears around the central part of the box that particles' centers cannot enter. When $b < 2 + 2\sqrt{3}$ is satisfied, the above equation is satisfied around $a = a^* = 4$ and the trajectory of the center of particles is given like Fig.3.4 (a). This is also the case for $a < a^* = 4$ where the trajectory of the center of particle is given like Fig.3.4 (b) if $2+2\sqrt{3} < b < b^* = 6$. In these cases, each trajectory of the center of particle is similar to what is observed in Sinai billiard[24]. In order to discuss these situations, we consider the $(a-d) \times (b-d)$ rectangular Sinai billiard which includes a hard sphere with diameter d ($d = 2$). Like correlated cell model[17], we can calculate the a-P_a relation of Sinai billiard analytically. For each particle in Sinai billiard, the entropy S is given by $S = log(A_r(a,b)A_v)$ and free energy F is given as $F = U - S$. (Boltzmann constant k_B and temperature T are set as 1.) Here, $A_r(a,b)$ and A_v are phase space volumes of, respectively, real space and velocity space, and internal energy U is constant because this system consists of hard walls and a hard sphere. $A_r(a,b)$ is given as

$$A_r = (a-d)(b-d) - \frac{\pi}{4}d^2 \cdots (a > 4) \tag{3.2}$$

$$A_r = (a-d)(b-d) - (a-d)\frac{d}{2}\cos\theta - \frac{d^2}{2}\theta \cdots (a \leq 4) \tag{3.3}$$

where $\sin\theta = \frac{a-d}{d}$ and $d = 2$. Using the above relations together with $P_a b = -\frac{\partial F}{\partial a}$, a-P_a relation of the system for $b < 6$ is obtained, and we can observe the liquid-solid phase transition like Fig.3.5 (a). In this case, the width $a = a^* = 4$ is a singular point and this point gives the maximal pressure independent of b. On the other hand, however, the a-P_a relation in simulation results (Fig.3.2 (a) and (b)) have the inflection point near the critical width $a = a_* = 4$, and the form of each curve is smooth. In addition, we consider a square box system in which a and b are varied with $a = b$. This system satisfies $b < 2+2\sqrt{3}$ around $a \sim a^*$. In the same way of the calculation of above rectangular Sinai billiard, the a-P_a relation of the $(a-d) \times (a-d)$ square Sinai billiard can be obtained analytically. In this calculation, the profile of the a-P_a relation of the square Sinai billiard is obtained as the almost same one as the results of the rectangular billiard. However, it is remarkable that $P_a(= P_b)$ decreases monotonically with the increase of $a(= b)$ in the simulation of two particles in the square box (Fig.3.5 (b))[20].

Finally, we discuss the mechanism of the appearance of plateau in $C(t)$, the auto-correlation function of each particle's position, near the width $a = a^*$ considering statistical properties of particles' trajectories. Now, we define $Pro_{\delta x}$ and $Pro_{\delta y}$ as the probability

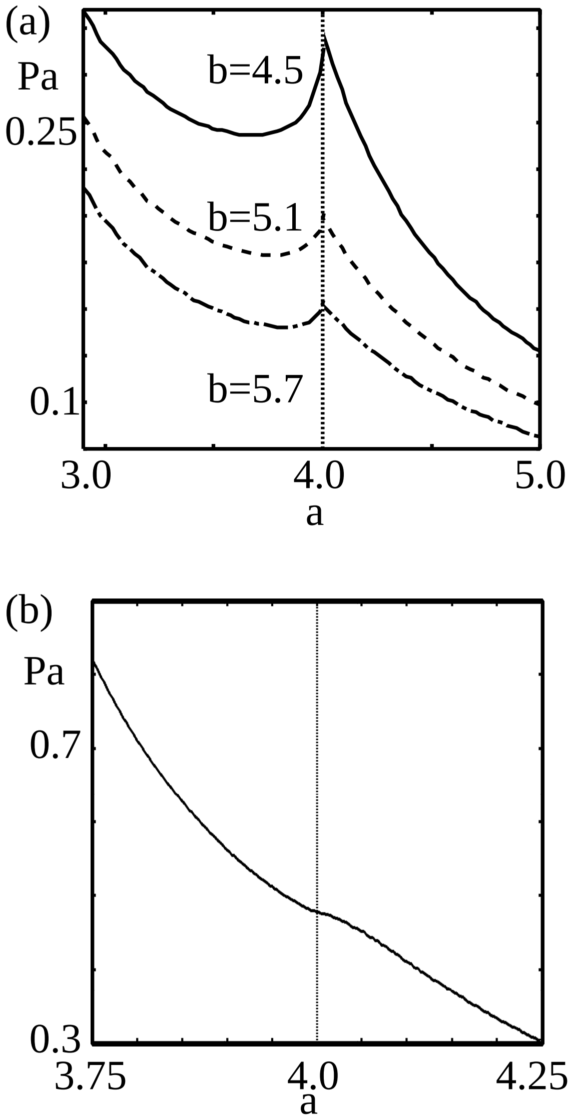

Figure 3.5: (a)a-P_a relations of rectangular Sinai billiard with $b = 4.5, 5.1$ and 5.7, and (b)a-P_a relations of two particles in square box.

distributions of δx and δy. Here, δx is horizontal component and δy is vertical component of relative position vector between centers of two particles. Figure 3.6 (a) and (b) are respectively δy-$Pro_{\delta y}$ relations and δx-$Pro_{\delta x}$ relations of the case $b = 4.3, 4.7, 5.1, 5.5, 5.9$ with $a = 4.1$. In Fig.3.6 (a), the maximum points of $Pro_{\delta y}$ are always far from the point $\delta y = 0$. In Fig.3.6 (b), however, the position of the maximum point of $Pro_{\delta x}$ depends on b. When b is small, the maximum points of $Pro_{\delta x}$ are far from the point $\delta x = 0$. This means that two particles tend to face each other on a diagonal line of box. By this tendency, it is rather easy for these two particles to exchange their positions both vertically and horizontally. Hence, the time at which $C(t)$ becomes 0 is relatively short. On the other hand, only one maximum point of $Pro_{\delta x}$ appears at $\delta x = 0$ when b is larger than the critical value $b^{**} \sim 5.0$. In this case, the height of box is enough large to change particle's positions almost freely but only in the horizontal direction. This is considered as the origin of fast relaxation in the simulation. This situation also means that two particles, in a statistical sense, tend to line up on a vertical line. In this case, the exchange of two particles' positions in vertical direction is cut across strongly. This fact originates the appearance of the plateau in $C(t)$, after which the slow relaxation starts.

3.4 Summary

In this chapter, liquid-solid phase transition and the long time correlation of two hard spheres confined in a two dimensional rectangular box is studied. Between the width of the box and the pressure at the side walls, the relation like Van der Waals equation is obtained. However, a finite range of the box width, in which the volume compressibility is negative, disappears when the height of this box passes through a critical value. The auto-correlation function of each particle's position is calculated near the critical width. According to the increase of the height of this box, the time at which this correlation become zero gets longer. Moreover, a fast relaxation and a slow relaxation are separated clearly by the appearance of plateau when the height of this box is sufficiently large. Thus, several characteristic natures of many particles systems with polydispersity are imitated in such an extremely simplified system. These relaxation processes are discussed considering the probability distribution of relative position of two particles. Still, for the relation between the width of the box and the pressure at the side walls, some discrepancies appear between the analytical and simulation results. Thus further consideration is required on the dynamical properties like the long time correlation. These topics seem to have strong relation with the slow dynamics in Hamiltonian dynamical systems[29]. In addition, the

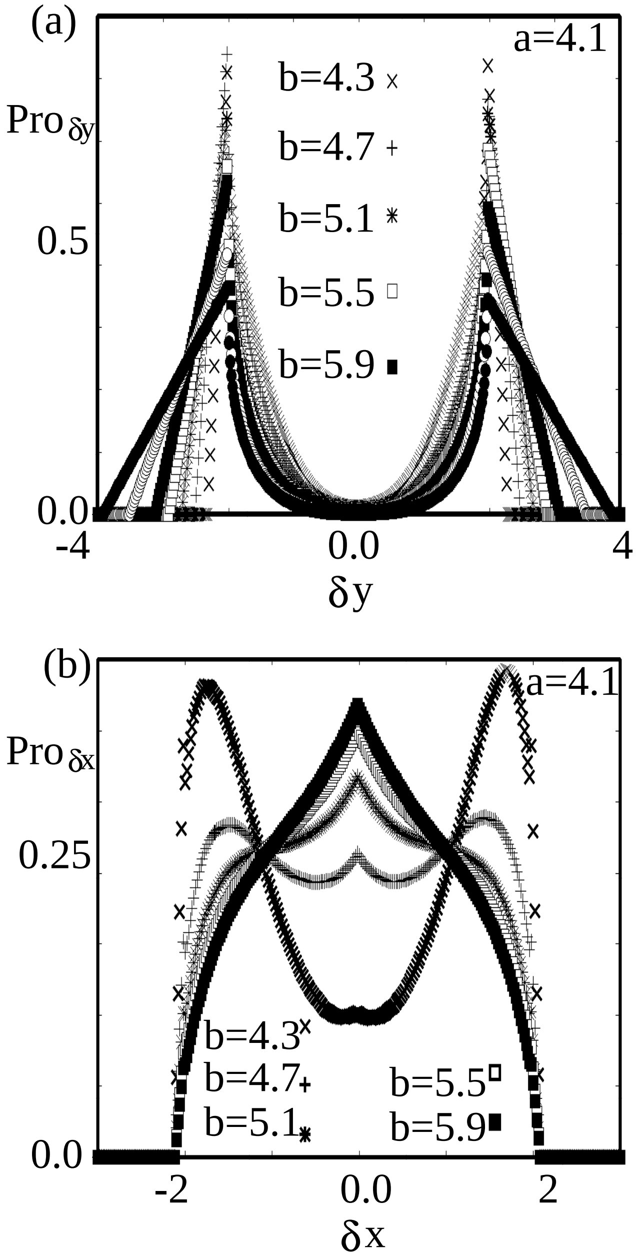

Figure 3.6: Probability distributions (a)$Pro_{\delta y}$ of vertical component of relative position vector δy, and (b)$Pro_{\delta x}$ of horizontal component of relative position vector δx between two particles with $a = 4.1$. $b = 4.3, 4.7, 5.1, 5.5$ and 5.9 from the bottom up near $\delta x = 0.0$ in (b).

pressure which works on walls is anisotropic in our system, while the pressure of the system with many particles is usually uniform. This also is a problems to be solved. Moreover, the understanding of the glass transition or the other non-equilibrium system[30] through our simple model is a future issue.

Chapter 4

Liquid-Solid Phase Transition and Change of Frictional Forces of the System with Two Particles in a Box

Abstract: In this chapter, the liquid-solid phase transition and the change of the frictional force of a system with two hard spheres in a two-dimensional rectangular box are discussed. Under controlling the pressure or the supply of energy from the wall, the solid-like state, the solid-liquid temporal coexistence state, and the liquid-like state are alternatively observed. The frictional force which works on particles and the mobility of the system are measured under the supply of the energy with an asymmetric external force. Characters of frictional forces for the 0 mobility state and that for the large mobility state are obtained like, respectively, that of the static and the dynamic frictions of solid-on-solid system. The strong temperature dependency is also observed in the profile of the relation between the above frictional force and the mobility. From above results, the relation between the friction and the velocity of a plate on granular layers which includes the hysteresis loop [S.Nasuno et al.,Phys. Rev. Lett **79** (1997) 949 et. al.] is discussed.

4.1 Introduction

The appearance of the static friction and the dynamic friction, and the change between them are familiar and important subjects of fundamental physics. They are universal phenomena which are usually observed at surfaces of macro-scale objects. From the microscopic point of view, the change between above two types of frictions is expected to have close relationship with the liquid-solid phase transition around surfaces[125, 128, 127, 131, 129]. Here, the liquid-solid phase transition in this case is caused by variances of external driving forces like shear forces, which means that this transition occurs under non-equilibrium states. By numerical simulations of systems containing $10^{1\sim4}$ hard or soft core particles, the liquid-solid phase transition with a Van der Waals loop was observed[1, 3, 10, 12, 13]. Very similar relations were observed also in the system with two hard spheres in a rectangular box (see chapter 3). Moreover, this system showed not only the solid-liquid phase transition but also the transition like glass transition with the appearance of α and β like relaxation and the disappearance of the Van der Waals loop. From these facts, we can expect that the appearances of above phase transitions are generically caused by the effect of the excluded volume independent of the number of associating particles. In this chapter, we try to discuss the appearance of the static and the dynamic frictions and the change between them through a simple model with a few modifications of that introduced in the previous chapter. First, phase transitions of the system under equilibrium and non-equilibrium states by controlling the supply of energy and the pressure in horizontal direction, are investigated. This controlled pressure corresponds to the normal reaction in the general treatment of friction. Based on these investigation, characteristic features of frictional forces in this system are discussed.

4.2 Two hard spheres system

The system of our considerations consists of two-dimensional hard sphere particles with unit mass and unit radius which are confined in a two-dimensional rectangular box (Fig. 4.1). The right wall with unit mass of the box can move in the horizontal direction. The position of the right wall is $X(t)$ ($X(t) > 2$) and the constant force $-f$ is working on this wall in the horizontal direction. The left wall is set at the origin of the horizontal axis and are connected to the energy source. The bottom of the box is set at the zero height of the vertical direction, and the position of the top of the box (the box height) is Y ($Y > 4$). All walls are rigid, and interactions between two particles, and, between a

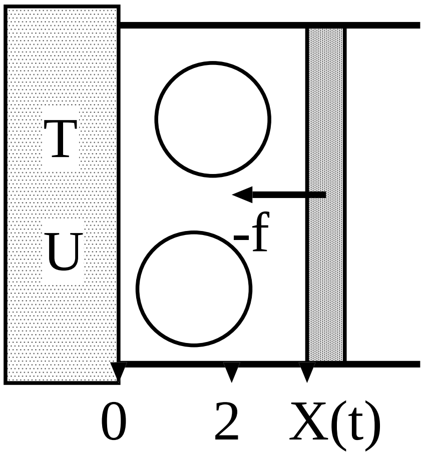

Figure 4.1: Illustration of two particles system in rectangular box with a moving wall (right) and energy sources (left)

particle and a wall without energy sources, are only through hard core collisions. These tasks are implemented in the following manner; the tangential velocities to the collision plane are preserved, while the normal component of relative velocity Δv_n changes into $-\Delta v_n$. A particle which hits the left wall connected to the energy source, with the velocity (v_h, v_v), will bounce back with the velocity (V_h, V_v) $(V_h > 0)$. Here, subscripts h and v indicate, respectively, the horizontal and the vertical direction. The velocity (V_h, V_v) is chosen ramdomly with the probability distributions $P_h(V_h)$ and $P_v(V_v)$ [31]

$$P_h(V_h) = T^{-1} V_h exp(-\frac{V_h^2}{2T}) \tag{4.1}$$

$$P_v(V_v) = (2\pi T)^{-\frac{1}{2}} exp(-\frac{(V_v - U)^2}{2T}) \tag{4.2}$$

where T is the temperature of the energy source. (We give the Boltzmann constant as 1.) The case with $U \neq 0$ means the asymmetric force working on the system from the energy source in vertical direction. We only consider the case of $Y > 4$ which means these two particles can exchange their positions in horizontal direction with each other. When $X(t) > 4$, these spheres can exchange their positions in vertical direction. On the contrary, these particles cannot exchange their positions in vertical direction when $X(t) < 4$. In the previous chapter, we fixed $X(t) = X$ and defined the state with $X > 4$ as the liquid state and that with $X < 4$ as the solid state. In this chapter, however, because we will treat probability distributions of $X(t)$ in the following discussions, we slightly modify definitions of these states as follows; The solid state is defined as the state in which the probability distribution of $X(t)$ has a peak at $X(t) < 4$, and the liquid state is defined as the state in which the distribution has a peak at $X(t) > 4$.

4.3 Liquid-solid phase transition with $U = 0$

First, we focus on the cases of $U = 0$ which are the same as the situation that a heat bath is connected to the left wall. Figure 4.2 is the probability distribution of the position of the right wall $X(t)$ for, respectively, when (a)$Y = 4.5$, (b)$Y = 5.0$, and (c)$Y = 5.5$ for typical values f under the same temperature T $(= 0.1)$. Independent of Y, each distribution has only one peak at $X(t) < 4$ for large value of f (solid state), or $X(t) > 4$ for small value of f (liquid state). For middle values of f, however, each distribution has two peaks for the case of $Y \leq 5.0$; One of them is at $X(t) < 4$ and the other is at $X(t) > 4$ (Fig. 4.2 (a)). This indicates, in the present situation, the system passes between the liquid state and the solid state. Thus, the discontinuous transition between the solid state and the liquid state appears like in the system with many hard spheres[10]. These two peaks become blunt with the increase of Y, and the probability distribution around $X(t) = 4.0$ becomes almost flat for $Y \sim 5.0$ (Fig. 4.2 (b)). Differently from the case of $Y \leq 5.0$, each distribution has always only one peak in the case of $Y > 5.0$ (Fig. 4.2 (c)), where this peak crosses the line $X = 4$ with no singularities for the middle f. The appearance and the disappearance of the discontinuous transition are considered to be strongly related to those of Van der Waals loop which were observed when the width of the box is fixed (see chapter 3). However, the height with no discontinuous transition is $Y > Y^* \sim 5.0$, while the one with no Van der Waals loop is $Y' > Y'^* \sim 6.0$ in the previous chapter. Our value Y^* is, if anything, similar to another critical height $Y'_c \sim 5.0$ for the previous model, where β and α like relaxations appear for $Y' \geq Y'_c$ (see chapter 3). If we fix the value f and change the value $\beta = 1/T$, we observe qualitatively the same results as the above.

4.4 Two hard spheres model and appearance and change of frictions with $U > 0$

Next, we discuss the cases with $U > 0$. In these cases, the system becomes non-equilibrium because of the asymmetric force working on particles in vertical direction along the left wall. Figure 4.3 is the probability distribution of the position of the right wall $X(t)$ for, respectively, when (a)$Y = 4.5$ with low temperature $(T = 0.1)$, (b)$Y = 4.5$ with high temperature $(T = 0.4)$, (c)$Y = 5.5$ with low temperature $(T = 0.1)$, and (d) $Y = 5.5$ with high temperature $(T = 0.4)$, for typical values U under constant value $f(= 1)$. Here, we

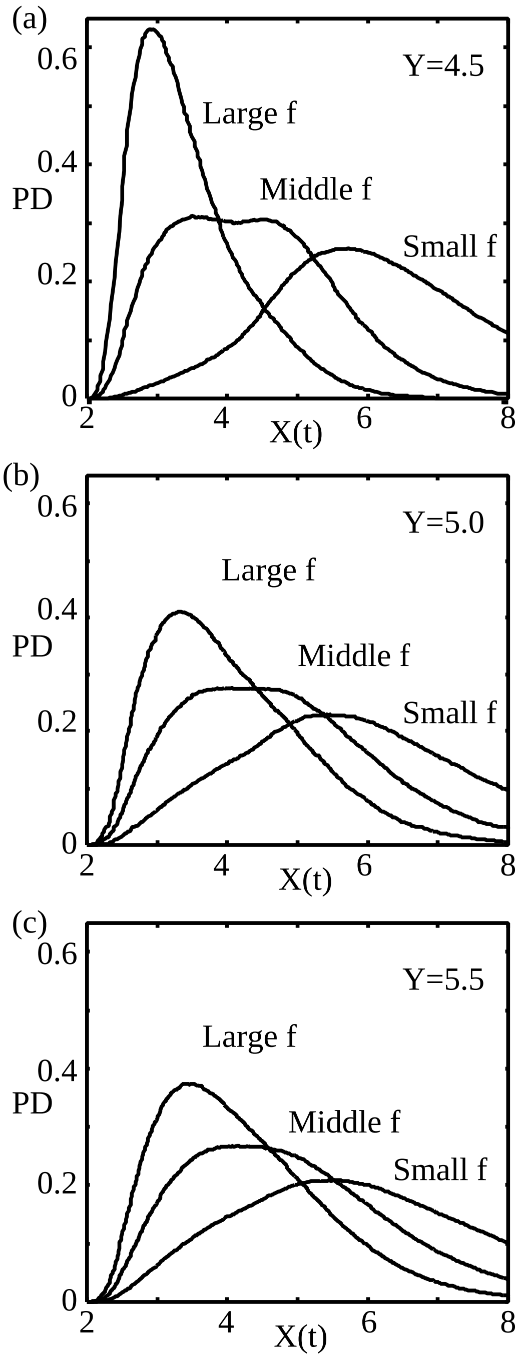

Figure 4.2: Probability distribution of the position of the right wall $X(t)$ (PD) for typical values f with, respectively, when (a)$Y = 4.5$ (Middle $f = 0.1725$), (b)$Y = 5.0$ (Middle $f = 0.1345$), and (c)$Y = 5.5$ (Middle $f = 0.1225$) under $T = 0.1$ and $U = 0$.

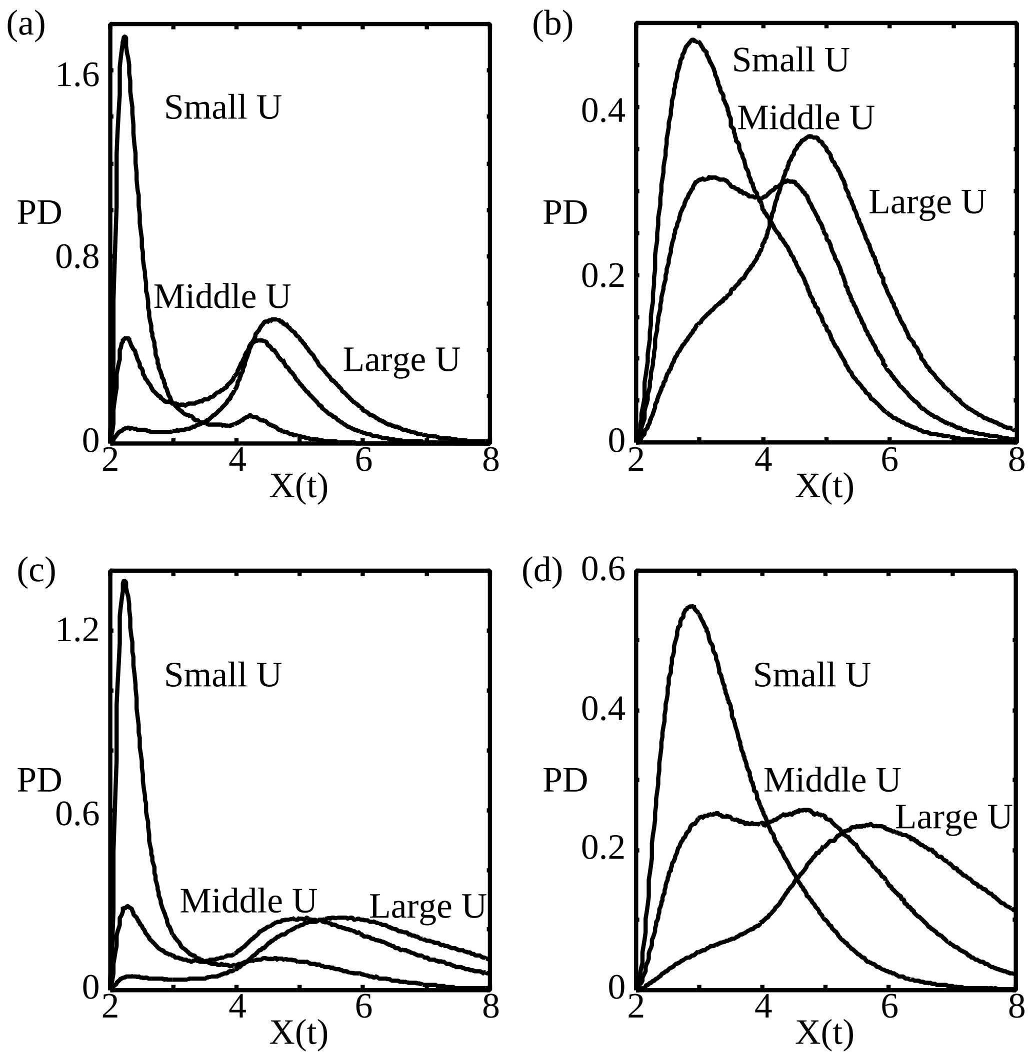

Figure 4.3: Probability distribution of the position of right wall $X(t)$ (PD) for typical values U and $f = 1$ with, respectively, (a)$Y = 4.5$ with $T = 0.1$ (Middle $U = 1.14$), (b)$Y = 4.5$ with $T = 0.4$ (Middle $U = 0.665$), (c)$Y = 5.5$ with $T = 0.1$ (Middle $U = 1.925$), and (d) $Y = 5.5$ with $T = 0.4$ (Middle $U = 1.25$).

set T with which the probability distribution of $X(t)$ has only one peak for $X(t) < 4$ (the solid state is realized) for the case of $U = 0$. The discontinuous phase transition between the solid state and the liquid state with the liquid-solid temporal coexistence state is realized for $Y \leq 5.0$ by varying the value U (Fig. 4.3 (a) and (b)). Differently from cases of the previous discussions with $U = 0$, however, such a discontinuous phase transition is observed also for cases with $Y > 5.0$. In these situations, two particles are compressed near the top wall of the box by the asymmetric force with $U > 0$. This means the region in which particles spend almost all the time becomes smaller in vertical direction. Then, the Y-dependent characters of the phase transition become blunt. With increase of T and Y, these two peaks become smoother and the top of the probability distribution of $X(t)$ for middle U comes close to be flat (Fig. 4.3(d)).

Now, we define the mobility m of the system as the average frequency of the change of sign of δy. Here, δy is the relative position between two particles in vertical direction. The solid state is realized when $m \sim 0$, and the liquid state is realized when m is large. From the asymmetric force characterized by the velocity U, the force $F_{ex} = \lim_{t\to\infty} \frac{1}{t}(\sum_{col}(V_v - v_v))$ works on particles at the left wall in average. Here, $\sum_{col}$ is the sum of individual collisions between the left wall and particles. Figure 4.4 is the relation between (a)U and m, and (b)U and F_{ex} for typical values T under constant values $f = 1$ and $Y = 5.0$. For small U, $m \sim 0$ and $F_{ex} \propto U$ are realized, and $m \propto U$ and $F_{ex} = constant$ are realized for large U. Here, F_{ex} for each U becomes large with T decreasing, although T dependencies of F_{ex} are small for large U. Moreover, each U-F_{ex} curve for small T has a peak which disappears for large T. When the width of the box becomes larger, m become larger. Then, frequency of collisions between particles and the left wall connected to energy source decreases. These facts make F_{ex} to be almost constant for large m although U increases. Figure 4.5 indicates relations between m and F_{ex} by increasing U for typical values T under constant values $f = 1$, where (a)$Y = 5.0$ and (b)$Y = 4.5$. Here, each state of the system is almost stationary in which m looks constant if averaged over the macroscopic time scale sufficiently larger than the mean free time of particles. Then, F_{ex} is regarded as the driving force to keep each steady state. This also means that the effective frictional force R, the magnitude of which is equal to that of F_{ex}, emerges in the system to inhibit the mobilization of the system. Hence, Fig. 4.5 also indicates the relations between the mobility m and the frictional force R. Here, f plays a role of the normal reaction of this system which is treated as the constant 1. Thus, the relations between m and R are equivalent to those of m and the effective friction coefficient $\mu = \frac{R}{f}$. In Fig. 4.5, for small T, R has a maximum value at a neighborhood of $m = 0$, and this decreases

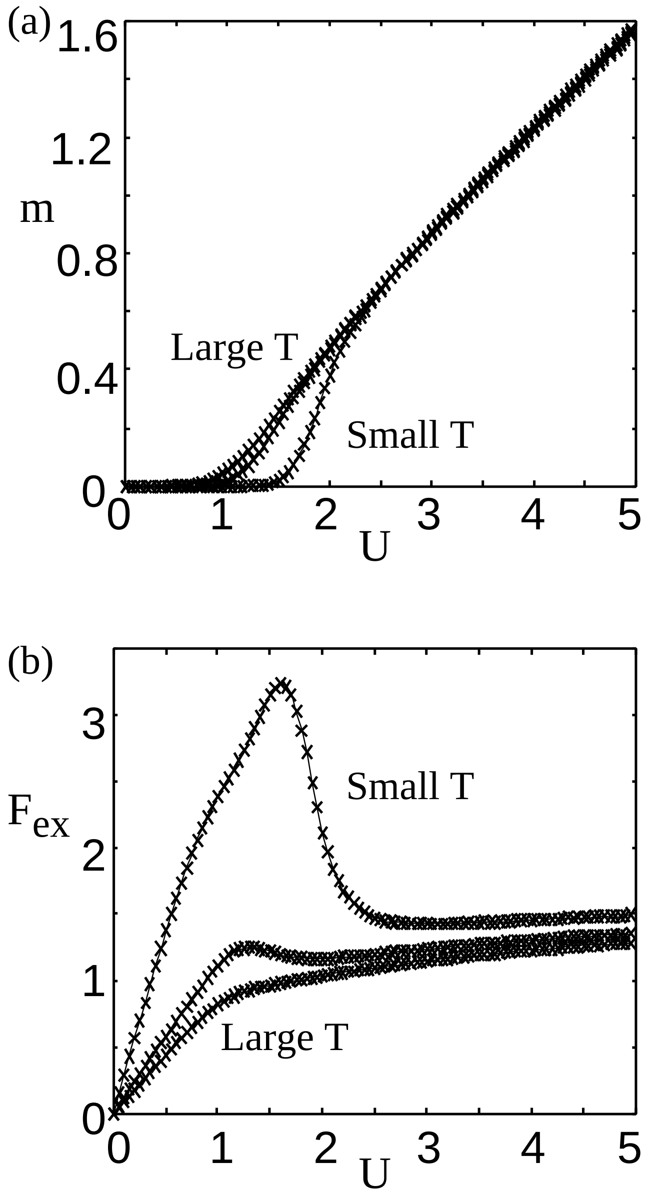

Figure 4.4: Relations between (a)U and m and (b)U and F_{ex} for typical values T ($T = 0.06$, 0.24 and 0.42) with $Y = 5.0$ and $f = 1$.

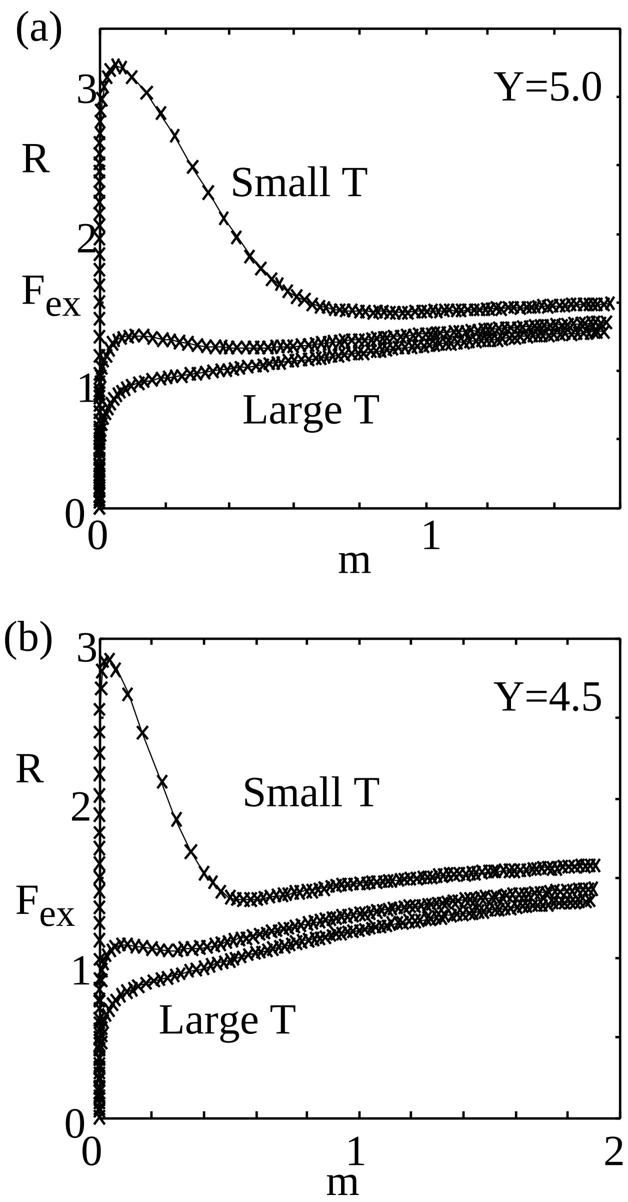

Figure 4.5: Relations between m and R (F_{ex}) for typical values T with, respectively, (a)$Y = 5.0$ ($T = 0.06$, 0.24 and 0.42) and (b)$Y = 4.5$ ($T = 0.05$, 0.21 and 0.37) ($f = 1$).

monotonically and becomes almost constant with the increase of m. These characteristics of m-R relation are similar to those of velocity-friction relations of solid-on-solid system which satisfies Coulomb-Amontons's frictions laws[125]. For large T, on the contrary, R increases monotonically and becomes almost constant value with the increase of m different from Coulomb-Amontons's frictions laws. When Y becomes small, R increases a little with m for large m (Fig. 4.5 (b)). However, this increase is small, and qualitative characteristics obtained in the above are considered to be independent of Y.

Figure 4.6 is the relations between, respectively, (a)m and the friction coefficient $\mu = \frac{R}{f}$, and (b)f and μ by increasing f for typical values T under a constant value U ($Y = 5.0$). In this case, the liquid state with large m and the solid state with $m = 0$ are realized for, respectively, small f and large f. In cases with $U = 0$, large f states are equivalent to small T states. Hence, it is natural that profiles of the relations for small m in Fig. 4.6 (a) become similar to those of relations with small T in Fig. 4.5. Because of the same reason, the probability distribution of $X(t)$ for large f also behaves similarly to those with small T in Fig. 4.3. In Fig. 4.6 (a), μ of the $m = 0$ states is obtained which is larger than μ of the large m state. Moreover, μ remains constant independently of m for large m. In Fig. 4.6 (b), the derivative $\frac{d\mu}{df}$ is small if f is small or large. This means the frictional force is almost proportional to the normal reaction in these region. These characteristics are also similar to those of solid-on-solid frictions which satisfy Coulomb-Amontons's frictions laws[125]. In Fig. 4.6 (b), for middle f, friction coefficients for each T increase with the increase of m. With the decrease of T, the friction constant increases sharply.

4.5 Qualitative mechanism of hysteresis loop of granular friction

Now, we focus on the relation between the velocity of a plate on granular layers and the friction between the plate and granular layers[127, 131]. Recently, from a sensitive experiment, Nasuno et al. found that the relation between the plate velocity and the frictional force makes a hysteresis loop[127]; The frictional force is multi-valued, which is less for decreasing velocity to 0 than for increasing velocity from 0. It is remarkable that a loop, which looks very similar to above one, can be created by combining m-R relations for large and small T (see Fig. 4.5). Thus, we try to understand qualitatively the mechanism of history dependencies of velocity-friction relations on granular layers from the m-R relations in Fig. 4.5. Here, m corresponds to the plate velocity and R corresponds to the friction on granular layers. We assume that the granular temperature T_g of the surface of granular layers plays similar roles to the temperature of energy source

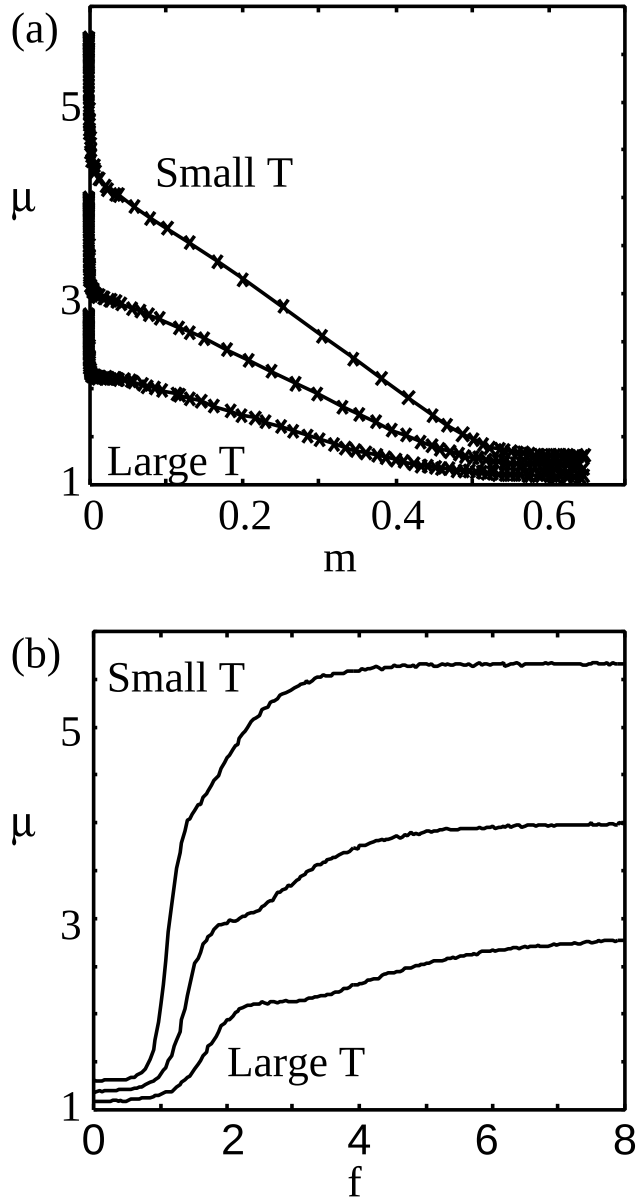

Figure 4.6: Relations between (a) m and μ, and (b) f and μ, for typical values T ($T = 2^{-5}$, 2^{-4} and 2^{-3}) with $Y = 5.0$ and constant U ($U = 2.0$).

in our system. Here, T_g is defined as the half of the mean-square of velocity fluctuation of each granular particle. Initially, the plate and each particle in granular layers do not move, where $T_g = 0$. Soon after the plate starts slipping, T_g increases but it is expected to be small at the early stage. Hence, the frictional force decreases with increasing the plate velocity on granular layers like m-R relations with small T in Fig. 4.5. When plate moves faster, however, T_g is expected to become large because the plate excites each particle in granular layers. Then, the frictional force is almost constant for finite plate velocity like m-R relations with middle or large T in Fig. 4.5. By this friction, in the final stage, the plate stops and T_g becomes 0 again. Thus, in this granular system, T_g varies with time and this variance of T_g iterates all along because the plate is pushed continuously. This iteration and the temperature dependency of the frictional force explain the appearance of such a hysteresis loop in granular materials.

4.6 Summary

In this chapter, we discussed the liquid-solid phase transition and the occurrence of static and dynamic frictions of the system with two particles in a rectangular box. First, we discussed the liquid-solid phase transition by controlling the pressure in horizontal direction or the temperature of a heat bath. When the height of the box is small, the discontinuous liquid-solid phase transition with the appearance of the liquid-solid temporal coexistence was observed. However, the liquid-solid phase transition becomes continuous when the height of the box is higher than a critical value. Next, we discussed the relation between the mobility and the frictional force of the system in which particles are excited by an asymmetric force in the vertical direction. In the simulation, we observed the frictional forces which are quite similar to the static friction and the dynamic friction observed in the solid-on-solid system. Moreover, we found that the relation between these frictional forces and the mobility strongly depends on the temperature of the heat bath. Taking these characteristics into consideration, we discussed the origin of the hysteresis loop in the granular friction. Our discovery of temperature dependency of these characters of frictions is an important result of our simulation. More discussions together with theoretical, numerical, and experimental studies are needed in the future. Also the analytical study of dynamical properties of frictional forces on granular layers is left as an important issue.

Chapter 5

Transition of the Effective Dimension of the Dynamics of Granular Materials in a Pipe

Abstract: In this chapter, phase transition of strongly excited granular materials in a 2D pipe is numerically investigated. Changing the ratio between width of the pipe and the height of the granular bed, we observe the transition between the 1 dimensional-like state and the actual 2-dimensional state. Moreover, it is found that the character of the transition changes when the magnitude of dissipation passes through a critical value.

5.1 Introduction

Granular materials exhibit various complex phenomena[32, 33]. These complex phenomena strongly depend on the characters not only of external forces but also of boundary condition. When granular materials in slim pipes filled with fluid (air, water, and so on) flow down or are fluidized by inducing fluid from the bottom, slugging is observed[66, 88]. In most investigations of such slugging, the effective dimension of the corresponding systems is regarded as 1[85, 86, 88]. On the other hand, two or more dimensional phenomena, such as bubbling and channeling, occur when granular materials are in a wider vessel[63]. The similar tendency is also observed for granular materials in a vibrating vessel[43, 44, 45, 46]. When the width of the vessel is small, most of particles take part in building solid structure in bulk and only particles near side walls flow down to the bottom[32, 44]. However, in a wide vessel, most of particles are strongly fluidized and form multi-roll structure like Bernard convection[46] From these facts, the behaviors of granular materials are entirely different between that in a slim vessel and that in a wide vessel. Then, an important problem occurs; what quantity determines 'slim' (one dimensional system) or 'wide' (two or three-dimensional system) for a given system? The purpose of this chapter is to make a quantitative criterion for this classification.

5.2 Considered system

Here, we simulate the following simplified situation[54, 55, 56]. The system consists of two dimensional particles of mass 1 and diameter d in a two-dimensional box under uniform gravity. The width of the box is a, and the height of the box is infinite. We employ the following particle model which is one of the simplest model of granular materials. The equation of the motion of the ith particle is

$$\ddot{\mathbf{x}}_i = -\sum_{j=1}^{N} \theta(d - |\mathbf{x}_i - \mathbf{x}_j|)\{\nabla U(d - |\mathbf{x}_i - \mathbf{x}_j|) + \eta(\mathbf{v}_i - \mathbf{v}_j)\} + \mathbf{g} \tag{5.1}$$

$$U(d - |\mathbf{x}_i - \mathbf{x}_j|) = \frac{k}{2}(d - |\mathbf{x}_i - \mathbf{x}_j|)^2 \tag{5.2}$$

here, θ is Heviside function, N is the total number of particles, k and η are, respectively, the elastic constant and the viscosity coefficient, and $\mathbf{x}_i(x_i, y_i)$, $\mathbf{v}_i(v_{x_i}, v_{yi})$, and $\mathbf{g} = (0, -g)$ are, respectively, the position, the velocity and the gravity of ith particles. In this model, the effect of particles' rotation is neglected. The system is driven by a simple energy source at the bottom of the box; a particle hitting the bottom with velocity (v_x, v_y) will bounce back with the velocity $(v_x, V(V > 0))$. We regard the box lies on the x axis $(y = 0)$, and $x = 0$ is the center of the bottom. The side walls of the box are put along $x = a/2$ and $x = -a/2$, and the viscosity which works between walls and particles is zero. At the initial condition, we put particles bed with thickness b on the bottom of the box. We simulate this system with several combinations of parameters (η, a, b), where a and b are sufficiently larger than the particle's diameter d. The above equations are calculated with the Euler's scheme. The time step δt is set small enough such that δx, the displacement of the ith particle during δt, does not exceed a given value. In our discussions, $(-g, V)$ is set so that the average height of the center of mass of the system $CM =< (\sum y_i)/N >_t$ is sufficiently larger than b.

5.3 Simulation

Figure 5.1 shows typical snapshots of the system for, respectively, (a) $a << b$ with $\eta = 1.0$, (b) $a >> b$ with $\eta = 1.0$, (c) $a << b$ with $\eta = 0.25$, and (d) $a >> b$ with $\eta = 0.25$. Here, we fixed $b = 20d$, whereas $(-g, V)$ of (a) is the same as that of (b), and $(-g, V)$ of (c) is the same as that of (d). In cases of (a) and (c), only the particles distribution in the horizontal direction is symmetric, and the center of mass of this system moves a little only in the vertical direction. On the other hand, the particles distribution is non-uniform in vertical and horizontal direction, and one convection appears in cases of (b) and (d). In order to characterize the system, we introduce the order parameter $L(t) = |\sum_i x_i(t)v_{yi}(t)|/N$ which indicates the strength of the convection. Figure 5.2 (a) and (b) are typical probability distributions of $L(t)$ which are given by each time series for, respectively, the cases of $a << b$ and those of $a >> b$ with $\eta = 1.0$. In Fig.5.2 (a), the peak of the probability distribution of $L(t)$ appears at $L(t) = 0$ which means there are no convection for the case $a << b$. In this case, the effective dimension of the system can be regarded as 1. We name such states as the '1D state'. On the contrary the peak of the probability distribution of $L(t)$ appears at $L(t) > 0$ in Fig.5.2 (b), which means a convection with finite magnitude appears in the system. In this case, the system is actually 2-dimensional system. We name such states with a convention as the '2D state'. Such a transition between the 1D state and the 2D state which depends on the relation between a and b is observed in a simple system.

In our simulation, particles are strongly excited by the energy source at the bottom of the box. Then, if we set an improper g for a small η or a small b, the height of particles diverges. In order to clear off such cases, we need to control g for several η and b. By

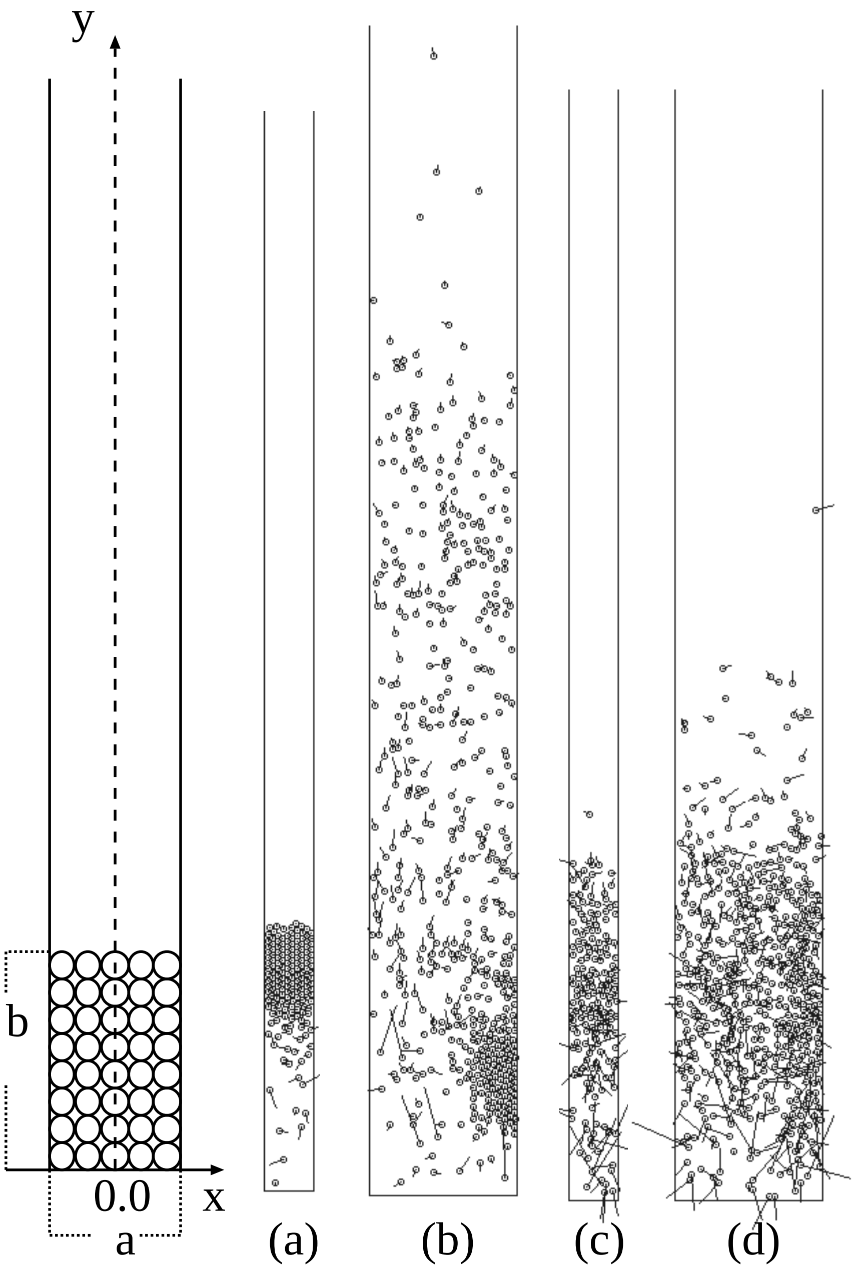

Figure 5.1: Illustration of 2D pipe and typical snapshots for, respectively, (a) $a << b$ with $\eta = 1.0$, (b) $a >> b$ with $\eta = 1.0$, (c) $a << b$ with $\eta = 0.25$, and (d) $a >> b$ with $\eta = 0.25$.

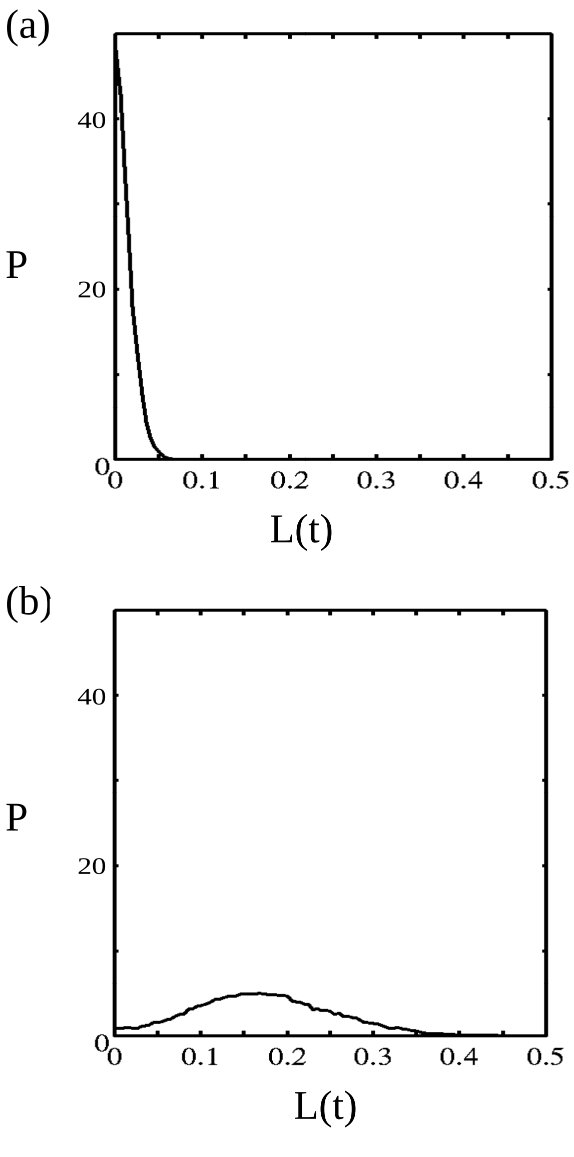

Figure 5.2: Probability distributions of $L(t)$ for, respectively, (a) $a << b$, and (b) $a >> b$.

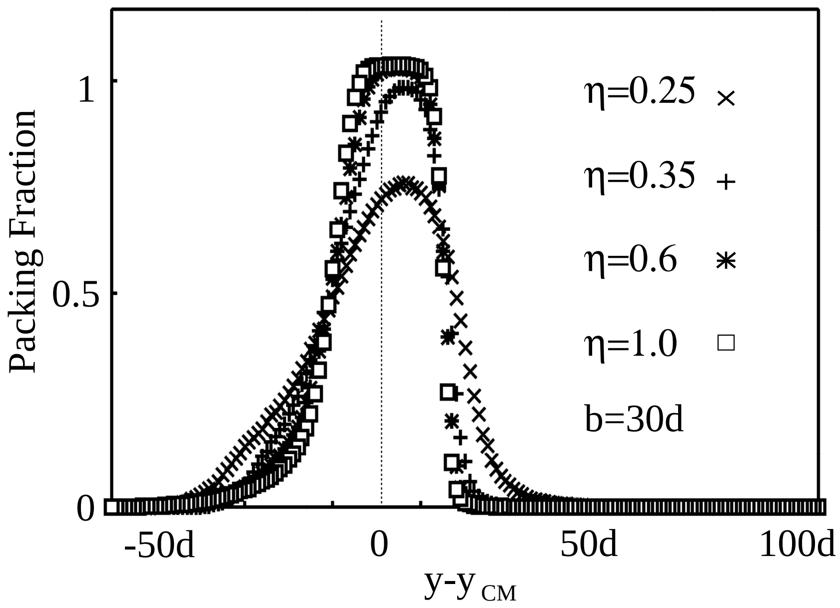

Figure 5.3: Packing fraction profile for y direction at $\eta = 0.25$,0.35,0.6, and 1.0.

the simulation, we found the fact that CM have almost the same values independent of a with $a << b$ for a fixed set of g, η, b and V. Hereafter, we fix V and determine the gravity g for a given set (η, b) independent of a. In our discussions, we set $V = 2$ and $g(\eta, b)$ with which $CM \sim 60d$ is realized for all cases of $a << b$. When we set $V = 3.0$ or $V = 4.0$, we can get qualitatively the same results as those of following discussions with $V = 2.0$.

5.4 Properties of one-dimensional system

Before the discussions of the transition width at which the 1D-2D transition takes place and of the character of the transition, we discuss the dependency of η in the 1D states. Figure 5.3 shows the time averaged packing fraction profile of the y direction as the function of $y - y_{CM}$ for several η with $a = 9d$ and $b = 30d$. Here, y_{CM} is the y component of center of masses of particles, and we define the packing fraction as followings. We divide the space by a lattice with the lattice constant d. Then, the number of centers of particle within each $d \times d$ square is the packing fraction in the square. The packing fraction of y direction is given as the average of them through the x direction for each y. For large η ($\eta = 0.6, 1.0$), each profile includes a flat region with large packing fraction near the center of mass of this system. These flat regions mean the existence of the solid structure

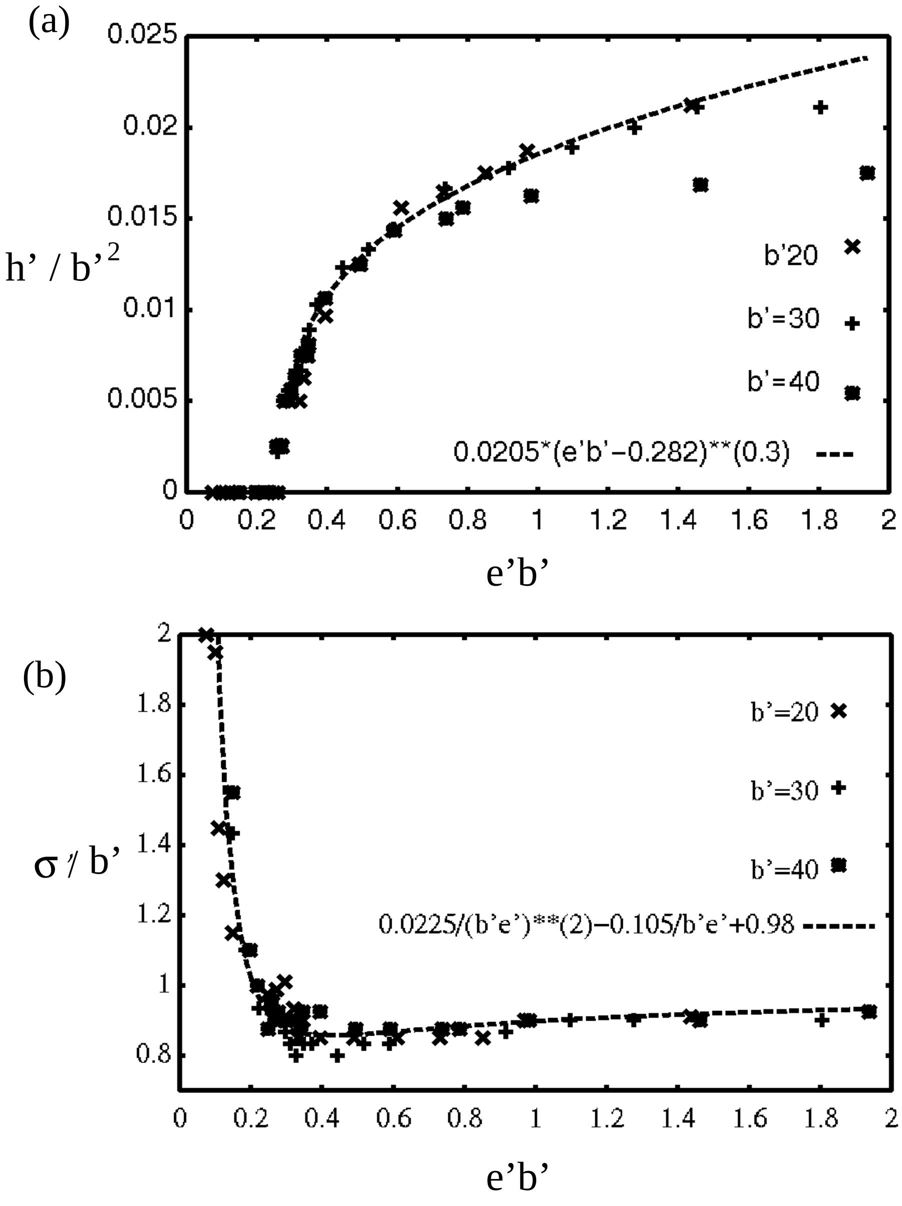

Figure 5.4: Relation between two rescaled values, (a) $e'b'$ and $\frac{h'(e')}{b'^2}$, and (b) $e'b'$ and $\sigma'(e')/b'$

in which particles are almost completely packed. The length of this flat region decreases as η decreases, and this length becomes 0 for $\eta = \eta^* \sim 0.38$. If $\eta < \eta^*$ ($\eta = 0.25, 0.35$), each packing fraction profile includes no flat region, and maximum packing fraction is smaller than that of $\eta > \eta^*$. It means that no solid structure is created for such small η. In other words, a transition between a state which includes the solid structure and the another state which includes no solid structure occurs at the critical value $\eta = \eta^*$. Similar results are obtained in the following two cases, $b = 20d$ and $b = 40d$. Now we introduce the following dimensionless values: $a' = a/d$, $b' = b/d$, and $e' = 1 - e$ where $e = exp(\pi\eta/(k - \eta^2)^{\frac{1}{2}}))$, and the length of the flat region $h(e') = h'(e')d$. ($h'(e')$ has no dimensions.) Here, e indicates the coefficient of restitution for head-on collisions between two particles[124]. The relation between two rescaled values, $(e'b')$ and $\frac{h'(e')}{b'^2}$, is obtained as shown in Fig.5.4(a). The rescaled critical point $(e'b')^*$ is determined independent of the system size, and the profile of this relation fits with

$$\frac{h'(e')}{b'^2} = h'_o|e'b' - (e'b')^*|^{0.3} \tag{5.3}$$

near $e'b' \sim (e'b')^* \sim 0.282$.($h'_o$ is constant.) Moreover, we introduce the cluster length $\sigma(e') = \sigma'(e')d$ ($\sigma'(e')$ has no dimensions.) which is defined as the distance between two nearest inflection points from the maximum point of the packing fraction profile. Thus, the relation between two rescaled values, $e'b'$ and $\sigma'(e')/b'$, are obtained as shown in Fig.5.4 (b). The profile of this relation fits with

$$\frac{\sigma'(e')}{b'} = \frac{0.0255}{(e'b')^2} - \frac{0.105}{e'b'} + 0.98. \tag{5.4}$$

We expect $\sigma'(e')/b' \to \infty$ for $e'b' \to 0$, and $\sigma'(e')/b' \sim 1$ for $e'b' \to \infty$.

5.5 Transition between the one-dimensional state and the two-dimensional state

Now, we discuss the character of the transition between the 1D state and the 2D state with the change of the vessel width. Here, we define this transition width a^* as the minimum width at which the 2D state appears in the system. Figure 5.5 shows the typical probability distributions of $L(t)$ for several width a around $a = \sigma(e')$. Here, (a) indicates the case $e' < e'^*$ ($\eta < \eta^*$) and (b) indicates the case $e' > e'^*$ ($\eta > \eta^*$)both for $b = 20d$. In Fig.5.5 (a), each profile of probability distribution of $L(t)$ includes only one peak. The position of peak is at $L(t) = 0$ for $a < \sigma(e')$. For $a > \sigma(e')$, however, the peak appears at $L(t) > 0$ and this peak moves as the width varies. Thus the continuous

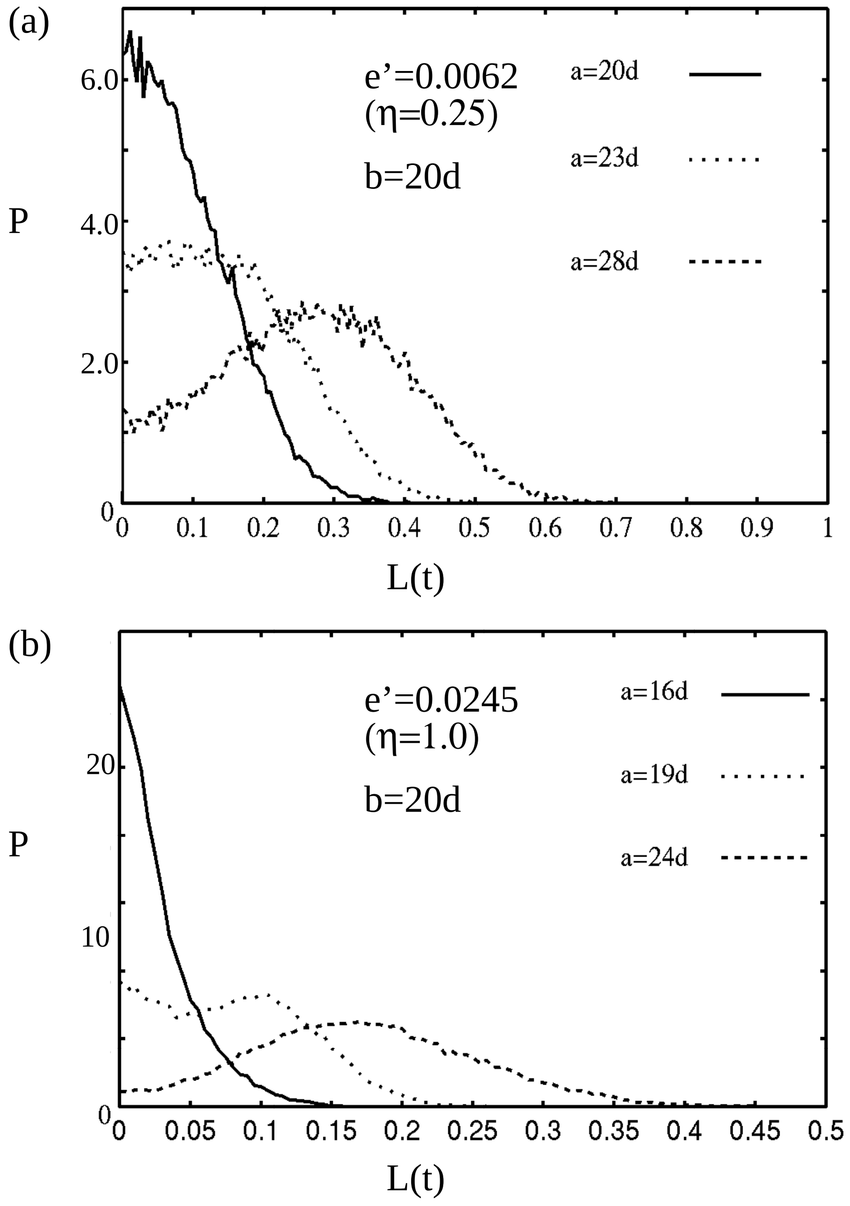

Figure 5.5: Typical probability distributions of $L(t)$ for (a) $e' < e'^*$ ($\eta < \eta^*$) and (b) $e' > e'^*$ ($\eta > \eta^*$) for several width around a critical value $a = \sigma(e')$.

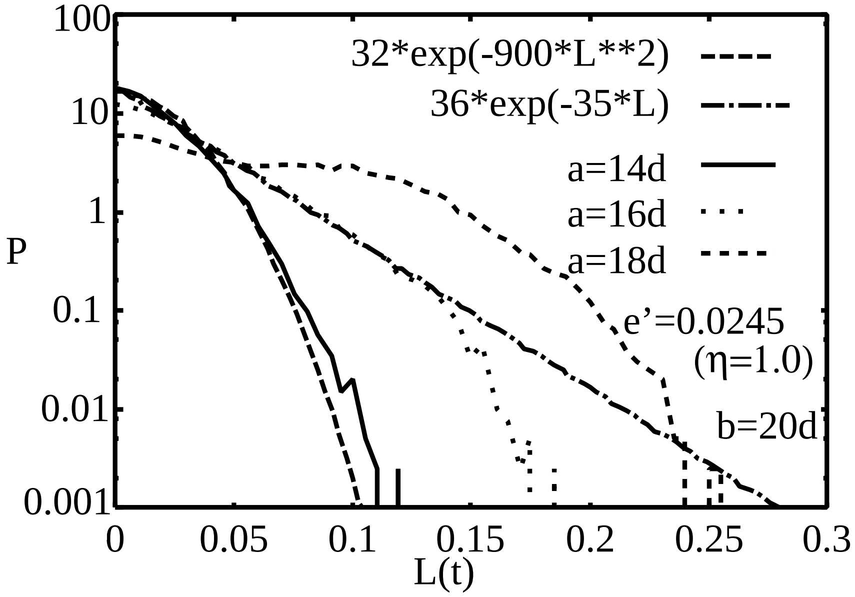

Figure 5.6: Semi-log scale profiles of probability distributions of $L(t)$ for respectively $a < \sigma(e')$, a is a little smaller than $\sigma(e')$ and $a \geq \sigma(e')$ with $e' \sim 0.247$ ($\eta = 1.0$)

transition between the 1D state and the 2D state appears for the case $e' < e'^{*}$ ($\eta < \eta^{*}$), and the transition width is given as $a^{*} \sim \sigma(e')$. In Fig.5.5 (b), on the contrary, probability distributions of $L(t)$ for a, which is a little larger than $\sigma(e')$, include two peaks at $L(t) = 0$ and $L(t) > 0$. This means that two locally stable states, one is the 1D state and the other is the 2D state, coexist and they appear periodically for the case of $e' > e'^{*}$ ($\eta > \eta^{*}$). In such cases, the system includes the solid structure when the 1D state is realized. In this solid structure, the friction between particles are strong because particles are densely packed. Hence, the solid structure is robust, and this originates the stability of the 1D state for $a > \sigma(e')$. Figure 5.6 shows the semi-log scale profiles of probability distributions of $L(t)$ for, respectively, $a < \sigma(e')$, $a \sim \sigma(e')$ and $a > \sigma(e')$. When $a' < \sigma'(e')$, the profile is proportional to $exp(-\gamma_0 L^2)$, which means that fluctuations of $L(t)$ are so small that they can be neglected. However, a profile which is proportional to $exp(-\gamma_1 L)$ is obtained when a is close to $\sigma(e')$, which means that the fluctuation from $L(t) = 0$ become large. Moreover, the profile includes two peaks at $L(t) = 0$ and $L(t) > 0$ when $a \geq \sigma(e')$. Then, the transition width a^{*} is regarded as $a^{*} \sim \sigma(e')$ for also $e' > e'^{*}$ ($\eta > \eta^{*}$). These results mean the following two facts. I) The critical width at which the 2D state can appear, is equal to the cluster length. II) The magnitude of dissipation separates the type of the transition between the 1D state or the 2D state. We obtain the similar results for the case

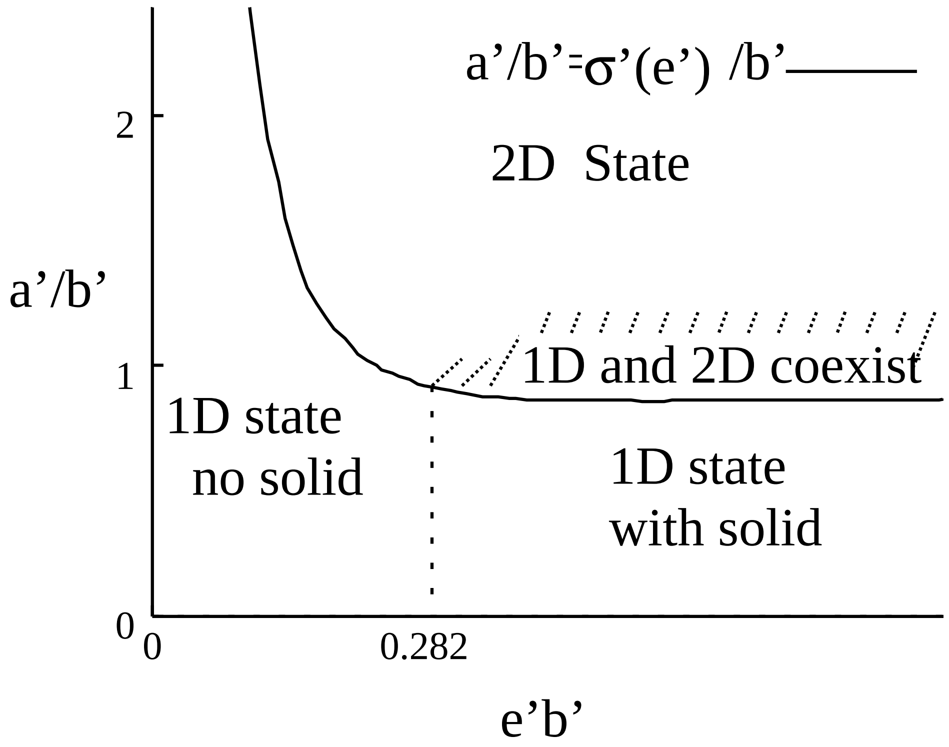

Figure 5.7: Phase diagram of the effective dimension of the system which depends on $e'b'$ and a'/b'

$b' = 30$. Then, by using rescaled parameter $e'b'$ and a'/b', the phase diagram is obtained as shown in Fig.5.7.

5.6 Summary

In this chapter, we simulated strongly excited granular materials in a 2-dimensional pipe. When the width of the system is small, a characteristic state, in which the effective dimension of particles' dynamics is regarded as 1, appears. We named this state as the 1D state. However, when the width of the system is larger than a critical width, the actual 2-dimensional state appears in which the convection is seen. We named this state as the 2D state. Moreover, we found that a critical width is equal to the length of the cluster which appears in the 1D state. The character of the 1D state depends on the magnitude of dissipation. When the magnitude of dissipation is larger than the critical value, the system includes solid structure. On the contrary, such solid structure disappears when the magnitude of dissipation is smaller than the critical value. According to the differences of the magnitude of dissipation, the following two types of behaviors appear in the system near the critical width. When the magnitude of dissipation is smaller than the critical value, the continuous transition between the 1D state and the 2D state appears. On the contrary, when the magnitude of dissipation is larger than the critical value, two meta-stable states, the 1D state and the 2D state, appear periodically for a little over the critical width. By another simulation, the existence of such a critical magnitude of dissipation is reported[59, 58]. The analytical derivation of this critical value is one of the most important issue for the research of granular materials. Moreover, simulations of more highly excited systems, larger systems, and the analytical study of the critical width for several magnitude of dissipation are important future issues.

Chapter 6

Size Segregation and Convection of Granular Mixtures Almost Completely Packed in the Rotating Thin Box

Abstract: In this chapter, size segregation of granular mixtures which are almost completely packed in a rotating drum is discussed with an effective simulation and a brief analysis. Instead of a 3D drum, we simulate a 2D thin rotating box which is almost completely packed with granular mixtures. The phase inversion of radially segregated pattern which was found in a 3D experiment are qualitatively reproduced with this simulation, and a brief analysis is followed. Moreover in our simulation, a global convection appears after radial segregation pattern is formed, and this convection induces axially segregated pattern.

6.1 Introduction

Granular materials exhibit various complex phenomena[32]. One example is size segregation which occurs by shaking or stirring them[103, 104, 105, 106, 107, 108, 110, 111]. Mixtures of granular materials which are partially-filled in horizontally rotating drum also segregate by size. Some of recent experiments have shown two types of segregation patterns[112, 113]. One of them is radial segregation where large particles accumulate near the walls of drum and small particles accumulate to the central region around the rotating axis. The other is axial segregation where the system evolves to form alternating bands one of which is rich in small particles and the other is rich in large particles. These phenomena have been explained by recent numerical and analytical studies[113, 114, 116, 115]. Most of these studies explained such segregation by considering the difference of dynamic angles of repose between those of large particles and small particles at flowing surface of granular bed. For radial segregation, another experiment reported that the mixed state and the reverse segregation appear when the angular velocity of rotating drum becomes large [120]. Here, the reverse segregation is defined such that small particles accumulate near the walls of drum and large particles accumulate to the central region around the rotating axis.

Recently, radial and axial segregation were observed in an experiment of a horizontally rotating drum which is almost completely filled with granular mixtures[121]. Moreover, as explained in the following, phase inversion between two types of radial segregation patterns takes place when w, the angular velocity of the rotating drum, passes through a critical value[122]. When $Aw^2 < g$, large particles accumulate near the wall of the drum and small particles accumulate to the central region. On the contrary, small particles accumulate near the wall of drum and large particles accumulate to the inner region of the drum like the reverse segregation when $Aw^2 > g$. Here, A is the radius of the drum, and g is the acceleration of gravity. In this system, there are little surface flow because the drum is almost completely filled with granular mixtures. Thus, the preceding numerical and analytical studies, which take into account the difference of dynamic angles of repose between large and small particles cannot explain these phenomena. In this chapter, we discuss the mechanism of such segregation and phase inversion phenomena in a rotating drum almost filled with granular mixtures. First, we reproduce experimental results with a simple simulation. Second, we make an analytical study of the phase inversion phenomena between two types of radial segregation.

6.2 Rotating thin box model

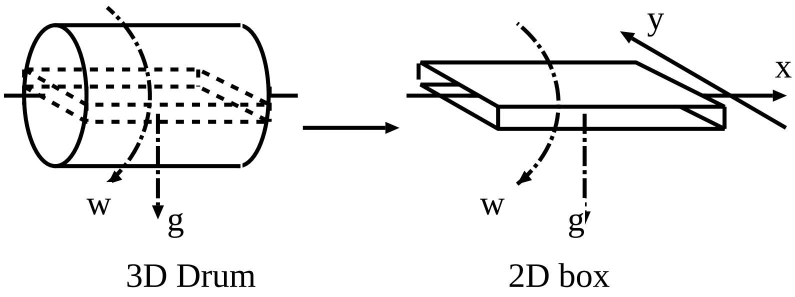

Figure 6.1: Illustration of 2D rotating thin box.

In order to simplify the simulation, we set the following situation. Instead of a 3D drum with the radius A and the width B, we use a 2D box which is rotating along a horizontal axis with the length $2A$ and the width B. Here, the length of the 2D box corresponds to the diameter of the 3D drum. The rotation axis of this box is the line of half length A, and this box rotates with angular velocity w (Fig.6.1). Our setup of the 2D thin box simulation is not the direct reflection of the 3D experiment. However, we believe it catches the intrinsic dynamics in the almost filled drum with little surface flow which plays an important role in the half filled drum. In other words, this is the simplest system with which one can look into the detailed dynamics of particles in the bulk. We employ the following particle model which is one of the simplest model of granular dynamics[43]. The equation of the motion of the ith particle is

$$\ddot{\mathbf{x}}_i = -\sum_{j=1}^{N} \theta(r_i + r_j - |\mathbf{x}_i - \mathbf{x}_j|)\{\nabla V(r_i + r_j - |\mathbf{x}_i - \mathbf{x}_j|) + \eta(\mathbf{v}_i - \mathbf{v}_j)\} + \mathbf{F}_i^{ex} \qquad (6.1)$$

$$V(r_i + r_j - |\mathbf{x}_i - \mathbf{x}_j|) = \frac{k}{2}(r_i + r_j - |\mathbf{x}_i - \mathbf{x}_j|)^2 \qquad (6.2)$$

here, θ is Heaviside function, N is the total number of particles, k and η are respectively the elastic constant and the dumping coefficient, and $\mathbf{x}_i(x_i, y_i)$, $\mathbf{v}_i(v_{x_i}, v_{yi})$ and r_i are, respectively, the position, the velocity and the radius of ith particles. The elastic constant k and the dumping coefficient η are related to the coefficient of restitution e and the collision time t_{col}, time period during collision[124] which are determined in the ideal two bodies collision. In this model, the effect of particles' rotation is neglected. We regard the rotating axis as x axis ($y = 0$), and the length direction (radius direction for 3D drum) as y direction in this simulation. $\mathbf{F}_i^{ex}$ is the external force which directly acts on the ith particle not by collision. Since gravitational and centrifugal force work on each particle, $\mathbf{F}_i^{ex} = (F_{x_i}^{ex}, F_{y_i}^{ex})$ is given as following.

$$F_{x_i}^{ex} = 0 \tag{6.3}$$

$$F_{y_i}^{ex} = y_i w^2 - g\sin(wt) \tag{6.4}$$

The above equations are calculated with the Euler's scheme. The time step δt is set small enough such that δx, the displacement of the ith particle during δt, does not exceed a given value. We set $2A = 7.43$, $B = 24.0$, $t_{col} = 0.05$, e between a pair of particles is 0.99, and $g = 3.0$. Moreover, boundaries of the box, $|y| = A$ and $|x| = \frac{B}{2}$ are given as the visco-elastic walls with $e = 0.95$. Total number of particles is $N = 750$, the ratio of particle numbers between large and small particles is 1:4, the ratio of average radius between them is 2:1, and 10% polydispersity for large and small particles' radius is given. The packing density which is defined as [the area of region occupied by particles]/[the area of 2D box] is estimated about 84%. It means this system is not completely packed. In practice, the movement of the center of the mass of particles appears through the rotation process in the simulation. However, the distance of this movement from the average position is almost the same as the average radius of small particles which is small enough compared to A. Hence, this system is regarded as an almost completely packed system. Because of such polydispersity and the movement of the center of mass of particles, each particle in the system barely moves.

6.3 Simulation

We pack particles at random at the initial condition (Fig.6.2 (a)) and simulate with several values of w. Figure 6.2 (b) (c) and (d) are typical patterns of radial segregation for (b)$w = 0.5$ ($Aw^2 < g$), (c)$w = 0.9$ (Aw^2 is a little larger than g), and (d)$w = 1.2$ ($Aw^2 > g$). Figure 6.2 (b) indicate that large particles accumulate near the wall of drum ($|y| = A$) and small particles gather around the central region when $Aw^2 < g$. Figure 6.2 (c) and (d) indicate that small particles accumulate near the wall of drum and large particles accumulate to the central region when $Aw^2 > g$. In Fig.6.2 (c), the region where large particles distribute is wider in the radial direction compared to Fig.6.2 (d). These results qualitatively correspond to the experimental results of rotating drum which is almost completely packed with granular mixtures[122]. The patterns illustrated in Fig.6.2 (c) and Fig.6.2 (d) are stable whereas the pattern like Fig.6.2 (b) evolves to the pattern like Fig.6.3 (c). This is because the fluctuation of large particles concentration

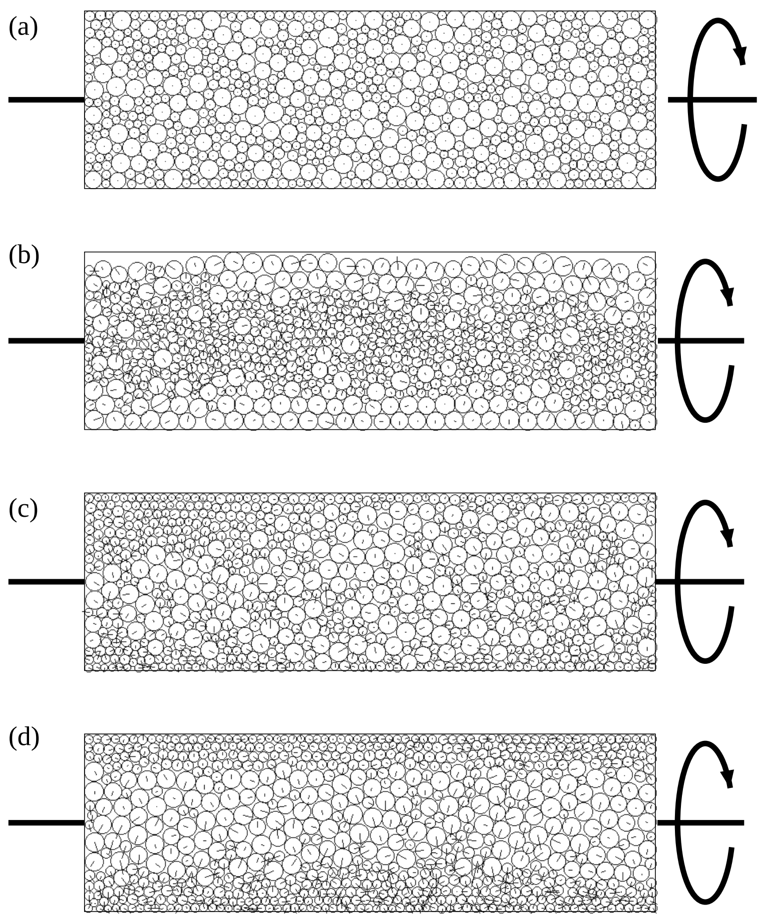

Figure 6.2: Typical snapshots of (a)initial condition, and radial segregation patterns respectively (b)$Aw^2 < g$, (c)Aw^2 is a little larger than g, and (d)$Aw^2 > g$.

in the axial direction grows up slowly as follows. Now, we consider the case that the direction of gravity is negative in y. It means that $y = -A$ corresponds to the bottom of the box. Near the bottom of the box, there exists a region in which large particles are packed. Above this region, the region in which small particle is rich exists. For convenience, we name boundaries between these two regions the S-L-boundary. Because of the fluctuation of large particles concentration near the bottom, the S-L-boundary has finite inclination. Small particles on this slope cannot invade the region in which large particle is rich because large particles are packed densely. However, through this boundary, small particles can flow down. Then, the amount of the small particles flow in $y < 0$ region is very small compared to that in the $y > 0$ region because particles in $y < 0$ region are packed more densely than in $y > 0$ region. Moreover, above the region rich in small particles, the region rich in large particle exists again. We name the boundary between these two regions the L-S-boundary. Large particles in this region cannot invade the region in which small particle is rich because they cannot go through small voids which appear in the region rich in small particles. Because of friction working at the L-S-boundary, however, some parts of large particles in this region near the L-S-boundary are dragged by the flow of small particles, which move down along the slope of the S-L-boundary. Hence, the axial concentration of large particles in this region fluctuates and this fluctuation grows up along S-L-boundary (Fig.6.3 (a)→(b)→(c)). The direction of gravity changes periodically between the negative direction and the positive direction in y with the rotation of the box. Thus, the above mentioned flow of particles in all around the system forms global convection along S-L-boundaries like Fig.6.4. Furthermore, the convection makes the fluctuation of large particles' concentration grow up, and changes the segregation pattern from the radial to the axial. Moreover, the axial segregation pattern is kept stable by the convection.

6.4 Mechanism of phase inversion

In order to discuss the phase inversion of the radial segregation pattern, we consider the following assumptions hold according to previous studies[103, 104, 105, 106, 107, 108, 110, 111]; Compared to large particles, small particles can move more easily in granular bed because they can move through smaller voids. It means that small particles are more directly drifted by external force than large particles. Then, we assume that small particles, compared to large particles, tend to move to the direction in which external force works. Large particles can also move through voids if sizes of them are larger than

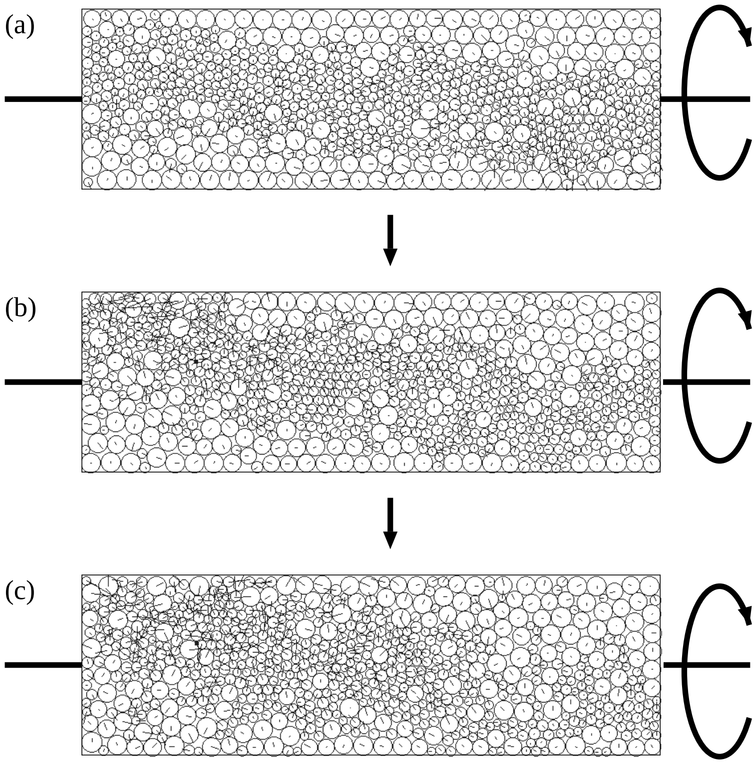

Figure 6.3: Snapshots of fluctuation growth of large particles concentration for axial direction ((a)→(b)→(c)), and typical axial segregation pattern (c).

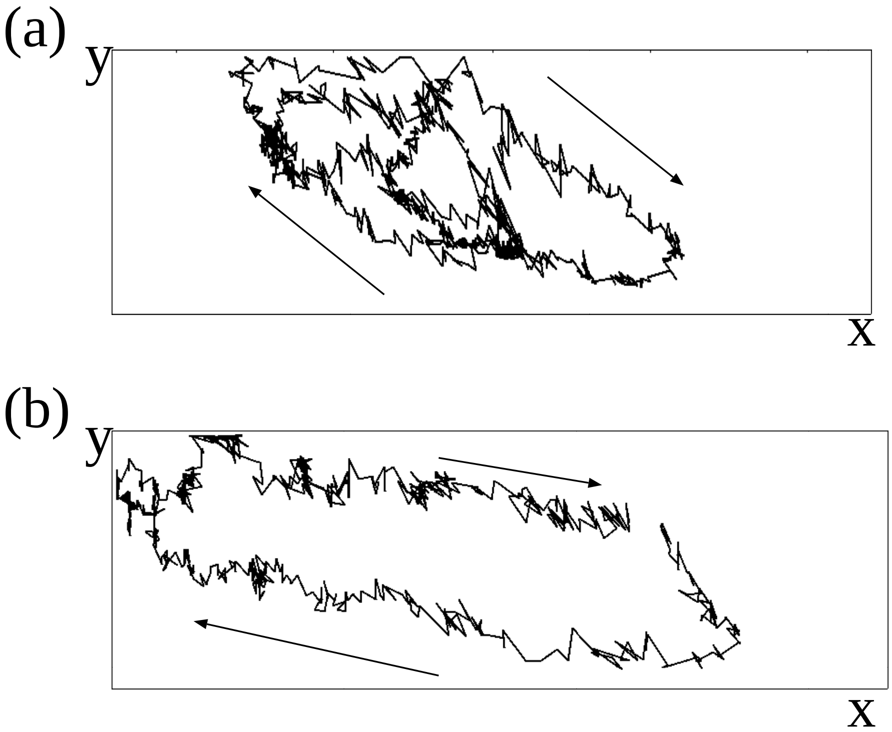

Figure 6.4: Trajectories of sample particles for 1600 rotation times of box. (a)One of small particles and (b)One of large particles.

that of large particles. Then, large particles tend to move to the low particles density region in which such large voids appear. By use of these assumptions, the mechanism of the phase inversion of radial segregation pattern is discussed. The force which works on each particle is given by eq.(3) and eq.(4). We put $(Y, Z) = (y\cos(wt), y\sin(wt))$. Here, the direction of gravitation is from $Z > 0$ to $Z < 0$. Now, the region of the drum is given by a circle $Y^2 + Z^2 \leq A^2$, and the region where $F_i^{ex} < 0$ for $y > 0$ and $F_i^{ex} > 0$ for $y < 0$ is given by another circle

$$Y^2 + (Z - \frac{g}{2w^2})^2 < (\frac{g}{2w^2})^2. \qquad (6.5)$$

In convenience, we name the former circle 'circle 1' and the latter 'circle 2'. The external forces work toward the center of circle 1 on each particle in circle 2, and toward the circumference of circle 1 in another region in circle 1. Now, the movement of particles in the region $Z < 0$ seems quite small compared to that in the region $Z > 0$ because the packing of particles in the $Z < 0$ region is more dense than that in the region $Z > 0$. Hence, we need to consider the movement of particles only in the region $Z > 0$. When $Aw^2 < g$, circle 2 covers up to the circumference of circle 1 in $Z > 0$ (Fig.6.5). It means that in most of region $Z > 0$, the external force works toward the center of the drum, so that small particles move toward the center of the drum. Because of the movement of small particles, low density region appears near the upper most position of the drum and large particles accumulate around there. On the contrary, when $Aw^2 > g$, circle 1 completely covers circle 2 (Fig.6.5). It means that small particles in circle 2 move toward the center of drum, and small particles out of circle 2 move toward the wall of drum. Then, since low particle density space appears around the circumference of circle 2, large particles accumulate there. The length between the center of circle 1 and the most far point on the circumference of circle 2 from the center of circle 1 is given by $\frac{g}{w^2}$. Hence, When $Aw^2 > g$, annular pattern the radius of which is estimated about $\frac{g}{w^2}$ is formed by large particles. Thus, the relation between the angular velocity of drum w and the radius $\bar{y}$ where large particles aggregate is given by

$$\bar{y} = A \cdots (w < (\frac{g}{A})^{\frac{1}{2}}) \qquad (6.6)$$

$$\bar{y} \sim \frac{g}{w^2} \cdots (w > (\frac{g}{A})^{\frac{1}{2}}). \qquad (6.7)$$

The phase inversion angular velocity w_c is given by $w_c = (\frac{g}{A})^{\frac{1}{2}}$.

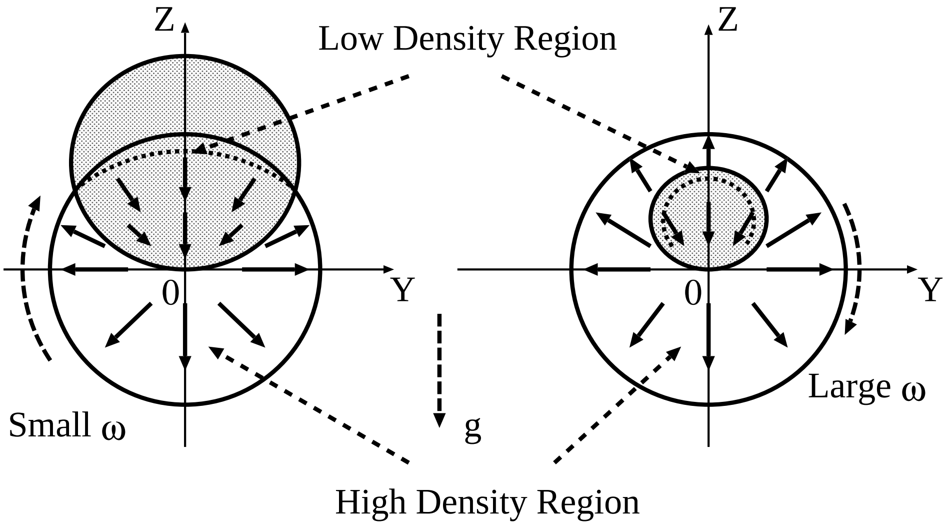

Figure 6.5: Direction of external force and distribution of particle density. White circles are 'circle 1', gray them are 'circle 2', and solid arrows indicate the direction of external force.

6.5 Summary

In this chapter, by use of simulations and brief analysis, we discussed the radial segregation and the axial segregation of granular mixtures which are almost completely packed in a horizontally rotating drum. Simulating a 2D horizontally rotating box, we reproduced two types of radial segregation patterns and the phase inversion between them, which have been found in previous experiments[122]. Furthermore, in this simulation, the global convection was observed to appear after the radial segregation pattern is formed, and this convection caused the axial segregation pattern. Moreover, by use of the competition between gravitational and centrifugal force which depends on the angular velocity of drum, we explained the phase inversion and found the critical angular velocity at which the phase inversion takes place. By this discussion, we also derivated the annularly segregated pattern reported in [122]. We expect that the clear annular pattern appears also in the simulation if we use the system which include larger number of particles. This is one of future issues. Moreover, in order to explain the phase inversion, we assumed that small particles, relatively, tend to move in the direction of external force and large particles move to the region of lower particle density. The justification of this assumption remains to be made.

Chapter 7

Dynamics of Two Equivalent Lanes Traffic Flow Model: Self-Organization of the Slow Lane and Fast Lane

Abstract: In this chapter, a simple two lanes traffic flow model using cellular automaton is investigated. As consequences of multi-lanes effects, following characteristic features of traffic flow appear. i)The fast and the slow lanes are spontaneously created. ii)The flow has non-unique values for a given density. iii)The hysteresis appears in the relation between flow and density.

7.1 Introduction and modeling of two lanes traffic flow

Recently, several traffic flow models have been proposed (see section 2.2). They investigated one lane traffic flow. However, real roads accompanied with sufficient number of observational data have more than one lane. Hence, in order to investigate the multiple lane effect, we simulate two lanes traffic flow models which include the effects of changing lanes.

We extend the one lane model by Nagel and Schreckenberg to that with two lanes ([76]). The system consists of cars and lanes. The number of lanes is two and cars number is varied as a control parameter. We number the cars in each lane in the order from the last to the top. Let x_n^i and v_n^i be, respectively, the position of the forefront and the velocity of the ith car at time step n in a lane, and X_n^j be the position of the forefront of the jth car in the other lane. The quantity d_n^i is the gap between the forefront of the ith car and the rear edge of the $i+1$th car i.e. $d_n^i = x_n^{i+1} - x_n^i - 1$ where 1 is the car length.

Velocity v_n^i takes one of five discrete values from 1 to 5, and the dynamical rules on each lane are equivalent, also the rules for changing lanes are set symmetrical between two lanes. The dynamics of the ith car from time step n to $n+1$ is determined by the set $\{x_n^i,\ v_n^i, v_n^{i+1},\ d_n^i,\ X_n^j\}$. Detailed rules are as follows;

I)When $v_n^i < d_n^i$; $x_{n+1}^i = x_n^i + v_n^i$ always holds, and $v_{n+1}^i = v_n^i + 1$ if $v_n^i < 5$, $v_{n+1}^i = v_n^i$ if $v_n^i = 5$. II)When $v_n^i = d_n^i$; $x_{n+1}^i = x_n^i + v_n^i$ always holds. If $v_n^{i+1} > v_n^i$, the car accelerates as $v_{n+1}^i = v_n^i + 1$ with probability P (accelerating probability), or, does not acelerate so that $v_{n+1}^i = v_n^i$ with probability $(1-P)$. For other cases $v_{n+1}^i = v_n^i$. III)When $v_n^i > d_n^i$; $x_{n+1}^i = x_n^i + d_n^i$ always holds. If $v_n^{i+1} < v_n^i$ and there are no jth cars satisfing $x_n^{i+1} = X_n^j$ with $X_n^j \le x_n^i + d_n^i < X_{n+1}^j$, then the ith car moves into the next lane without changing velocity ($v_{n+1}^i = v_n^i$). If $x_n^{i+1} = X_n^j$ and $X_n^j \le x_n^i + d_n^i < X_{n+1}^j$ holds for some jth car, the ith car decelerates as $v_{n+1}^i = v_n^i - 1$. On the other hand, if $v_n^{i+1} > v_n^i$ then $v_{n+1}^i = v_n^i$. For all other cases, $v_{n+1}^i = v_n^i - 1$.

7.2 Simulation

We simulate for the two cases, (1)$P = 0$ (deterministic case) (2)$P = 0.5$ (stochastic case). Here we define the car density ρ as (The number of occupied sites)/(The system size) and flow f as $\frac{\sum_i v^i}{(systemsize)}$ where (system size) means (length of road (= number of sites per one lane))$\times$(2 (= number of lanes)).

Firstly we discuss the case (1). Because the non-trivial relation between the flow and the density and the interesting dynamics of the system appears for $0.1 \leq \rho \leq 0.2$, we forcus on these densities regime. (The results for other densities are similar to those of the previous traffic flow models.(see section 2.2)) The boundary condition is set periodic and positions and velocities of cars are set random at the initial condition.

Figure 7.1 is a typical spatio-temporal evolution of the stationary states where dots mean individual cars and each car runs from the left to the right. Each stationary state is composed of a 'free flow region' and one type of 'cluster'. Here a 'free flow region' means the region in which every car has the maximum velocity ($v_n^i = v_f = 5$). Conversely, a 'cluster' means the region in which the gap between the successive two cars takes one value and equal to their velocity v_c less than the maximum velocity, that is $v_n^i = v_c = d_n^i$, and $v_c \leq 4$. The clusters are classified into 4 types according to v_c. In particuler if v_n^i is 1, the cluster is named as 'jam phase'. Moreover 'accelerating region' ('decelerating region') exists between a free flow region and the forefront (rear end) end of a cluster. In this region cars accelerate from v_c to v_f (decelerate from v_f to v_c) and $v_n^{i+1} = v_n^i + 1$ ($v_n^{i+1} = v_n^i - 1$).

Figure 7.2 shows relations of the density and the flow which are taken at 50000th time step after initial conditions with various densities of cars. In this diagram, some branches grow from the line $f = 5\rho$ for $0.1 < \rho < 0.2$. It means the flow is not determined as a unique function of the car density. This result is incompatible with that of the previous models (see section 2.2), yet it agrees with observational reports of real systems.([67],[68],[69]). Moreover each branch has its own spatial-temporal evolution of the system. For example, when the relation between the flow and the density belongs to the branch (a) in Figure 7.2, the system behaves like Figure 7.1 (a). This figure indicates that clusters which are composed of the cars which run with $v_n^i = v_c = 1$ appear in both lanes in a symmetric way. On the contrary, when the relation between flow and density belongs to the branch (b) in Figure 7.2, the system behaves like Figure 7.1 (b). This picture indicates that one of these lanes includes one type of cluster with $v_c = 3$, and the other lane is completely occupied by the free flow region. The only difference between two systems, (a) and (b), is the initial distribution of cars. In such a way, even if the dynamical rules between two lanes are symmetric, according to the small difference of initial conditions, two types of stationary states can appear. We call one of them 'symmetric state' (Fig.7.1 (a)) and the other 'asymmetric state' (Fig.7.1 (b)). Thus, the symmetric state or the asymmetric state appear for each branches in Figure 7.2. Figure 7.3 shows the relations between the car density and the average velocity difference between two lanes. Because the average velocity difference in the asymmetric state is larger than that in the

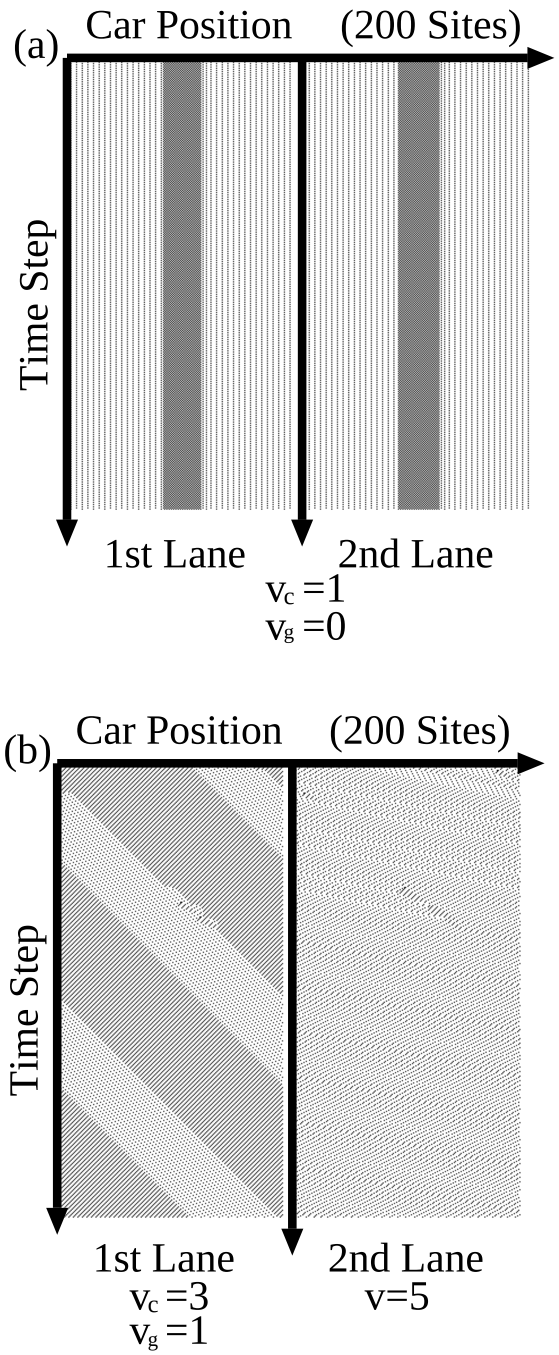

Figure 7.1: Two typical spatio-temporal evolutions of the stationary state for P=0. (a) The symmetric state. (b) The asymmetric state.

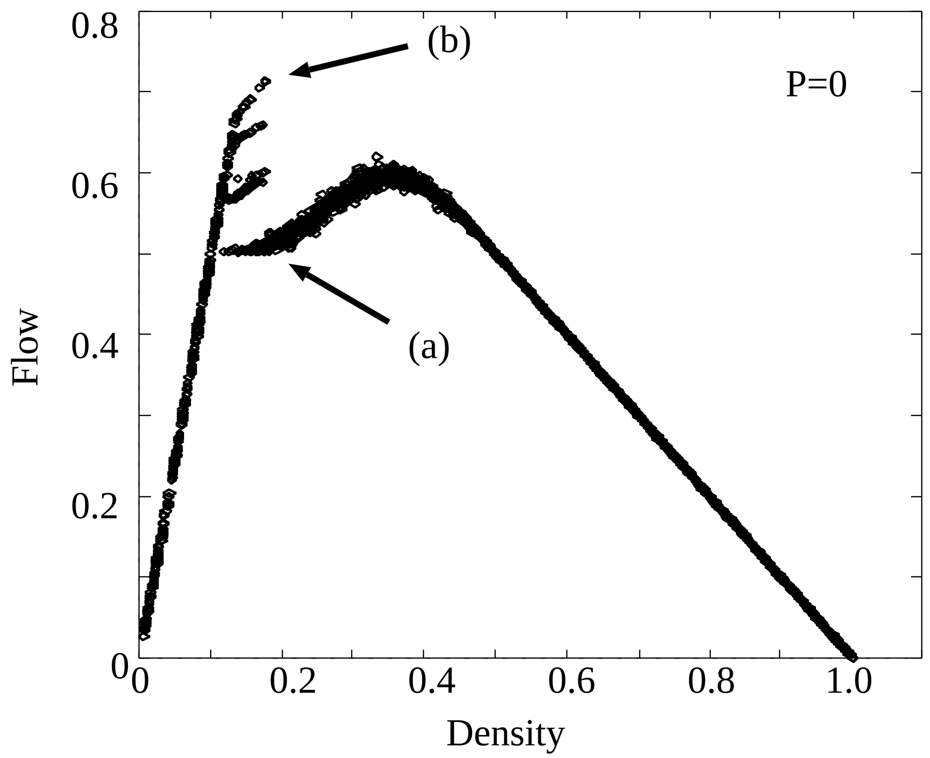

Figure 7.2: The relations between flow and density for P=0. Some branches exist for $0.1 \leq \rho \leq 0.2$.

symmetric state, Fig. 7.3 means that symmetric and asymmetric states coexist for the density $0.1 \leq \rho \leq 0.2$.

Investigating our results in more detail, we find the following facts. In Figure 7.1, each cluster has unique group velocity v_g which is given as $v_g = \frac{v_c - 1}{2}$. Here the cluster's group velocity is defined as the average velocity of the forefront of the cluster, and v_c is the individual car's velocity in the cluster. Similarly, if a free flow region exists in front of a cluster, the gap d between a car and its preceding in the free flow region is given by $d = 2v_f - v_c$. For $0.1 \leq \rho \leq 0.2$, the relation between the density ρ and the flow f for each state is nicely fitted by the following relations,(Fig.7.4).

i)When the symmetric state is realized,

$$f = \frac{1}{2} + v_g \rho. \tag{7.1}$$

ii)When the asymmetric state is realized,

$$f = \frac{3}{4} - \frac{1}{2(v_f + 1)} + v_g(\rho - \frac{1}{2(v_f + 1)}). \tag{7.2}$$

Here v_g is the group velocity of the cluster which finally survives in each stationary state

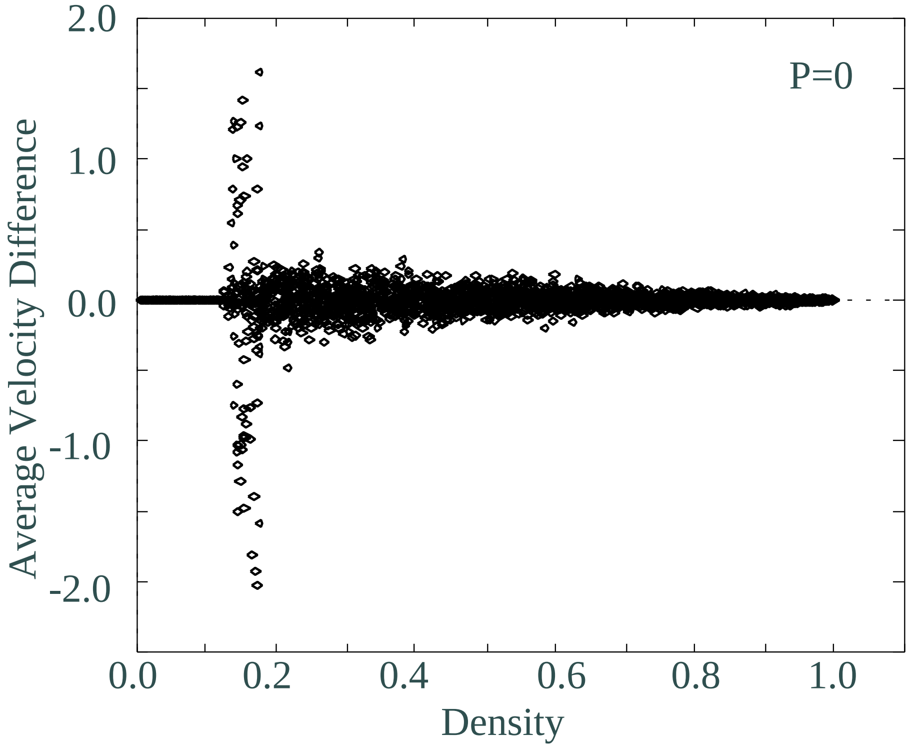

Figure 7.3: The relation of average velocity difference between two lanes and car density for P=0.

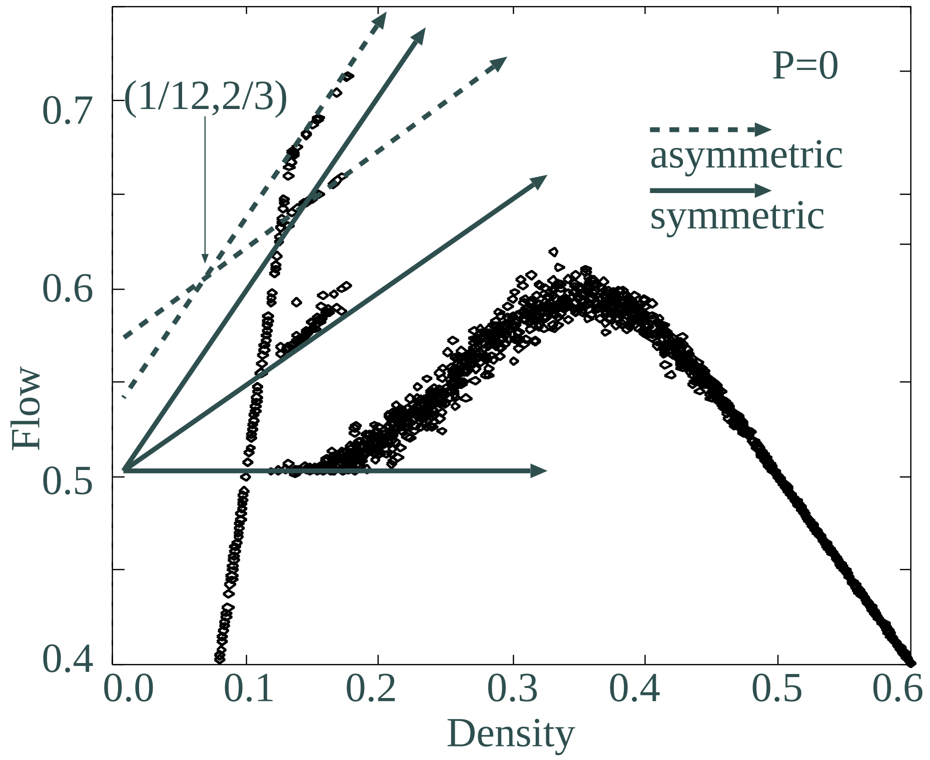

Figure 7.4: The relations between the flow and the density for P=0. Each branch is fitted by the equation (7.1) or (7.2) depending on its symmetry.

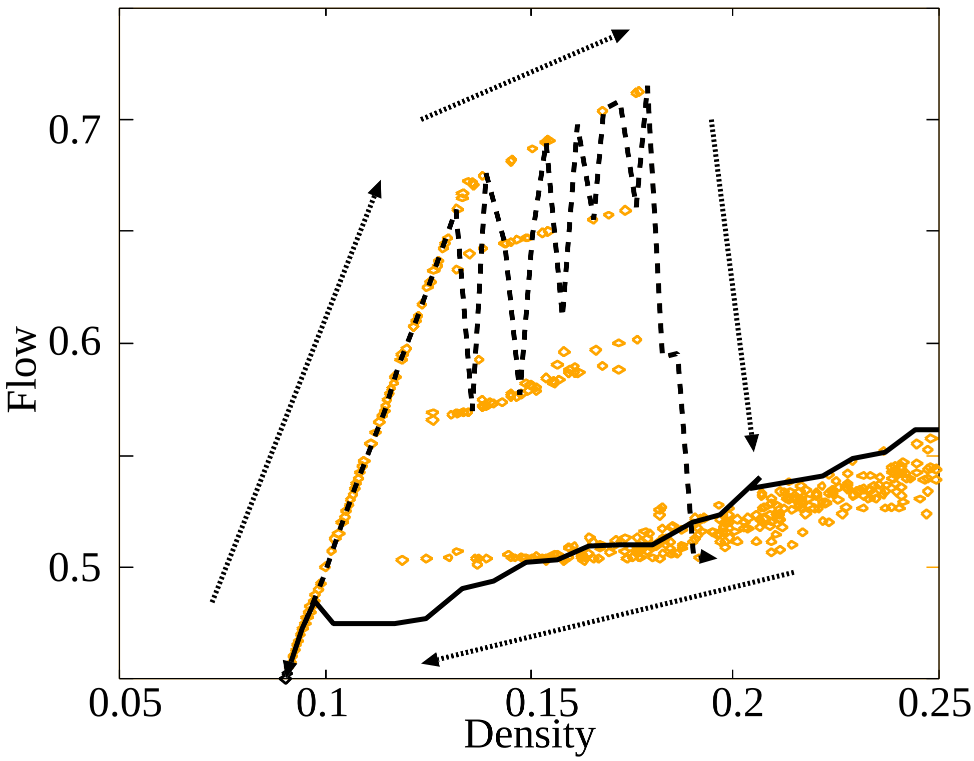

Figure 7.5: Hysteresis exists in the relation between flow and car density.

and $v_f = 5$. For both cases, considering the fact that v_g sensitively depends on the initial configuration and is not uniquely determined by ρ, f is a non-unique function of ρ. Moreover, when we add cars one by one at random positions so that the car density increases from 0.1 to 0.3, the flow changes along the upper branches in Figure 7.2. However, when we remove cars so that the car density decreases from 0.3 to 0.1, the ρ-f relation varies along the lowest branch of Figure 7.2. It means the hysteresis exists in the relation between the flow and the density. (Fig.7.5)

7.3 The relaxation processes to the symmetric state and the asymmetric state

Now, we discuss in what way the symmetric state and the asymmetric state appear and which type of clusters finally survives in the system. For this purpose, we consider the dynamics of clusters in the relaxation processes of the system. Consider the situation in which two isolated clusters named 'the preceding cluster' and 'the following cluster' are in the same lane. The rate of outgoing cars from the preceding cluster during unit time is $\frac{v_f}{d_{f(pr)}+1}$ and that from the following cluster is $\frac{v_f}{d_{f(fol)}+1}$. Here $d_{f(pr)} = 2v_f - v_{c(pr)}$ ($d_{f(fol)} = 2v_f - v_{c(fol)}$) and $v_{c(pr)}$ is the v_c of the preceding cluster ($v_{c(fol)}$ is the v_c of the following cluster). The gap d_{fc} between a forefront car of the free flow region lying between two clusters and the rear-end car of the preceding cluster satisfies $0 \leq d_{fc} \leq d_{f(fol)}$. If $v_f \geq d_{fc}$, d_{fc} turns to $v_{c(pr)}$ at the next time step, which means a leading car in the free flow region is absorbed into the preceding cluster. Hence, the rate of cars joining in the preceding cluster within unit time is given by $\frac{v_f}{d_{f(fol)}+1}$. From these facts if $v_{c(pr)} > v_{c(fol)}$, the number of outgoing cars is larger than that of cars absorbed into the preceding cluster. Hence the length of the preceding cluster continues to decrease and finally disappears. Similarly if $v_{c(pr)} < v_{c(fol)}$ the preceding cluster grows up, and if $v_{c(pr)} = v_{c(fol)}$ the length of the preceding cluster is kept unchanged. When $v_{c(pr)} < v_{c(fol)}$, the following cluster occasionally catches up with the preceding cluster before disappearing. Then, from the dynamical rule, the forefront car of the following cluster must decelerate from $v_{c(pr)}$ to $v_{c(fol)}$ when the car cannot change the lane. Hence, the cars in the following cluster will be incorporated into the preceding cluster and finally the following cluster disappears. Figure 7.6(a) indicates these processes. Secondly, consider the situation where two clusters in different lanes occupy neighboring regions of each other. When v_cs of neighboring clusters in different lanes are different, the forefront of the faster cluster moves faster than that of the slower cluster. However, the rear edges of them tend to correspond through changing lane of individual cars near the rear-most of these clusters. This means that by the contact of two clusters in different lanes, the car number of the slower cluster decreases and that of the faster cluster increases. Hence the slower cluster becomes shorter and shorter and finally disappears (Fig.7.6 (b)). In this way asymmetric states are spontaneously formed. (When v_cs of those clusters are the same, both of these clusters survive stably because of no interactions like the above. This means that symmetric states are stable.)

Finally we consider two scenarios for the nucleation of a new cluster. One is; When a cluster disappears, the accelerating region and the decelerating region contact with each other. Then a seed of new cluster is formed by two cars which have the velocity $v_c + 1$. Here v_c is the car velocity of the cluster which has just disappeared. From this seed, a new cluster with a group velocity faster than before is occasionally produced. The other is; When cars come in a lane from the next lane which has clusters, the local car density of the lane increases. Then a seed of a new cluster is occasionally created in the lane. However, such seeds of new clusters are unstable against weak fluctuations in the system because they are small. Hence, only when the number of incoming cars is sufficiently large, these seeds of new clusters will survive to grow up to form stable clusters.

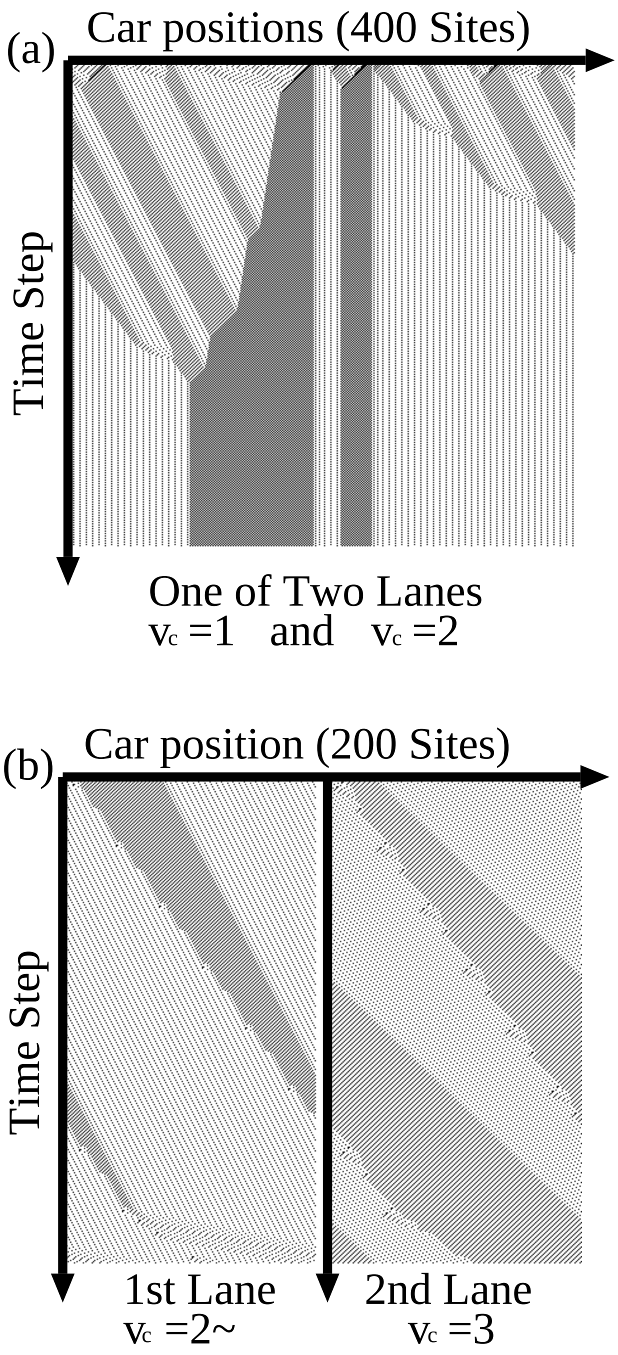

Figure 7.6: Spatio-temporal evolutions of relaxation processes. (a) The interactions of some clusters which appear in a lane. (b) The interactions of two clusters which appear in different lanes occupying neighboring regions of each other.

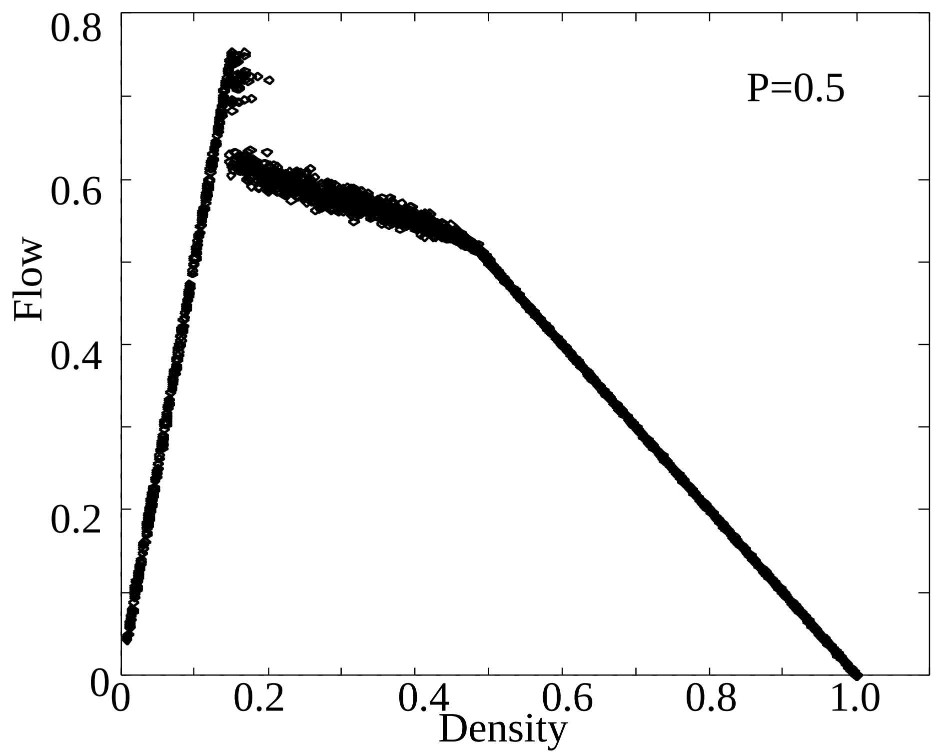

Figure 7.7: The relations between the flow and the car density for P=0.5. Similar to the case of P=0, the flow is not a unique function of the density.

In such ways, the system is relaxed to the asymmetric state which has larger flow compared to symmetric states, or, to the symmetric state according to the initial condition.

7.4 Results of stochastic model

Finally we study the cases where stochastic effects are introduced in the system. For $P = 0.5$, the behaviors of the system are qualitatively the same as that in the deterministic case ($P = 0$), however, in contrast to the case $P = 0$, v_g has negative values. (Fig.7.7 and Fig.7.8) Since the jam phase has the negative group velocity on real roads, the stochastic case seems more realistic than the deterministic one.

7.5 Summary

To summarize, some novel properties of traffic flow are reproduced using a two lanes traffic model. The fast lane and the slow lane are spontaneously formed even if the rules for

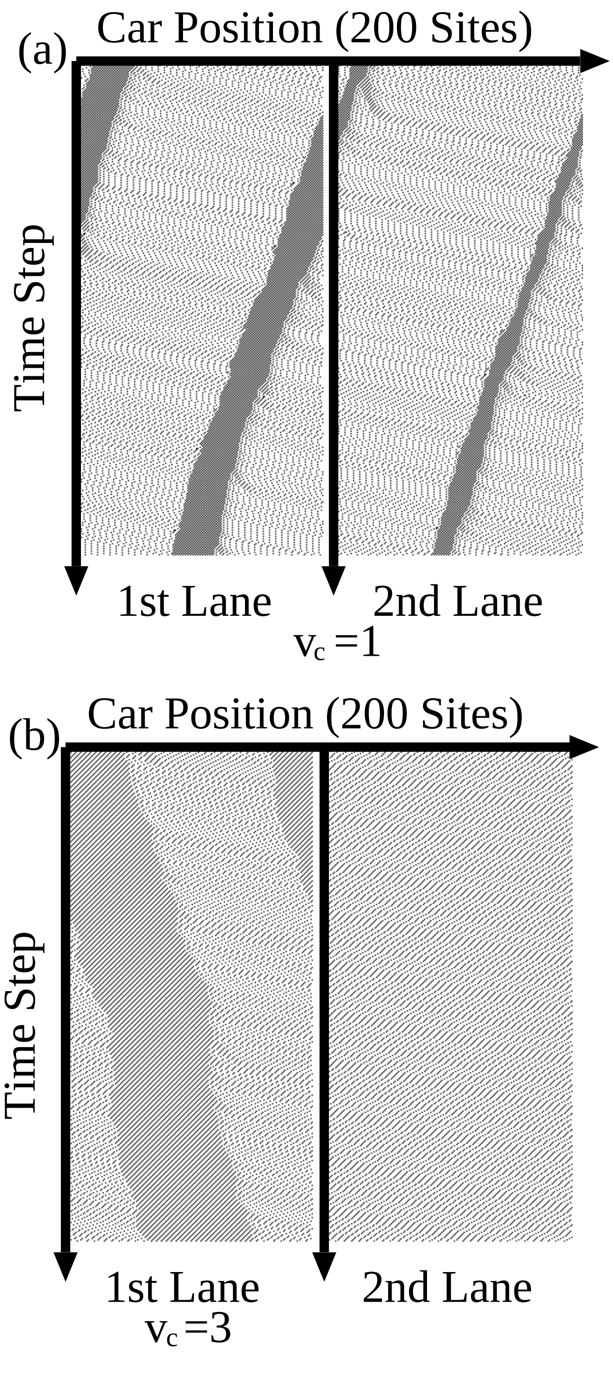

Figure 7.8: Two typical spatio-temporal evolutions of the stationary states for P=0.5. (a)A symmetric state. (b)An asymmetric states.

changing lane are set symmetric between two lanes though it is not always the case. In other words, two types of stationary states 'symmetric state' (Fig.7.1(a)) and 'asymmetric state' (Fig.7.1(b)) appear for the same density according to the initial condition. The flow of the stationary state is not a unique function of the density. According to the type of the stationary state and that of the clusters finally surviving in the system, the value of flow is determined. Moreover, the hysteresis is seen in the relation between flow and density.

Chapter 8

The Dynamics of Rule $184++C$: A Simple Model for the Complex Dynamics of Various Particles Flow

Abstract: In this chapter, a cellular automaton named Rule $184++C$ is proposed as a meta-model to investigate the flow of various complex particles. In this model, unlike the granular pipe flow and the traffic flow, not only the free-jam phase transition but also the free-intermediate, the intermediate-jam, and the dilute-dense phase transitions appear. Moreover, the freezing phenomena appear if the system contains two types of different particles.

8.1 Introduction

Recently, the flow of materials which consist of numerous discrete elements, for example the granular pipe flow, the traffic flow, and so on are investigated analytically, experimentally, and numerically (see section 2.2). They succeeded to explain various phenomena in these systems, e.g. the free-jam phase transition and the $1/f$ fluctuation of the local density[75, 86, 73, 88] However, it is a fact that the behavior of the granular pipe flow depends on materials filled in the pipe[66, 88]. For example, when long range interaction like Coulomb force, the inhomogeneity of softness, or the form of materials is taken into account, the system is expected to behave in a more complex manner. Now, to discuss such complex flows of various particles, we propose a simple meta-model which we name cellular automaton (CA) Rule $184 + +C$.

8.2 Explanation of Rule 184++C

The dynamics of Rule $184 + +C$ is based on that of Rule 184. The Rule 184 is taken as the simplest models of the traffic and granular flow. Here, in addition to the Rule 184 dynamics, as the $+C$ rules, we employ a set of simple rules for the velocity change of individual particles. The dynamics of each particle is described by the equations

$$v^i_{n+1} = F(v^i_n, v^{i+1}_n, d^i_n) \tag{8.1}$$

$$x^i_{n+1} = x^i_n + v^i_{n+1} \tag{8.2}$$

where we number the particles i from the upper part of the traffic stream to the downward. The quantities x^i_n and v^i_n are the position and the velocity of the ith particle at time step n, and d^i_n is the number of empty sites between ith and $i+1$th particles. The function $F(v^i_n, v^{i+1}_n, d^i_n)$ and the velocity v^i_n take 0 or 1, whereas $F(*)$ obeys the following rules;

I)When $d^i_n > 1$, $F(v^i_n, v^{i+1}_n, d^i_n) = 1$ always holds, and when $d^i_n = 0$, $F(v^i_n, v^{i+1}_n, d^i_n) = 0$ always holds.

II)When $d^i_n = 1$, $F(v^i_n, v^{i+1}_n, d^i_n)$ takes 0 or 1 which depends on the type of particle at i. Since v^i_n takes 0 or 1, the combination of (v^i_n, v^{i+1}_n) takes one of the following four patterns: $(0,0)$, $(0,1)$, $(1,0)$, $(1,1)$. For each combination, F takes the value 0 or 1. Hence, 16 types of rules for $F(v^i_n, v^{i+1}_n, d^i_n)$ (from $\{F(0,0,1) = 0, F(0,1,1) = 0, F(1,0,1) = 0, F(1,1,1) = 0\}$ to $\{F(0,0,1) = 1, F(0,1,1) = 1, F(1,0,1) = 1, F(1,1,1) = 1\}$) are considered . In other words, we define 16 types of particles according to the function $F(v^i_n, v^{i+1}_n, d^i_n)$. Now, we name the type of particles using the rule number C which is defined like Wolfram's method[81]

$$C = 2^0 F_C(0,0,1) + 2^1 F_C(0,1,1) + 2^2 F_C(1,0,1) + 2^3 F_C(1,1,1). \tag{8.3}$$

If the type of all particles is $C = 15$, the dynamics is the same as CA Rule 184. The boundary condition is set periodic and the position and the velocity of particles are set random at initial conditions. Hereafter, first, simulation results for pure systems in which all particles have the same C are introduced. Also the statistical and the dynamical properties for each stationary state are discussed. Second, the simulation of mixed systems in which various C particles coexist are discussed.

8.3 Simulation results of particles flow for each C

In Fig.8.1 are the typical fundamental diagrams which are the relations between particle density ρ and the flow f for each C. Here, ρ is defined as (the number of occupied sites by particles)/(the total number of sites), and f is defined as $< \sum_i v_n^i >$/(the total number of sites) where $< ... >$ means the time average. These fundamental diagrams are classified into the following three types: (i) the two phases type (2P-type) where $C = 0, 4, 5, 6, 8, 10, 12, 13, 14$,or 15, (ii) the three phases type (3P-type) where $C = 2, 9$ or 11, and (iii) the four phases type (4P-type) where $C = 1, 3$ or 7. The property of the steady state for the 2P-type is following; When ρ is low, all particles move at each time step, while slugs appear in the system if ρ is higher than a critical value. Here, the term 'slug' means an array of particles which do not move i.e., $v_n^j = 0$, $v_n^{j+1} = 0...$. Generally, slugs move backward in the traffic stream keeping the internal spatial pattern of them invariant. Each of them is kept by the balance between the incoming free-flow particles from the upward and the out-going free-flow particles to the downward. As such, with ρ increases, the phase transition from the 'free-flow state' (without slug) to the 'jam-flow state' (with slug) occurs. This property is qualitatively the same as known results of recent traffic and granular flow models (see section 2.2). In particular, the dynamics of the pure particle system with $C = 12$ ($F_{12}(0,0,1) = 0$, $F_{12}(0,1,1) = 0$, $F_{12}(1,0,1) = 1$, $F_{12}(1,1,1) = 1$) is equivalent to those of the deterministic traffic flow model proposed by Takayasu and Takayasu[75]. Differently from such systems, the 3P-type systems include the parameter region of the 'intermediate-flow state'. At the intermediate values of ρ between those corresponding to the free-flow state and those corresponding to the jam-flow state, the third state which is different from the former two states, takes place as shown in Fig.8.2 (b) and (e). Among the 3P-type systems, we discuss the pure systems with $C = 11$ and $C = 9$.

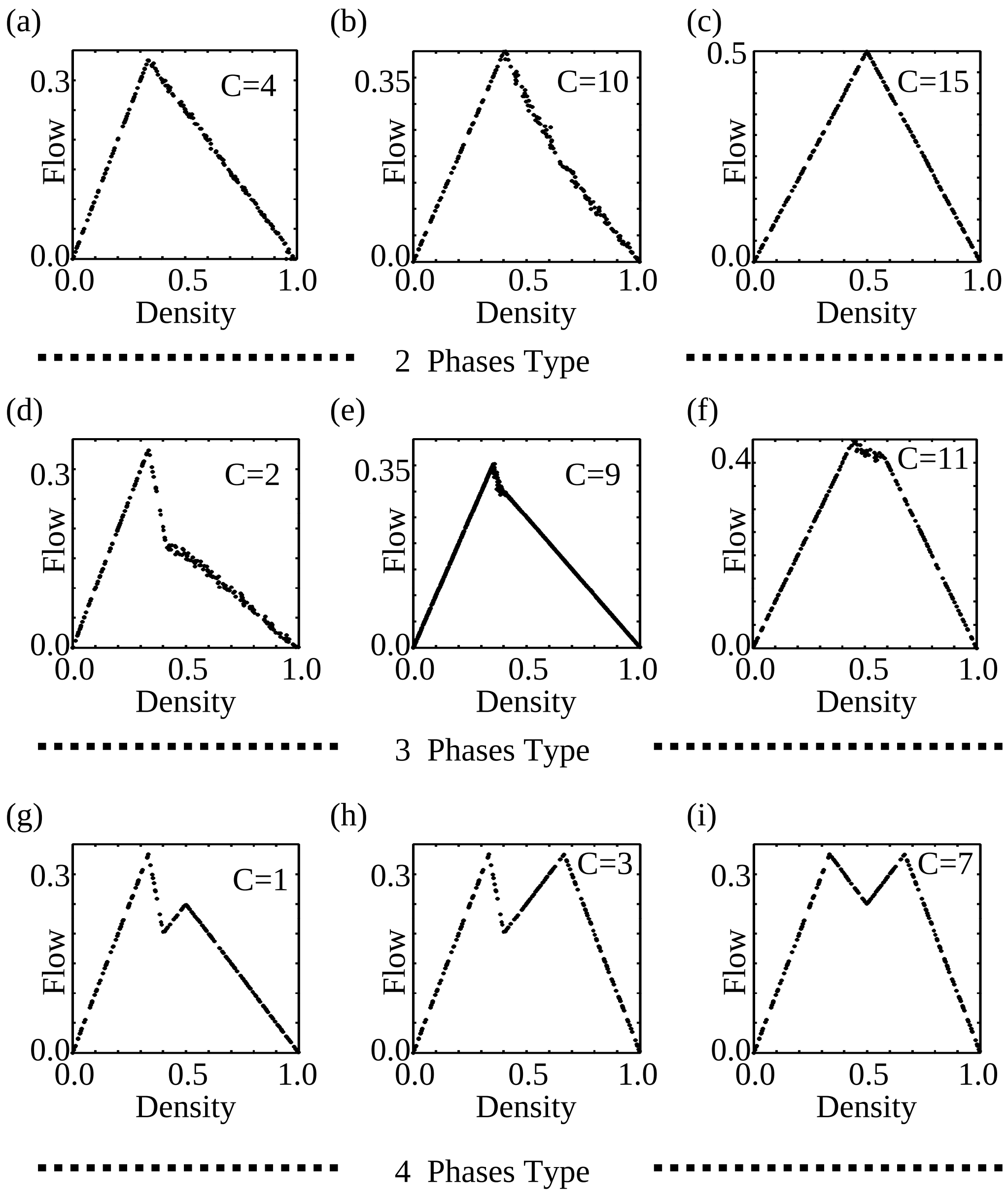

Figure 8.1: The typical fundamental diagrams for each C. There are three types of fundamental diagrams, (a)(b)(c) 2P-type, (d)(e)(f) 3P-type, and (g)(h)(i) 4P-type.

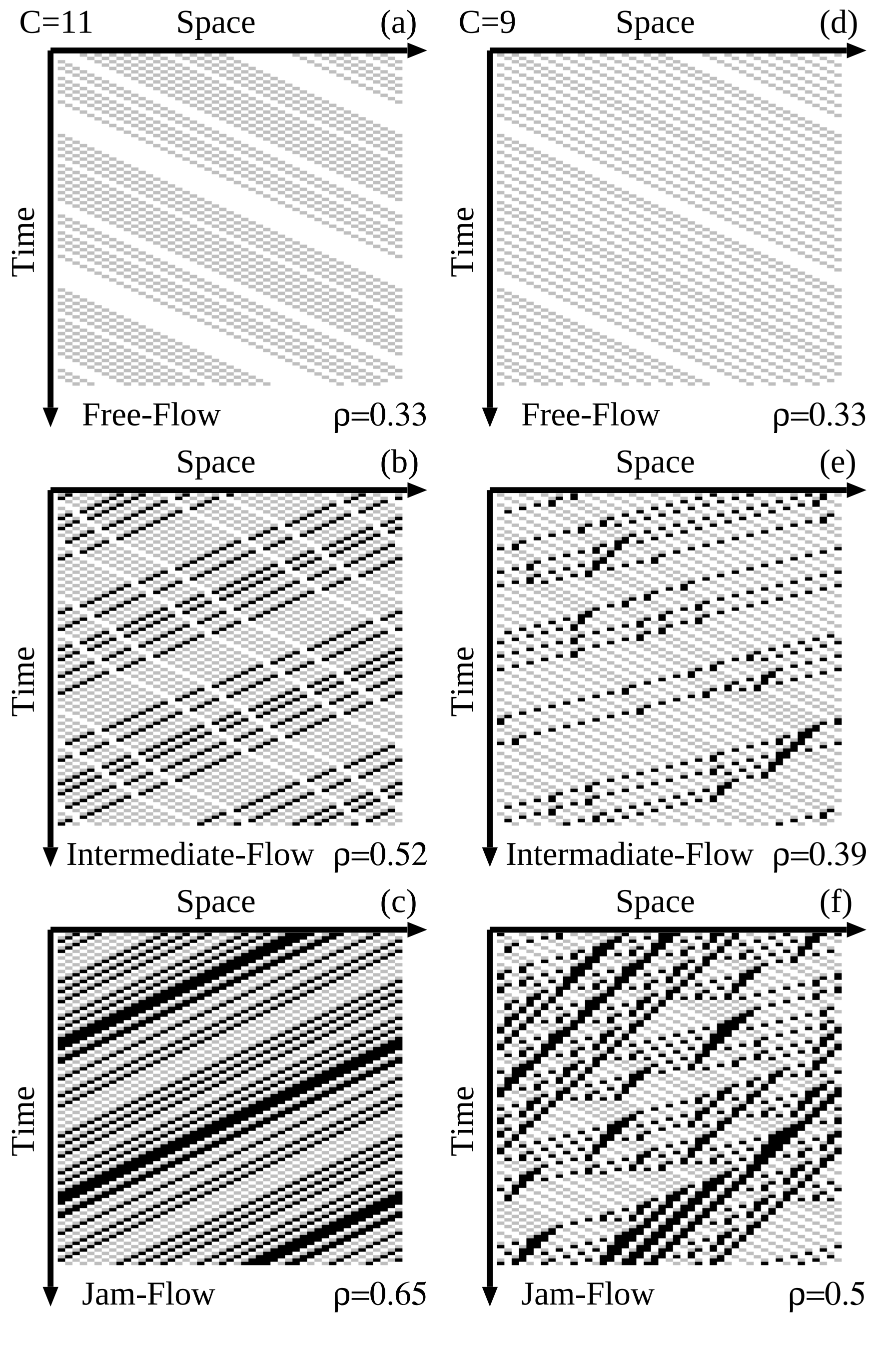

Figure 8.2: The space-time evolutions of the stationary states of $C = 11$ particles system ((a),(b),(c)), and $C = 9$ ((d),(e),(f)), where black dots means $v = 0$ particles and gray dots means $v = 1$ particles. They indicates, respectively, the free-flow ((a) and (d)), the intermediate-flow ((b) and (e)), and the jam-flow ((c) and (f)).

Fig.8.2 (a) (b) and (c) show the space-time evolutions of the stationary states of the pure systems with $C = 11$ ($F_{11}(0,0,1) = 1$, $F_{11}(0,1,1) = 1$, $F_{11}(1,0,1) = 0$, $F_{11}(1,1,1) = 1$). They, respectively, correspond to (a) the free-flow state (b) the intermediate-flow state, and (c) the jam-flow state. Here, dots represent individual particles where black dots indicate particles with $v = 0$ and gray dots indicate particles with $v = 1$. The behaviors of particles in (a) and (c) of Fig. 8.2 are qualitatively the same as the space-time evolutions of the 2P-type systems. In the free-flow state, more than two successive empty sites appear in front of some particles because the particle density is low. In the jam-flow state, slugs appear and survive stably because the particle density is high. Unlike these two kinds of states, stable slugs and more than two successive empty sites coexist in the intermediate-flow state (Fig.8.2(b)). Fig.8.2 (d) (e) and (f) show the space-time evolutions of the stationary states of the system with $C = 9$ ($F_9(0,0,1) = 1$, $F_9(0,1,1) = 0$, $F_9(1,0,1) = 0$, $F_9(1,1,1) = 1$). There are two types of slugs. Isolated slugs consist of only one particle j with $v_n^j = 0$, whereas large slugs consist of more than two particles with $v_n^j = 0$, $v_n^{j+1} = 0 \cdots$. Moreover, the backward propagation velocity of large slugs is slower than that of isolated ones. In the jam-flow state, (Fig.8.2.(f)), some large slugs remain stable in the system. In the intermediate-flow state, however, large slugs are unstable and repeat creation and annihilation irregularly in space and time(Fig.8.2(e)). The intermediate-flows are novel flow phase which have not been reported in the observation of real traffic flow or the granular flow. However, the space-time patterns like Fig.8.2(e) and (f) are similar to those of stochastic model[79] which describes the realistic traffic flow.

Next, we discuss the properties of the 4P-type systems. As an example, the system with $C = 3$ particles ($F_3(0,0,1) = 1$, $F_3(0,1,1) = 1$, $F_3(1,0,1) = 0$, $F_3(1,1,1) = 0$), is considered . In Fig.8.3 are typical space-time evolutions for several densities. When density ρ is low ($0 < \rho < \frac{1}{3}$), the free-flow state is realized, and when ρ increases ($\frac{1}{3} < \rho < \frac{2}{5}$), some slugs emerge, which means the free-jam transition take place like in the 2P-type systems (Fig.8.3 (a) (b)). Within slugs of the latter ρ region the gap d_n^j between particle j and $j+1$ is not zero, and repeats $d_n^j = 1$ and $d_{n+1}^j = 2$ by turn. Moreover, the spatial patterns in these slugs are periodic with the unit $v_n^j = 1$, $v_n^{j+1} = 0$, $d_n^j = 1$ and $d_n^{j+1} = 2$. In other words, these slugs are more dilute than what we see in the 2P-type and the 3P-type systems wherein gaps d are all 0. Thus, we name these slugs 'dilute slugs' and this state the 'dilute jam-flow state'. When $\rho = \frac{2}{5}$, the system is completely filled with dilute slugs. If ρ increases more ($\frac{2}{5} < \rho < \frac{2}{3}$), unlike the 2P-type systems, different type of slugs from the dilute slug appear (Fig.8.3 (c)). The spatial pattern of these slugs is periodic with the unit $v_n^j = 1$, $v_n^{j+1} = 0$,similarly with the dilute slug.

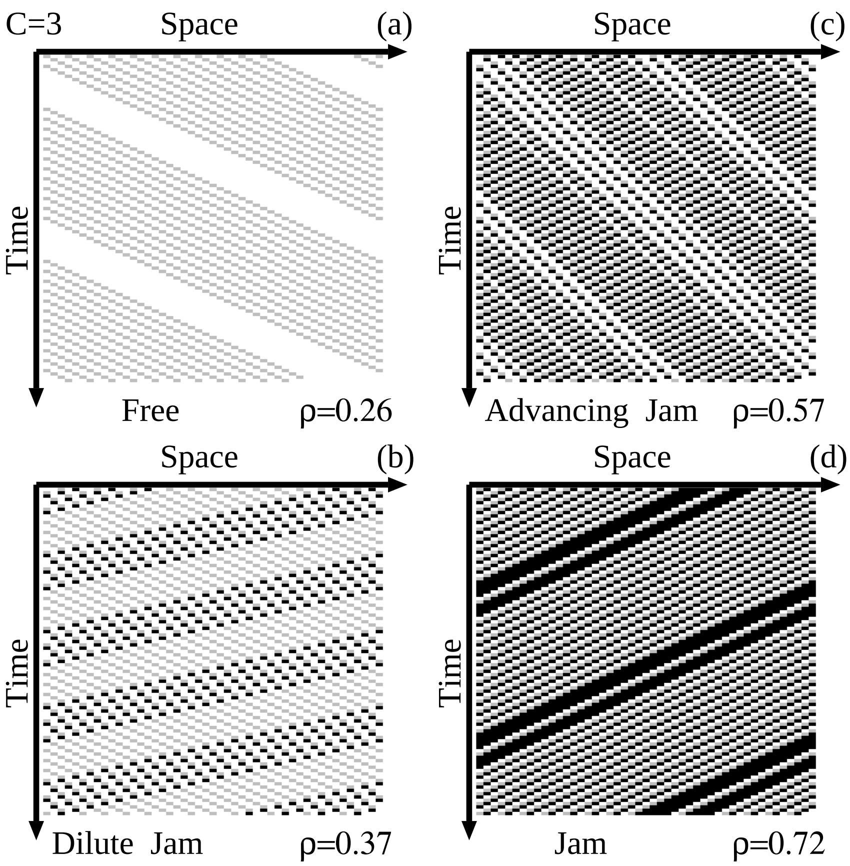

Figure 8.3: The space-time evolutions of the stationary states of $C = 3$ particles system, respectively (a) the free-flow, (b)the dilute jam-flow, (c) the advancing jam-flow, and (d) the hard jam-flow.

However, in this case, gaps in front of particles j and $j+1$ repeat the combinations ($d_n^j = 0$, $d_n^{j+1} = 1$) and ($d_{n+1}^j = 0$, $d_{n+1}^{j+1} = 1$) by turn. Moreover, the direction of movement of those slugs is downward, and these slugs are surrounded by dilute slugs. Now, we name these unusual slugs 'advancing slugs' and this state the 'advancing jam-flow state'. Moreover, in the advancing jam-flow state, the flow increases in proportion to ρ, in which sense the advancing jam-flow state is similar to the free-flow state.When the density increases more ($\rho > \frac{2}{3}$), slugs in which gaps d_n^j are zero appear (Fig.8.3 (d)), and the flow turns again to a decrease function of ρ. We call this state the 'hard jam-flow state'. As such, with the increase of ρ, three phase transitions: the free-dilute,the dilute-advancing, and the advancing-hard transition, appear. The characters of the first and the third are like what we see in the 2P-type systems because the flow sharply turns from the increasing function to a decreasing function at the transition point. So both of them are, in a wide sense, the free-jam transition. On the other hand, the second is the transition between the low density (dilute) regime and the high density (dense) regime. The similar transitions also appear for $C = 1$ and $C = 7$ systems. However, these transition have not been observed in the real traffic flow nor in the granular flow. They are considered to appear if the interactions between particles are more complex than those between drivers or between granular particles.

It is noted the 3P-type systems and the 4P-type systems , respectively, have common rules which hold among each of them. The 3P-type systems share the rules, $F_C(0,0,1) = F_C(1,1,1)$ and $F_C(1,0,1) = 0$. These rules mean that when a particle comes close to the preceding particle, repulsive force works between the two. On the other hand, the 4P-type systems share the rules ,$F_C(0,0,1) = 1$ and $F_C(1,1,1) = 0$. Here, the rule $F_C(0,0,1) = 1$ indicates that effective attractive force works on a particle when this particle and the preceding one are close each other and they are at standstill (i.e. $v_n^j = v_n^{j+1} = 0$). Similarly, $F_C(1,1,1) = 0$ indicates that effective resistance acts on a particle when this particle and the preceding one are moving. (i.e. $v_n^j = v_n^{j+1} = 1$). According to such effective forces, several flow phases mentioned above are realized.

So far we have discussed the statistical aspects of our systems. Now, we consider the dynamical properties of the above. For this purpose, apart from the classification of the system according to the fundamental diagrams, the space-time evolutions are divided in three types: i) The regular flow regime ($C = 0, 2, 3, 5, 8, 10, 11, 12, 14$ or 15); where space-time evolution is regular and the flow f is constant with time (As shown in Fig.8.2 (a) (b) (c), and Fig.8.3). ii) Oscillatory flow regime ($C = 1, 4, 7,$ or 13); where f oscillates with time. For example in the $C = 7$ particles system, the velocities of individual particles in

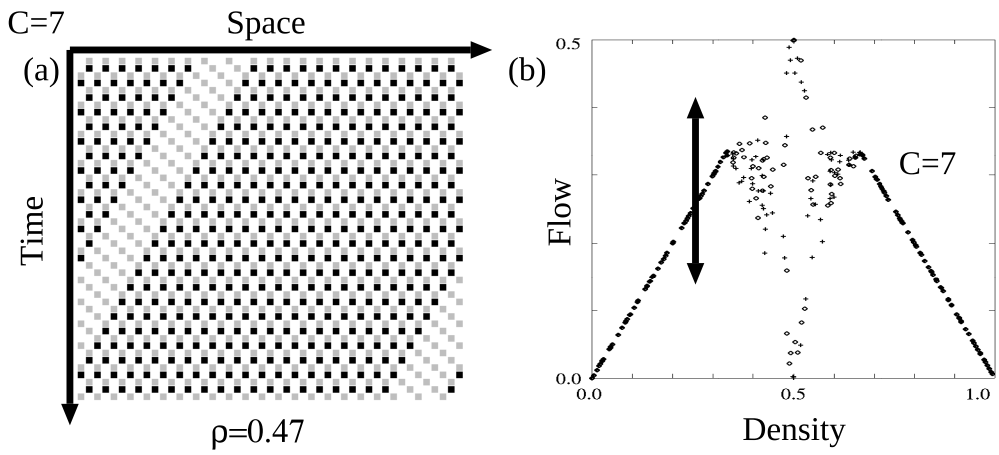

Figure 8.4: (a) The space-time evolutions of the stationary states of $C = 7$ particles system. (b) The fundamental diagram of $C = 7$ particles system at even time and odd time.

dilute slugs synchronize each other to oscillate between 0 and 1 (Fig.8.4 (a)). Therefore, f oscillates with large amplitude (Fig.8.4 (b)). iii) The chaotic flow regime($C = 6$, or 9); where the space-time evolution of particles and the time evolution of f are chaotic. (Examples are shown in Fig.8.2 (e), (f) and Fig.8.5 (a).) In particular, in the $C = 9$ particles system, the flow has $1/f$ fluctuation near the critical density ($\rho \sim 0.38$) of the phase transition between the intermediate-flow state and the jam-flow state (Fig.8.5 (b)). Both types of particles ($C = 6$ and $C = 9$) share the symmetric dynamics $F_C(0,0,1) = F_C(1,1,1) \neq F_C(0,1,1) = F_C(1,0,1)$. In other words only such systems obeying the symmetric rules behave chaotic if the system is pure.

8.4 Flow of mixed particles systems

Here, we focus on the mixed systems in which two types of particles are mixed and compare their behaviors to those of the pure systems. Figure 8.6 are two typical fundamental diagrams of two types of pure systems and that of mixed systems of these types of particles. Here, the ratio of two types of particles is 1 : 1. In most cases, the relations like Fig.8.6 (a) are realized. However, the relations like Fig.8.6 (a) also are realized for some cases. Here, the flow of the mixed systems is smaller than that of respective pure particles systems. To discuss them, as an example, we consider mixed systems with $C = 2$ and $C = 4$ particles. (For $C = 2$: $F_2(0,0,1) = 0$, $F_2(0,1,1) = 1$, $F_2(1,0,1) = 0$, $F_2(1,1,1) = 0$. For $C = 4$: $F_4(0,0,1) = 0$, $F_4(0,1,1) = 0$, $F_4(1,0,1) = 1$, $F_4(1,1,1) = 0$.) Figure 8.7 (a) is a

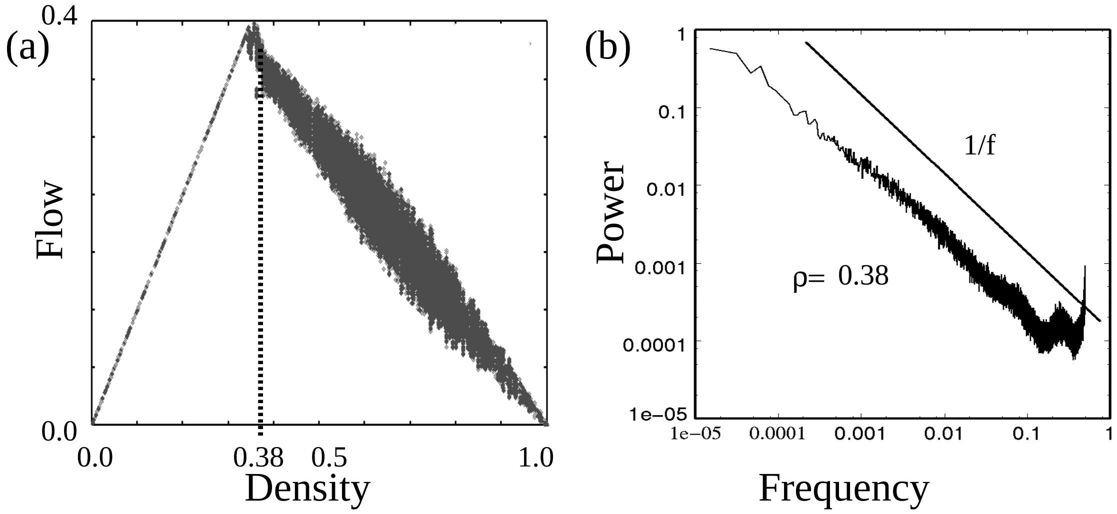

Figure 8.5: (a)The fundamental diagram at long time. (b)The power spectrum of the flow fluctuation of $C = 9$ particles system near the critical density ($\rho \sim 0.38$) of middle-jam transition.

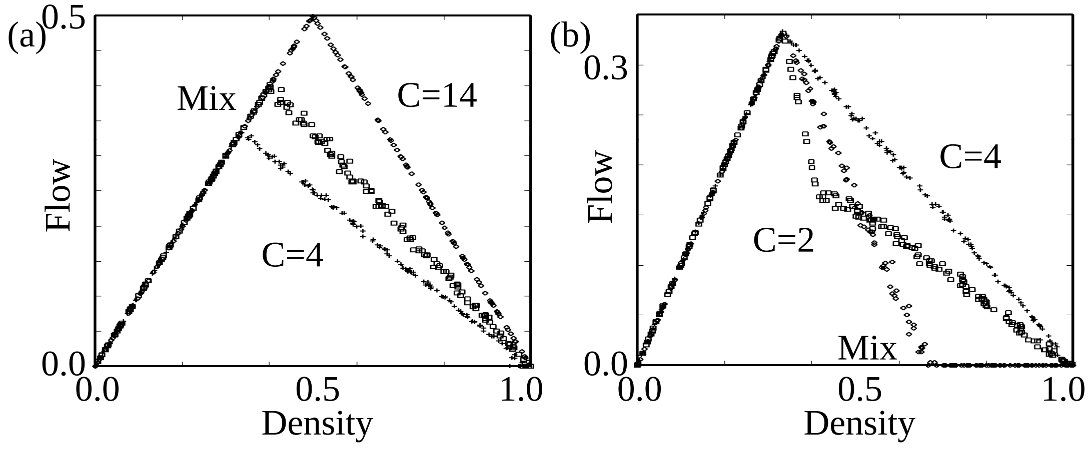

Figure 8.6: The typical fundamental diagrams of two pure particles systems and the mixed particles systems. The rate of particles is 1:1. (a) Normal type. (b)Decreasing type.

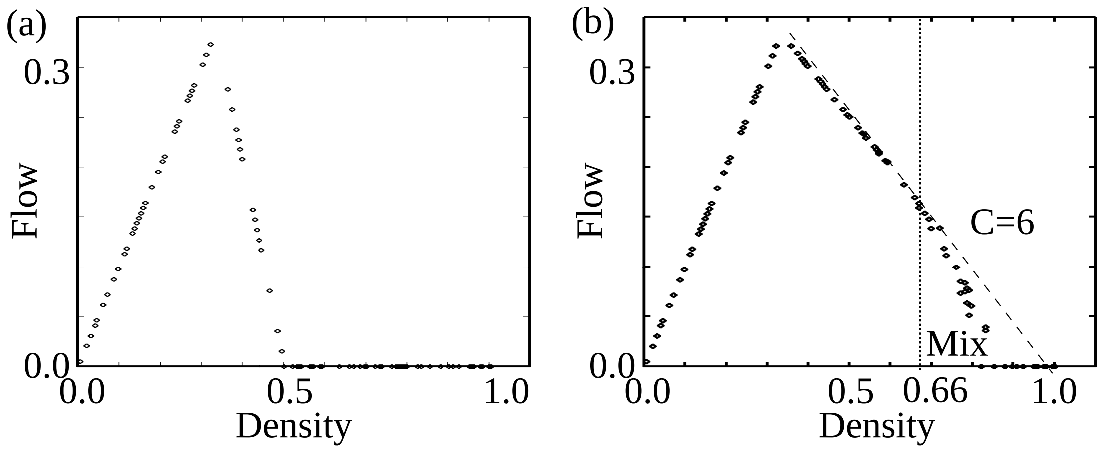

Figure 8.7: The fundamental diagrams of the system in which a $C = 4$ particle is added to pure $C = 2$ particles (a) and done to pure $C = 6$ particles (b).

fundamental diagram of the almost pure $C = 2$ particles system except one $C = 4$ particle inside. Compared to the pure $C = 2$ particles system, the flow is drastically little, and in particular, no flow for $\rho > 0.5$. The origin of such behavior is as follows. When ρ is sufficiently large, that is most of gaps d_n^i between successive particles are not larger than 1, the dynamics of each particle mainly obeys the function $F(v_n^i, v_n^{i+1}, 1)$. Once the $C = 4$ particle stops, this particle remains stationary if d_n^i remains not larger than 1. Moreover, in such d_n^i, the $C = 2$ particle remain stationary when the preceding particle dose not move. In other words, a $C = 4$ particle works as the coagulant of $C = 2$ particles, and changes characters of the whole system. Such relation appears also in different pairs of particles e.g., $C = 6$ and $C = 4$ for $\rho > 0.66$ (Fig.8.7 (b)), and $C = 2$ and $C = 12$. The mechanism of the freezing phenomena in these systems is qualitatively the same as the above. Moreover, $C = 4$ and $C = 12$ particles, both of which work as the coagulant in the above mixed systems, share common rules $F_2(0, 0, 1) = 0$ and $F_2(0, 1, 1) = 0$.

8.5 Summary

To summarize, various properties of complex materials flows are realized using a meta-model named CA Rule 184 + $+C$. Unlike the preceding CA models of the granular particles flow and the traffic flow, two types of novel relations between the density and the flow are realized in some types of particles systems. One is realized in the three phases type systems in which the free-intermediate and the intermediate-jam phase transitions occur with the increase of particle density. The other is observed in the four phases type systems in which not only the free-jam but also the dilute-dense transitions are realized. When these systems are classified from another point of view, there are three types of flow regimes: the regular flow regime, the oscillatory flow regime, and the chaotic flow regime. The particles in the chaotic flow systems share the the symmetric rules. The relationship between such symmetric rule and the chaotic behavior remains to be studied in the future. Moreover, when two types of particles are mixed in a system, one may work as a coagulant of the other. In other words the characters of pure particles systems drastically change by the addition of only a few number of different type of particles. The present CA rules are the straight extension of the rule 184. Hence, it is expected that some of $F_C(*)$ particle systems describe the behaviors of traffic flow or the granular flow more faithfully than the rule 184 whereas some of $F_C(*)$ will not. In practice, behaviors of a chaotic flow system ($C = 9$) are similar to those of stochastic model for the real traffic flow[79], and the dynamics of the systems with $C = 12$ is equivalent to that of the deterministic traffic flow model[75]. A more systematic discussion on what of above $F_C(*)$ are suitable for the model of real traffic flow is one of the future issues.

Chapter 9

Summary

In this thesis we discussed various types of phase transitions which appear in systems consisting of hard spheres or granular particles. We chose these systems because they are not only simple and easy to handle, but possess, as shown in the previous chapters, intrinsic characters of various many body systems in equilibrium and non-equilibrium states, with energy conservation and dissipation. Actually, using these simple systems as our computational models, we reproduced several types of phase transitions and peculiar dynamics in molecules systems like liquid-solid transition, glass transition, and those in granular materials under external force like transition between static and dynamics friction, size segregation, jam formation and so on.

If we care again the simplicity of these systems, in some cases with only two hard spheres, and take notice of the common features among them, we arrive at one conclusion that a dominant origin of all the above rich behaviors is the exclusion effect of finite volume particles with finite number. That means, if we carefully prepare the system with small number of particles with finite volume, a wide variety of nontrivial behaviors in various many body systems is easily investigated through simple models with rather a small number of particles with finite volume. This is, in a sense, opposed to the concept of thermo-dynamical limit which has conventionally been used in statistical mechanics to explain various phenomena in many body systems.

Yet, this is the resultant correspondence between the dynamics of finite systems and the statistics of infinite system with the lack of essential reasoning, the understanding of which should be one of the most attractive issue left for us. In parallel, treatments with simplified descriptions like present investigations of granular materials or hard spheres systems should be extended to more complex phenomena. For examples, chemical reactions in non-equilibrium states, motions of proteins, evolutions of ecological systems etc., are expected to be attacked in a similar way. We believe these investigations will offer a first step for the discoveries of universal mechanism which causes surprisingly rich behaviors of systems consisting of many simple elements.

Appendix A

Introduction of Distinct Element Method

In chapter 5 and 6, we used very simple particles model for each granular particle. This is because our main purpose of this thesis was to discuss various phenomena realized in systems with simple elements. However, we often need more realistic model of granular materials to simulate more sensitive phenomena or to discuss them quantitatively. Here, we show one of the realistic numerical method called Distinct Element Method (DEM), which simulates the more quantitative dynamics of granular materials than ours. The brief method used in chapter 5 and 6 was introduced by simplifying this realistic method.

In DEM model, translational motion and rotational motion of each particle are considered. Equations of each particle's motion are described as

$$m_i \ddot{\mathbf{x}} = \sum_{<i,j>} \theta(d - |\mathbf{x}_i - \mathbf{x}_j|)(\mathbf{F}_n^{ij} + \mathbf{F}_t^{ij}) + \mathbf{F}_{ex}, \tag{A.1}$$

$$I\dot{\omega} = \frac{d}{2} \sum_{<i,j>} \theta(d - |\mathbf{x}_i - \mathbf{x}_j|)(\mathbf{n} \times \mathbf{F}_t^{ij}), \tag{A.2}$$

where $\theta(x)$ is Heviside function, $\mathbf{x}$ and ω are the position and the angular velocity of the ith particle with diameter d and moment of inertia I. $\mathbf{F}_n^{ij}$ and $\mathbf{F}_t^{ij}$ are normal and tangential components of contact forces which are obtained by

$$\mathbf{F}_n^{ij} = \mathbf{n}\{F_{repl} - \eta_n \mathbf{n}(\dot{\mathbf{x}}_i - \dot{\mathbf{x}}_j)\} \tag{A.3}$$

$$\mathbf{F}_t^{ij} = \begin{cases} \mathbf{F}_{non-slip}^{ij} \cdots (F_{non-slip}^{ij} < \mu F_n^{ij}) \\ \mu \mathbf{t} F_n^{ij} \cdots (otherwise) \end{cases} \tag{A.4}$$

$$\mathbf{F}_{non-slip}^{ij} = \mathbf{t}\{F_{min} - \eta_t[\mathbf{t}(\dot{\mathbf{x}}_i - \dot{\mathbf{x}}_j) + \frac{d}{2}(\omega_i + \omega_j)]\} \tag{A.5}$$

where, η_n and η_t are viscosity coefficients of the normal direction and the tangential direction, and μ is the dynamical friction coefficient. Usually, $F_{repl} = -k_n x^a$ is used for repulsive force between particles as the function of the overlap length x with spring constant k_n. In most cases, $a = 1$ (Hook force) or $a = \frac{3}{2}$ (Heltz force) is used. For the tangential direction, the force $F_{min} = -k_t x'^b$ called Mindlin force is used where x' is the total shear displacement during one contact, and k_t is the virtual spring constant. When $a = 1$, the overlap length between two particles which contact with each other obeys the linear differential equation

$$\ddot{x} + 2\eta_n \dot{x} + 2k_n = 0. \tag{A.6}$$

By solving this equation, the elastic constant $e = exp(-\eta_n t_{col})$ $(t_{col} = \pi/(2k_n - \eta_n^2)^{\frac{1}{2}})$ is given as a constant value independent of collision velocity.

Still, some points to be improved are left in this method. For example, the number of parameters is large, and the determination of proper set of parameters for individual situations is not an easy task which is now on active discussion[143].

Bibliography

[1] W.W. Wood and J.D. Jacobson, J. Chem. Phys **27** (1957) 1207; B.J Alder and T.E Waiwright, J. Chem. Phys **27** (1957) 1208; J. Chem. Phys **33** (1960) 1439;

[2] E.Fermi, J.Pasta and S.Ulam, in Collected Papers of Enrico Fermi, edited by E.Segre,(University of Chicago, Chicago, 1965) vol.2 978

[3] B.J. Alder and T.E. Waiwright, Phys. Rev. **127** (1962) 359

[4] W.G. Hoover and R.M. Ree J. Chem. Phys **49** (1968) 3609

[5] S.T. Chui, Phys. Rev. Lett. **48**, (1982) 933

[6] J.M. Kosterlitz and D.J. Thouless, J. Phys. C **6** (1973) 1181 ;B.J. Halpin and D.R. Nelson, Phys. Rev. Lett. **41**, (1978) 121 ;A.P. Young, Phys. Rev. **B19** (1979) 8155

[7] B. Joos and M.S. Duesbery, Phys. Rev. Lett. **55**, (1985) 1997

[8] N.D. Mermin and H. Wagner, Phys. Rev. Lett. **17**, (1966) 1133

[9] K.J. Strandburg, Rev. Mod. Phys. **60** (1988) 161;

[10] J.A. Zollweg and G.V. Chester, Phys. Rev. **B46** (1992) 11186; J. Lee and K.J. Strandburg, Phys. Rev. **B46** (1992) 11191

[11] J.A. Zollweg, G.V. Chester and P.W. Leung, Phys. Rev. **B39** (1989) 9518;

[12] J.P Hansen and L Verlet, Phys. Rev. **184** (1969) 151;

[13] W. Vermhlen and N. Ito, Phys. Rev. E **51** (1995) 4325

[14] H.E Stanley, INTRODUCTION TO PHASE TRANSITIONS AND CRITICAL PHENOMENA. Clarendon Press Oxford (1971);J.M. Ziman, MODELS OF DISORDER. Syndics of the Cambridge Press (1979); W.G Hoover, Computational Statistical Mechanics, Elsevier Science B. V. (1991)

[15] see for example N.E Cusack, THE PHYSICS OF STRUCTURALLY DISORDERED MATTER , University of Sussex Press (1987), and references in this book.

[16] For example, G.M. Zaslavsky, Chaos in Dynamical System (Harwood Academic, New York, 1985)

[17] B.J. Alder, W.G. Hoover and T.E. Wainwright, Phys.Rev.Lett **11** (1963) 241; Dh. Dellago and H.A. Posch, Physica A **230** (1996) 364

[18] E. Dickinson and R. Parker, Chem. phys. Lett. **79** (1981) 3

[19] I. Moriguchi, AIP CONFERENCE PROCEEDINGS **519** (2000) 244 "Weighted-density functional theory: Application to freezing of polydisperse hard-spheres" Bulletin of Tohwa University, 1999, Vol.25, 237; H.Xu and M.Baus, Phys. Rev. E **61** (2000) 3249

[20] R.J.Speedy Physica A **210** (1994) 341

[21] For example, Science **267** (1995) 1924,1935,1939,1945 and 1947 M.D. Edinger, C.A. Angell and S.R. Nagel, J. Phys. Chem. **100** (1996) 13200

[22] J. Matsui, T. Odagaki and H. Hiwatari, Phys. Rev. Lett **73** (1994) 2452; C. Monthus and J.P. Bouchaud, J.Phys. A **17** (1984) 5915;

[23] T. Muranaka and Y. Hiwatari, Phys, Rev. E. **51** (1995) 2735; R. Yamamoto and A. Onuki, Phys, Rev. E. **58** (1998) 3515; W. Kob et al., Phys. Rev. Lett **79** (1997) 2827 K.Kim and R.Yamamoto, Phys. Rev. E, **61**, (2000) 41

[24] K. Shinjo, Phys. Rev. B, **40**, (1989) 40

[25] R.K.Bowles R.J.Speedy Physica A **262** (1997) 76

[26] L.Santen and W.Krauth, Nature (London) **405** (2000) 550

[27] M.Matsuo, (private communications)

[28] E.Leutheuβer, Phys. Rev. A, **29**, (1984) 2765; U. Bengtzelius, W.Götze and A.Sjölander, J.Phys. A **17** (1984) 5915; J. Bosse and Y. Kaneko, Phys. Rev. Lett **74** (1995) 4023; K. Kawasaki, Nonequilibrium and phase transition. (in japanese) Asakura (2000)

[29] Y Aizawa, Prog. Theor. Phys.,**71** (1984) 1419; G Benettin, Prog. Theor. Phys. Suppl, **116** (1994) 207; G Benettin, L Galgani and A Giorgilli Phys. Lett **A 120** (1987) 23; Y.Y Yamaguchi and T Konishi, Prog. Theor. Phys.,**99** (1998) 139; Y.Y Yamaguchi, Moderately Chaotic Hamiltonian System: Structure and Motion in High-dimensional Phase Space, Ph.D thesis of Nagoya University; L Meza-Montes and S E. Ulloa, Phys,Rev. E. **55** (1997) 6319

[30] Dh. Dellago and H.A. Posch and W.G. Hoover, Phys,Rev. E. **53** (1996) 1485

[31] R.Tehver, F.Toigo, J.Koplik and J.R.Banavar, Phys. Rev. **E57** (1998) 57

[32] H.Hayakawa, H.Nishimori, S.Sasa, Y-h. Taguti, Jpn. J. Appl. Phys. **34** (1995), 397

[33] H.M.Jeager and S.R.Nagel, Science **255** (1990) 1523

[34] L.P. Kadanoff, Rev.Mod.Phys **71** (1999) 435

[35] S. Hidaka, et.al, The Introduction of Simulations of Granular Materials (Huntai Kougaku Kai, in Japanese 1998)

[36] I.Goldhrirsch and G.Zanetti, Phys. Rev. Lett. **70**, 1619(1993).

[37] P.Evesque and J.Rajchenbach, Phys. Rev. Lett. **62**,(1989) 44.

[38] F.Melo, P.B.Umbanhowar and H.L.Swinney Phys. Rev. Lett. **75** (1995) 3838 ;P.B.Umbanhowar F.Melo and H.L.Swinney Nature. **382** (1996) 793

[39] C.Bizon, M.D.Shattuck, J.B.Swift, W.d.McCormic and H.L.Swinney Phys. Rev. Lett. **80** (1998) 57

[40] K.M.Aoki and T.Akiyama Phys.Rev.E **77**, (1996) 4166

[41] S.C. Venkataramani and E. Ott, Phys. Rev. Lett. **80**, (1998) 3495

[42] P.A. Cundall and O.D.L. Stark, Geotechnique **29**, (1979) 47 ;Y.-h.Taguchi, Bussei Kenkyuu **61**, (1993) 1

[43] Y.-h.Taguchi, Phys. Rev. Lett. **69**, (1992) 1367 ;J.A.C.Gallas, H.J.Herrmann and S.Sokolowski Phys. Rev. Lett. **69**, (1992) 1371

[44] E.L.Grossman, Phys.Rev.E **56** (1997) 3290.

[45] K.M.Aoki, T.Akiyama, Y,Maki and T.Watanabe Phys.Rev.E **54** (1996) 874.

[46] K.M.Aoki and T.Akiyama Phys.Rev.E **58**, (1998) 4629.

[47] K.Hamada, (Master Thesis Doshisya Univ. 1997)

[48] T.Ohtuski, Y.Takemoto, T.Hata, S.Kawai and A.Hayashi, Int.j.Mod.Phys. B **7** (1993)1865

[49] Y.-h.Taguchi and H.Takayasu, Europhys.Lett **30**, (1995) 499.

[50] Y.Murayama and M.Sano, J.Phys.Soc.Jpn **67** (1998) 1826

[51] Y.-h.Taguchi Europhys.Lett **24**, (1993) 203.

[52] T. Shinbrit, D. Khakhar, J.J. McCarthy and J.M. Ottino, Phys. Rev. Lett. **79**, (1997) 829.

[53] H.Hayakawa and D.C.Hong, Phys. Rev. Lett. **78**, (1997) 2764. Daniel C. Hong, Su Yue, Phys. Rev. E **58**, (1998) 4763

[54] Y.DU, H.Li and K.P.Kadanoff Phys. Rev. Lett. **74**, (1995) 1268

[55] E.L.Grossman, T.Zhou and E.Ben-Naim Phys.Rev.E **55**, (1997) 4200.

[56] M.Isobe and H.Nakanishi, J.Phys.Soc.Jpn. **68**, (1999) 2882.

[57] A.Kudroll, M.Wolpert, and J.P.Gollub, Phys. Rev. Lett. **78**, (1997) 1383.

[58] R.Ramirez, D.Risso and P.Cordero, Phys. Rev. Lett. **85**, (2000) 1230.

[59] T.S.Komatu, J.Phys.Soc.Jpn. **69**, (2000) 5.

[60] T. S. Komatu and H.Hayakawa Phys.Lett. A **183** (1993) 56.

[61] T.Ooshida and T.Kawahara Phys.Rev.E **56**, (1997) 511.

[62] H.Hayakawa and K.Ichiki, Phys.Rev.E **51**, (1995) 3815.

[63] K.Ichiki and H.Hayakawa, Phys.Rev.E **52**, (1995) 658.

[64] K.Ichiki and H.Hayakawa, Phys.Rev.E **57**, (1998) 1990.

[65] T.Musha and H.Higuchi Jpn.J.Appl.Phys **15** (1976) 1271.

[66] S.Horikawa, T.Isoda, T.Nakayama, A.Nakahara and M.Matsushita, Physica **A233**(1996),699 ;A.Nakahara and T.Isoda: Phys.Rev.E **55**(1997) 4264.

[67] D.Helbing, Phys.Rev.**55** (1997) 25.

[68] B.S.Kerner and H.Rehborn, Phys.Rev.lett, **79** (1997) 4030.

[69] D.Huzita, Koutuu genshou to Koutuu youryou (Gijutushoin,1987).

[70] S. Yukawa and M. Kikuchi, Int.J.Mod.Phys. C **11** (2000) 221

[71] S.Yukawa, M.Kikuchi and S.Tadaki, J.Phys.Soc.Jpn.**63** (1994) 3609.

[72] S.Yukawa and M.Kikuchi, J.Phys.Soc.Jpn.**64** (1995) 35.

[73] S.Yukawa and M.Kikuchi, J.Phys.Soc.Jpn.**65** (1996) 916.

[74] M.Fukui and Y.Ishibashi: J.Phys.Soc.Jpn. **65** (1996) 1868.

[75] M.Takayasu and H.Takayasu, Fractals **1** (1993) 860.

[76] K.Nagel and M.Schreckenberg, J.Phys.I.France **2** (1992) 2221.

[77] K.Nagel and H.J.Herrmann, Physica **A199** (1993) 254.

[78] K.Nagel and M.Paczuski, Phys.Rev.**E51** (1995) 2909.

[79] M.Schreckenberg, A.Schadschneider, K.Nagel, N.Ito, Phys.Rev.**E51** (1995) 2939.

[80] M.Rickert, K.Nagel, M.Schreckenberg and A.Latour, Two Lane Traffic Simulations using Cellular Automata (preprint,1996).

[81] S.Wolfram: "Cellular Automata and Complexity",Addison-Wesley. Reading. Massachusetts. (1994)

[82] G.F.Newell, Oper.Res.**9** (1961) 209 ;G.B.Whitham, Proc.R.Soc.London,Ser A **428** (1990) 49

[83] M.Bando, K.Hasebe, A.Nakayama, A.Shibata, and Y.Sugiyama, Phys.Rev.**E51**, 1035 (1995).

[84] B.S.Kerner and P.Konhäuser: Phys.Rev.E **50**(1994) 54.

[85] T. S. Komatu and S.-i. Sasa: Phys.Rev.E **52** (1995) 5574. ;T. S. Komatu, PhD Thesis(Tohoku University, 1996)

[86] G.Peng and H.J.Herrmann: Phys.Rev.E **51**(1995) 1745.

[87] Y.Sugiyama and H.Yamada, Phys.Rev.E55, 7749 (1997).

[88] O.Moriyama, N,Kuroiwa, M,Matsushita, and H,Hayakawa: Phys.Rev.lett,**80**(1998)2833.

[89] H.Hayakawa and K.Nakanishi, Phys.Rev.E **57** (1998) 3839. ;H.Hayakawa and K.Nakanishi, Prog.Theor.Phys.Suppl.**130** (1998) 57

[90] S.Wada and H.Hayakawa J.Phys.Soc.Jpn. **67** (1998) 763.

[91] T.Takaai and H.Hayakawa Proceedings of Symposium on Simulation of Traffic Flow (1997) 33.

[92] Y.Igarashi, K.Itoh and K.Nakanishi, pat-sol/9810007.

[93] K.Hasebe, A.Nakayama and Y.Sugiyama, preprint

[94] T.Nagatani, Phys.Rev.E **58** (1998) 4271.

[95] N. Mitarai and H. Nakanishi, J. Phys. Soc. Jpn. **68** (1999) 2475; Phys. Rev. Lett. **85** (2000) 1766

[96] S.Tadaki, M.Kikuchi, Y.Sugiyama and S.Yukawa, J.Phys.Soc.Jpn **67** (1998) 2270.

[97] K.Nishinari and D.Takahashi, J.Phys.A **31** (1998) 5439. Flow (1998) 33.

[98] T.Nagatani, Phys.Rev.**E45**,(1993) 3290 .

[99] S.Tadak and M.Kikuchi: Phys.Rev.E**E50** (1994) 4564.

[100] S.Tadaki and M.Kikuchi: J.Phys.Soc.Jpn.**64** (1995) 4504.

[101] T.Horiguchi and T.Sakakibara, Physica A **252** (1998) 388.

[102] M. Takayasu, H. Takayasu and T. Sato, Physica A **233** (1996) 824.

[103] C.Williams, Powder Technol. **15** (1976) 245 et.al ;A.Rosato, K.J.Strandburg, F.Prinz and R.H.Swendsen, Phys. Rev. Lett. **58**, 1038 (1987) ;R.Jullien and P.Meakin, Phys. Rev. Lett **69**, 640 (1992)

[104] J.Duran, J.Rajchenbach and E.Clement, Phys. Rev. Lett **70**, 2431 (1993)

[105] G.C.Barker, A.Mehta and M.J.Grimson, Phys. Rev. Lett **70**, 2194 (1993)

[106] J.B.Knight, H.M.Jaeger and S.R.Nagel, Phys. Rev. Lett. **70**, 3278 (1993).

[107] D.Brone and F.J.Muzzio, Phys. Rev. E. **56**, 1059 (1997).

[108] H A.Makse, S.Havlin, P.R. King and H.E.Stanley, Nature 6623 (1997) 379 ;H A.Makse, P.Cizeau and H.E.Stanley, Phys. Rev. Lett. **78**, 3298 (1997).

[109] M. Noguchi, Master Thesis at Ibaraki University (in Japanese. 2000)

[110] Savage and Lun, J Fluid Mech **189**, 311 (1988).

[111] J.T.Jenkins NATO ASI Series, Series E: Applied Siences - Vol.350 Physics of Dry Granular Media (H.J.Herrmann, J.-P.Hovi, and S.Luding) 645

[112] O.Zik, D.Levine, S.G.Lipson, S.Shtrikman and J.Stavans, Phys. Rev. Lett. **73**, 644 (1994); ;Y.Oyama, Bull. Inst. Phys. Chem. Res. Jpn. Rep. **18**, 600 (1939). ;M.B.Donald and B.Roseman, British Chem. Eng. **7**, 749, 823 (1962). ;S.Das Gupta, D.V.Khakhar and S.K.Bhatia,Chem. Eng. Sci. **46**, 1531 (1991): Powder Technol. **67**, 145 (1991). ;M.Nakagawa, Chem. Engg. Sci. **49**, 2544 (1994). ; G.H.Ristow and M.Nakagawa, Phys. Rev. E **59**, 2044 (1999). ; K.M.Hill and J.Kakalios, Phys. Rev. E **49**, 3610 (1994); Phys. Rev. E **52**, 4393 (1995); ;K.M.Hill, A.Caprihan and J.Kakalios, Phys. Rev. Lett. **78**, 50 (1997). ;E.Clement, J.Rajchenbach and J.Duran, Europhys. Lett. **30**, 7 (1995). ;F.Cantelaube and D.Bideau, Europhys. Lett. **30**, 133 (1995).

[113] K.Ueda and R.Kobayashi, Proceedings, 1997 Meeting of Japan Society of Fluid Mechanics (1997 - 7) 413.

[114] T.Yanagida, Phys. Rev. Lett. **82**, 3488 (1999)

[115] S.Sakamoto, Jounal of the Society of Powder Technology Jpn Vol**35** 7 (1998) 508

[116] S.Puli and H. Hayakawa, Physica A **270**, 115 (1999).

[117] B.Levitan, Physica A **249**, 386 (1998).

[118] L.Prigozhin and H.Kalman, Phys. Rev. E **57**, 2073 (1998).

[119] J.Rajchenbach, Phys. Rev. Lett. **65**, 2221(1990).

[120] J H.Bytnar, J.O.G Parent, H.Henein and J Iyengar, International Journal of Powder Metallugy. **31**, 37(1995).

[121] M.Nakagawa, NATO ASI Series, Series E: Applied Siences - Vol.350 Physics of Dry Granular Media (H.J.Herrmann, J.-P.Hovi, and S.Luding) (1998)703

[122] M.Nakagawa, (To appear in Powder Technology)

[123] K.M. Aoki and N.Ito Phys. Rev. **E54** (1996) 1990

[124] $t_{col} = \pi/(2k - \eta^2)^{\frac{1}{2}}$, $e = exp(-\eta t_{col})$[43]

[125] For example, H. Matsukawa, Mathematical Science **433** (2000) 41 (in Japanese) and references there; V. Zaloji, M. Urbakh and J. Klafter, Phys. Rev. Lett. **81** (1998) 1227; E. Granato and S.C. Ying, Phys. Rev. Lett. **85** (2000) 5368

[126] C.H. Scholz, Nature (London) **391** (1998) 37

[127] S.Nasuno, A.Kudrolli and J.P.Gollub, Phys. Rev. Lett. **79** (1997) 949 ;S.Nasuno, A.Kudrolli, A.Bak and J.P.Gollub Phys. Rev. E **58**(1998) 2161.

[128] F. Heslot, T. Baumberger, B. Perrin, B. Caroli, and C. Caroli, Phys. Rev. E **49** (1994) 4973

[129] A. Subbotin, A. Semenov and M. Doi, Phys. Rev. E **56** (1997) 623 ;K. Sato and A. Toda, J.Phys.Soc.Jpn **68** (1999) 77

[130] P.A. Tompson and G.S. Grest, Phys. Rev. Lett. **67**, 1751 (1991).

[131] H. Hayakawa, Phys, Rev. E. **60** (1999) 4500; H. Hayakawa, Prog.Theo. Phys.Suppl

[132] J.M. Carlson and A.A. Batista, Phys. Rev. E **53** (1996) 4153

[133] R.A. Bagnold, The Physycs of Blown Sand and Desert Dune (Mathuen, 1941)

[134] H.Nishimori and N.Ouchi, Int.J.Mod.Phys **B7** (1993) 2025; Phys. Rev. Lett. **71**, 197 (1993)

[135] H.Nishimori, M.Yamasaki and K.H.Andersen, Int.J.Mod.Phys **B12** (1998) 257; H.Nishimori, M.Yamasaki, Preprint; B.T. Werner, Georogy **23** (1995) 1107

[136] R. Kawamura, Reports of Scientific Technology Institute in Tokyo Univ. (in Japanese) (1951) 95;

[137] L.Vanel, D.Howell, D.Clark, R.PpBehringer, and E.Clement, Phys, Rev. E. **60** (1999)

[138] S.Luding , Phys, Rev. E. **55** (1997) 4720

[139] C.Eloy and E.Clement J.Phys I France**7** (1997) 1541

[140] H.G.Matuttis, Granular Matter **1** (1998) 83

[141] A. Daerr and S. Douady, Nature (London) **399** (1999) 241; Eur.Phys.Lett. **47** (1999) 325; Eur.Phys.J. B **11** (1999) 131

[142] T.S. Komatsu, S. Inagaki, N. Nakagawa and S. Nasuno, cond-matt/0008086

[143] H.Kuninaka and H.Hayakawa, cond-mat/0011294

[144] T. Komatsuzaki and S.R. Berry, J. Chem. Phys. 110 (1999) 9160; R.J. Hinde and S.R. Berry, J. Chem. Phys. 110 (1999) 2942

[145] A. Awazu, To apear in Phys. Rev. E

[146] A. Awazu, Now submitting

[147] A. Awazu, Now submitting (To appear in Proceedings of Powder and grains 2001)

[148] A. Awazu, Phys. Rev. Lett. **84**, (2000) 4585;

[149] A. Awazu, J.Phys.Soc.Jpn. **67**,(1998) 1071

[150] A. Awazu, Phys. Lett. A **261**, (1999) 309

Acknowledgements

First of all, I would like to thank Prof. Hiraku Nishimori for valuable advice and discussions, continuous support and encouragement, and careful reading of the manuscript. I also thank Prof. Hitoshi Kaneta, Prof. Yosuke Kayanuma, Prof. Masayoshi Tajiri, for valuable discussions and helpful advice.

I am also grateful to Prof. Hiroshi H. Hasegawa, Prof. Hisao Hayakawa, and Prof. Satoshi Yukawa for valuable discussions and helpful advice. I also acknowledge thankfully that discussions with the following people have been beneficial to my investigation: Prof. Shoukichi Kanno, Prof. Shinya Watanabe, Prof. Naoko Nakagawa, Dr. Teruhisa Komatsu, Prof. Akio Nakahara, Prof. Nobuyasu Ito, Prof. Shin-ichi Sasa, Prof. Kunihiko Kaneko, Prof. Keiichi Tainaka, Dr. Masaharu Isobe, Prof. Katsuhiro Nishinari, Prof. Ken Sekimoto, Prof. Shinji Takesue, Prof. Mitsusada M Sano, Dr. Kengo Ichiki, Prof. Yoshiyuki Y. Yamaguchi, Prof. Makoto Kikuchi, Prof. Tsuyoshi Chawanya, Prof. Satoru Nasuno, Prof. Tsuyoshi Hondou, Prof. Masami Nakagawa, Mr. Miki Matsuo, and members of Nishimori Lab. at Osaka Pref. Univ., Hayakawa Lab. at Kyoto Univ. Ito Lab. at Tokyo Univ., and Information Mathematical Sciences Group at Ibaraki Univ..

Researches in this thesis were supported in part by Grant-in-Aid for JSPS Fellows 10376. A part of the computation in this thesis was done by use of many free softwares on UNIX or Linux System.